Schafer

IFE Reactor Studies

February 1999

Prepared by:

Schafer Corporation
1901 N. Ft. Myer Drive
Suite 800
Arlington, VA 22209
703/558-7900

Task Report – Naval Research Laboratory
Contract N00014-97-D-2014/001

Table of Contents

Executive Summary:

This report detail the effort undertaken by Schafer Corporation during the period between 1 July 1998 and 1 February 1999 in support of NRL efforts to define the requirements and key scaling parameters for possible future laser fusion power reactors driven by large krypton fluoride excimer lasers. While laser-driven fusion is not a new topic, the last study performed for DoE was the Sombrero study undertaken in 1992. In addition to being somewhat dated, this effort was also terminated ahead of the planned schedule, resulting in some areas of the concept that were not thoroughly explored. Nonetheless, it seemed prudent to take Sombrero as the baseline approach, or point of departure.

Studies of the effects on both cost and efficiency of variations in possible laser operating modes and concepts are presented as Appendix 1. It is important to appreciate that while both the DoE and DOD communities have long appreciated the potential scalability of KrF lasers, this is not the same as stating that these issues have been extensively explored. While SDIO looked at the utility of megawatt class excimer lasers for ABM missions in the early to mid-1980's, virtually all of the work was at the system level of analysis and little work was done in terms of determining how to make such lasers a reality. The only DoE work prior to Nike was the Aurora effort at Los Alamos and much lower scale laboratory efforts at the basic research level in the 1970's. A consequence of this history is that in determining how to develop the laser technology from the single pulse Nike level to that appropriate for a repetition-rated, long-lived reactor driver, the technologists have to start at a rather basic level in order to avoid the indeterminate results which are the almost invariable consequence of trying to proceed on too many parallel technological fronts at one time. The 5 Hz, 30-cm aperture Electra laser under development at NRL is a conservative, logical and prudent first step beyond Nike. While our efforts endorse this as the first step, it was also clear that one might not achieve the performance in either laser efficiency or capital cost per unit laser pulse energy necessary for an attractive reactor. This task tried to examine the potential of various directions of further development after Electra in terms of their potential for approaching the longer-term needs of the program.

The conceptual reactor studies effort was divided into two main sections:

1 It was assumed in all cases that the very effective induced spatial incoherence (ISI) approach pioneered by NRL on the Nike laser would be used to control final pulse duration and smoothing on the pellet. The laser studies showed that it might be advantageous to operate the laser amplifiers at as long a pulse duration for the gain as would prove feasible. Most simply put, the effect of longer pulse duration was to linearly increase the amount of energy obtained

from each amplifier module. As an example, if everything performs as postulated, then a microsecond pulse laser would require half the amplifier modules of a 500-nanosecond pulse laser, halving the capital cost of the most expensive parts of the laser structure. Even longer pulses would be consistent with the large physical footprint of the architecture of a reactor site, even with the increased number of optics modules. To a point, longer pulses might also help to increase the electrical efficiency of the laser. Other than the laser study, the main efforts in updating Sombrero were in the area of target chamber and optics, which were not well defined at the end of the Sombrero effort. In the optics area, a new technology, fusion bonding of crystalline optical materials has come of age since the sombrero study. In many ways the most desirable optical window for the electron beam-pumped laser modules would be sapphire (crystalline Al_2O_3); however, at the present time the largest high quality zero degree orientation (the one that is needed to avoid birefringent effects) window element that can be obtained is about 15 cm by 30 cm in optical aperture. Fusion bonding offers a technique which could allow larger windows to be fabricated from these 15 x 30 cm^2 elements arrayed as a mosaic. Several design iterations were run with Onyx Optics, Inc. the company that has developed and patented this process, and an approach identified which would be affordable for the Electra Device (30 cm x 30 cm aperture), would allow demonstration of 60 x 60 cm Nike sapphire windows during the current effort, and would allow fabrication of meter x meter optics if needed for a reactor driver module. The Sombrero study assumed that the target chamber would operate at a low internal pressure, ~ 1 torr of argon or another inert gas, and relied on differential pumping to retain all tritium in the reaction vessel, as diffusion into the target chamber building, which was also to be operated at an internal pressure of ~ 1 torr, could dramatically increase the cleanup cost of tritium-contaminated material for the facility at end of useful life. In the current study, an alternative to this phase of the sombrero design is presented which allows: (1) operation of the surrounding facility at normal pressure with no tritium contamination issue; (2) a material window, nominally fused silica, which is protected from direct exposure to particles and radiation from the target and which separates the atmospheric pressure and low pressure regions; (3) use of a low pressure differential aerodynamic window, ~1 torr on either side, separating outer and inner parts of the target chamber; (4) the only optic exposed to the target is a grazing incidence mirror. The aero window occurs at a beam waist. This location could also be fitted with a gate valve to close it completely in the event of a malfunction where a tritium release could otherwise result. An issue with the original Sombrero concept that was identified was that it assumed a single pellet injection system. In an engineering sense, this is not a realistic choice as this allows the power plant to fail from a single point failure in this system. The optimum number of injection systems clearly has to be two or more. This point has not been pursued further because of limited funding, but , it is clear, that careful

study is necessary to define a pellet injection system that has: (1) high redundancy to avoid single point failures; (2) the capacity to operate continuously at full rated load for months at a time; (3) the ability to operate at reduced load in times of low system need for electricity; and, (4) the ability to do all of these and deliver high quality pellets to the focal region accurately at a (manufacturing plus amortized capital) cost not exceeding $0.25 per pellet.

2 A second line of effort proceeded from a very different point of view. In this effort, a parametric analysis was done to determine the interrelationships of laser pellet gains, laser efficiencies and the allowable final cost of power for ICF fusion to be economically viable. From this model, presented in Appendix 2, not only can the requirements in laser efficiency be scoped out, but, given reasonable assumptions from the power industry, the effect of the final desired Cost of Energy and the fusion pellet performance on the allowable capital cost of the laser.

For a future IFE power plant one must optimize the cost of electricity (COE) of the plant, consistent with physical and engineering reality. Therefore, the two studies must dovetail seamlessly. That is the "sweet spot" for reactor operation and that for laser performance are contiguous, if not identical. Actually, it is not so simple, as the regime in which most high energy per pulse ultraviolet excimer lasers has operated has been strongly influenced either by the application at hand, which historically was not inertial confinement fusion, or by the requirement to produce maximal single pulse energies from the funding available for laser proof-of-concept experiments, and by available reliable pulsed power equipment.

This is why the two studies from radically different bases are useful. The reactor power plant conceptual study helps to define what are practical and needed goals for a fusion laser development task; the excimer laser study helps to define what can possibly expected from krypton fluoride lasers in the future, if not in the past. Between the two studies, one can discern a region of overlap where this laser technology may be able to achieve capital and operating cost requirements, as well as illuminating the efficiency requirements to make a fusion reactor practical and an economically attractive producer of electrical power.

The third appendix is a draft of a plan Schafer Corporation put together for NRL as a "strawperson" approach to managing the type of experimental investigation needed to determine how well a relevant KrF laser can operate in the real world, as distinct from in a model. Folded into the concept is how one could manage a parallel alternate (solid state)laser development, if that proves practical. The key to this plan is to focus on the form of the management plan and the seniority of people required to carry it forward and not the specific nominees.

The fourth appendix presents a preliminary design performed by Schafer for the magnet assembly of the Electra 30-cm aperture repetitively pulsed laser, which NRL is developing in the first phase of the current DoE program.

The fifth appendix presents a preliminary design by TRW, Inc. for a floe loop for the Electra laser.

Appendix 1

Inertial Fusion Energy

Laser/Fusion Reactor Development Plan

October 1998

TABLE OF CONTENTS

1.0 INTRODUCTION:

For over forty years the scientific community has been intrigued by the prospects of developing fusion energy. The hope was to produce a cost effective, safe and environmentally friendly energy source, which would have an almost unlimited source of fuel. The original and still the main focus of the energy community has been the magnetic fusion energy (MFE) approach. The significantly less funded energy concept, inertial fusion energy, (IFE), has had to leverage its concepts off of technologies from the MFE program that were applicable as well as those that were developed in support of the Department of Defense and DOE Defense Programs. While these investments were significant, the major contributions that they provide an IFE program are to develop phenomenology which can suggest IFE approaches but not provide the answers of the technical and engineering issues required to develop an IFE power plant.

The result of this has been that the focus of the IFE program was less on building large devices to demonstrate detailed technical issues and more on using the defense program results coupled with analysis to create potential energy power plant constructs which would provide attractive costs of electricity and thus be of interest to the energy industry. Coupled with this, the community addressed some of the key technical issues in a few well-chosen experiments.

In 1992, conceptual designs were completed for two IFE power plants by a consortium of industry and university scientists. These were performed under the Prometheus study which looked at both an indirect drive heavy ion beam concept and a direct drive laser beam concept. The Osiris study, which was for an indirect drive concept using a heavy ion beam as the driver, and the Sombrero study, which was for a direct drive concept using a Krypton Fluoride (KrF) laser as the driver. The Osiris and Sombrero studies were complementary for the two concepts and will be the baseline for further discussions. Both studies produced power plant concepts where the cost of electricity was between 5-7 cents/kW-hr, and the capital costs appear to be competitive and environmental issues can be addressed and mitigated. Thus IFE should be competitive with other power systems. In addition, experiments demonstrated to date show no technology showstoppers and confirmed/demonstrated several key technical concepts. Thus IFE remains as a realistic option as a fusion energy source. This program plan addresses the near term program proposed to address only a laser fusion power plant based on the direct drive concept. In this concept, the target absorbs the laser light directly rather than using the laser (or ion beam) to create thermal x-rays which are then absorbed by the target. While the near term plan focuses on key technical issues, it is, however, put in the context of those activities required to build an operational fusion power plant. To date, the program has made two major advances. Scientists at the Naval research Laboratory (NRL) have developed a high gain target design which can be traced to experiments. These designs are within the performance bounds of the Sombrero study and provide one anchor for its conclusions. The second achievement has been the development of the Nike KrF laser, also at NRL. This system has demonstrated the spectral bandwidth and spatial beam uniformity that is required to implode direct drive

targets and not incur deleterious plasma instabilities. These are necessary steps on the way to demonstrating the enormous potential of IFE.

The demonstration of all technical and engineering issues relating to the design of a fusion reactor in toto is a project of considerable complexity and could well take decades to complete and several billions of dollars in current day [1998] funds to reach the stage where the private power providers would feel comfortable with taking this over as part of their future. At present, the MFE Program is faced with such a dilemma where continued development of integrated systems, which are almost an a priori requirement of today's technologies, are of the scale where these full-scale developments would preclude pursuing other options, even those with better economic potential.

In the current IFE program we wish to take advantage of the fact that inertial confinement fusion is **modular**, unlike magnetic confinement fusion. That is, we can separately develop and test the major components of such a fusion power plant without building a complete plant. This has significant advantages in that it allows the development of a program plan that addresses the key issues in either a series or parallel manner, i.e. not all issues need to be addressed simultaneously, or at the same level of vigor. Having stated this, it is important to understand that while one can identify issues which with each element (laser, chamber, target) of a laser IFE concept, the one that needs to be addressed next is to understand the demonstrated scaling of KrF laser technology. Data obtained from laser modules can then be used to validate designs, performance and costs of an eventual IFE KrF laser driver. In addition, it is important to rekindle engineering efforts at a low initial state of activity. This will reduce the lead time for later engineering activities related to the elements of the system. These include efforts related to chamber design (wall materials, coolants, containment, breeding, target injection, optical beam propagation) and target development (design refinements, manufacture). Thus, while the near term focus will be on validating driver engineering and performance issues, valuable activity on the other long-lead elements of an eventual system will be undertaken to focus subsequent activity. The reactor and target concepts will be developed such that even the driver can be changed to a different one if it can be made applicable for a direct drive concept. While NRL will be responsible for developing the case for a direct drive laser fusion reactor employing krypton fluoride lasers to implode the target, Lawrence Livermore National Laboratory (LLNL) will be responsible for developing the case for a direct drive laser fusion reactor employing diode pumped solid state lasers (DPSSL), with ultraviolet frequency conversion, to implode the target.

This document will mainly address only the Phase I: Concept Validation phase the effort, an initial phase lasting four years in which the major priority is to identify and resolve key technical issues. Assuming this effort is successful, the program in the 2003 time frame will decide on initiating a Scaling Validation activity based on whether KrF and/or DPSSL, is ready to build a full scale 30-50 kilojoule repetition rate laser beamline. This activity will be ongoing from 2004 to 2010, with the goal of providing the engineering data needed to design [and cost] a Phase III: Engineering Prototype Inertial Confinement Fusion Facility. This facility would provide the opportunity to demonstrate a laser driven fusion reactor and would provide a full-scale evaluation of the engineering

readiness of the technology. Assuming success, the Phase IV: Demo Power Plant would follow with the selected technology. The following figure shows the conceptual and overall schedule through Phase II along with the Phase I projected cost:

Table 1.-I

Phase I Budget *(M4)*	FY 99	FY 00	FY 01	FY 02
Krypton-fluoride Lasers {includes development, target design & fabrication &chamber design)	9.5	20	23	17
Diode Pumped Solid State Lasers {includes development, target design & fabrication &chamber design)	1	6	7	11
TOTALS	10.5	26	30	28

Table 1.-II Overall program plan for Phase I and II of the laser effort:

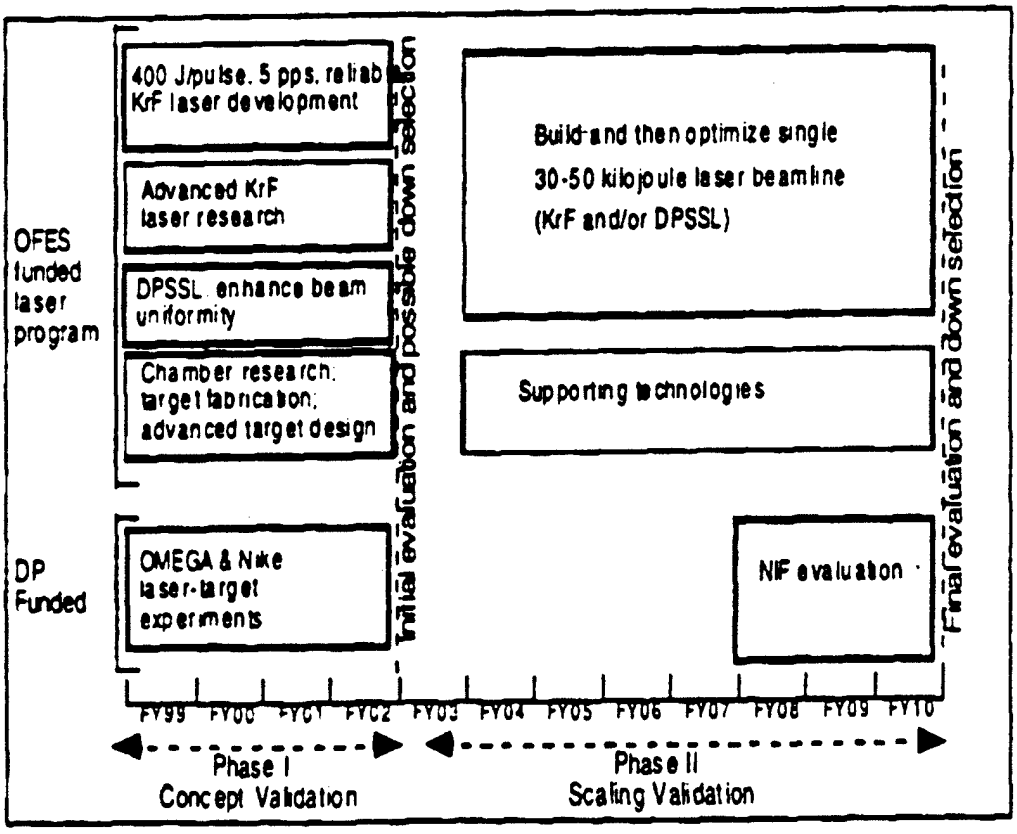

2.0 Direct Drive Fusion Power Plant Concept

2.1 Plant Parameters:

The system design is based on the Sombrero study. Sombrero was a 1000 Mwe, KrF-laser driven power plant design performed in 1992 for DOE. There will be a number of areas where new data indicates a need to update Sombrero. These will be noted in the Sombrero description; revision may or not be a part of the proposed program, depending on its criticality. As an example, the Sombrero chamber was proposed to be constructed of a low-activation carbon/carbon (C/C) composite. Data developed since the study was completed indicate that alternate materials might be better choices, based on thermonuclear neutron damage. As there appear to be numerous possible alternate first wall materials, and as the MFE program will be actively researching this issue, we do not propose any effort, at this time on the IFE program. The first wall was proposed to be protected with 0.5 Torr of xenon buffer gas. The issue of preferred gas fill should be addressed on this program, as it involves issues of laser propagation through a turbulent optical medium and the effect of that turbulence on the laser uniformity on target. Solid Li_2O particles flowing by gravity through the blanket were proposed as the primary coolant and breeding material. This moving bed solid breeder blanket concept has all the advantages of solid breeders but none of the disadvantages, such as the need for a high pressure gas coolant and a separate He gas loop for tritium extraction. Helium is used to fluidize the particles for transport around the heat transport loop. Liquid lead is used in the intermediate loop to transfer heat to a steam generator and a double reheat steam power cycle.

The KrF driver uses e-beam pumped amplifiers and angular multiplexing for pulse compression. The laser uses relatively small (~60 kJ) final amplifiers and a new plasma cathode technology which will be developed on this program for the e-beams in order to improve the laser system efficiency. Amplifiers are grouped in four-unit modules to minimize hardware requirements. Sixty beams are used to provide uniform target illumination. Grazing incidence metal mirrors are used as the final optical component to remove the dielectric focusing mirrors from the direct line of sight of high-energy neutrons. The key plant operating parameters are listed in Table 2.1 -I

Table 2.1. -I Sombrero Power Plant Operating Parameters

Power (MW)	2,677.0
Energy Driver Energy (MJ)	3.4
Target Gain	118.0
Target Yield (J)	400.0
Rep Rate (Hz)	6.7
Fusion Multiplication	1.08
Total thermal Power (MW)	2,891
Power Conversion Efficiency (%)	47
Gross Electrical Power (MWe)	1,359
Driver Efficiency (%)	7.5

Driver Power (MWe)	304
Auxiliary Power (Mwe)	55
Net Electrical Power (Mwe)	1,000
Tritium Breeding Ratio	1.25

2.2 SOMBRERO CHAMBER DESIGN

A cross-section of the 1992 Sombrero chamber is shown in Figure 2.1, and the key design parameters are given in Table 2.2.-I As proposed in the Sombrero study, the chamber is assembled from twelve (12) wedge-shaped, modules that are totally independent of each other with separate Li_2O inlet and outlet tubes. The chamber has a cylindrical central section with conical ends; a radius of 6.5 m at the midplane and an overall height of 18 m. Each module is subdivided both radially and circumferentially into coolant channels as shown in Figure 2.2. The carbon structure fraction increases from about 3% at the front to 50% at the rear of the blanket, thus providing an integral reflector which does not require cooling. The first wall (FW) thickness is 1.0 cm. The thickness of the cooling channel behind the first wall varies from 7 cm at the midplane to 37 at the upper and lower extremities, making the flow area constant along the entire FW from top to bottom. This is done to ensure a constant velocity at the FW where a high heat transfer coefficient is needed.

TABLE 2.2-I SOMBRERO CHAMBER DESIGN PARAMETERS

First Wall Radius at Midplane (m)	6.5
Overall Internal Height (m)	18
First Wall Thickness (cm)	1.0
Maximum Stress in First Wall (Mpa)	43
Blanket Thickness (m)	1.0
Total thermal Power (MW)	2,981
Surface Power (MW)	803
Blanket Power (MW)	2,088
Li_2O Inlet Temperature (^0C)	550
Li_2O Average Outlet Temperature (^0C)	740
Li_2O Flow Rate (kg/s)	5,590
Max Li_2O Velocity at FW (m/s)	1.15
Number of Blanket Modules	12
Structural Mass Per Module (Tonne)	37.8
Number of Beam Ports	60
Li_2O Mass in chamber (kg)	670,000
Total Li_2O Inventory (kg)	2,000,000

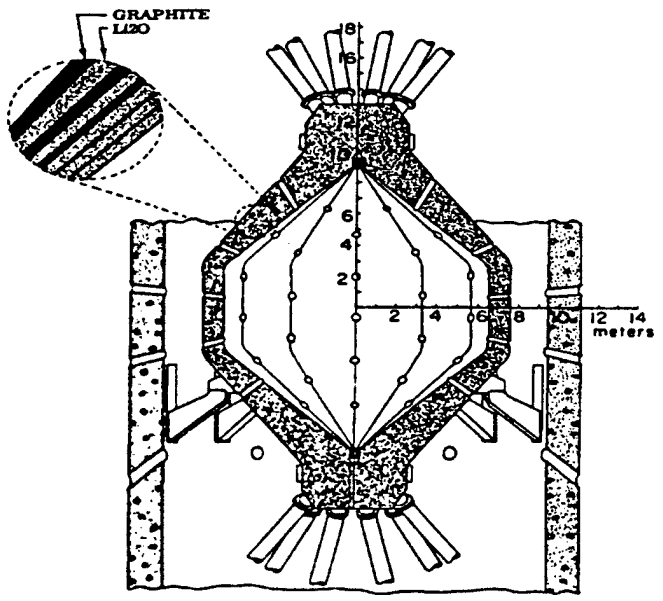

FIGURE 2.1 CROSS-SECTION OF SOMBRERO CHAMBER

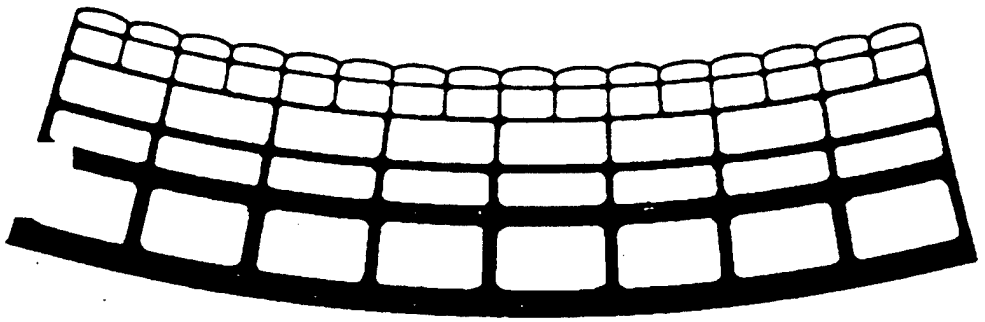

FIGURE 2.2 CROSS SECTION OF SOMBRERO BLANKET

The Li_2O particles with a size range of 300-500 μm have a void fraction of 40% in the moving bed, and the grains are 90% of theoretical density. The Li_2O particles enter the top of the chamber from a manifold that doubles as a cyclone separator to remove the particles from the He gas that is used to transport Li_2O through the intermediate heat exchanger (IHX). After the particles enter the chamber, they flow under the force of gravity through the chamber and exit at the bottom. The Li_2O velocity at the FW is 1.15 m/s and each succeeding radial zone has progressively lower velocities towards the rear of the blanket. Low pressure (0.2 Mpa) He gas flows counter-current to the particles in the chamber coolant channels; this helps maintain a steady movement of the particles and prevents the formation of clustering or compaction. A thin coating of SiC on the inner

surface of the coolant channels aids in sealing the C/C composite structure against He gas leakage into the chamber. The Li_2O inlet temperature to all of the zones is 550 °C, but the outlet temperature is 700 °C for the FW coolant channel and 800 °C for the rear zones. The total mass flow rate of 2×10^7 kg/hr has an equilibrated outlet temperature of 740 °C. Flow in the different zones is controlled with baffles located at the bottom of the chamber to ensure that there will be no voids in the blanket. After going through the chamber, the particles are transported around the loop and through the IHX in a fluidized or entrained state by He gas.

The FW is protected from x-rays and ions by 0.5 torr of Xe gas. Since the beam ports are open to the reactor building, the whole building also has 0.5 torr of Xe gas. A certain amount of He leakage into the building can be tolerated without degrading the reactor performance. Innovative ideas for separating He from Xe, such as diffusion membranes, must be incorporated into the Xe recycling system. (This is an area where newer concepts than those used in Sombrero for protecting optics and confining tritium, such as use of aerodynamic windows, or gas curtains, will have to address the issues of maintaining the chamber atmosphere during operations.)

As noted above in this proposal, more recent data suggest that Carbon and Carbon composite structures may not withstand continued operation as well as was expected in 1992. A different material for the reactor vessel will be required; at present, probably either an aluminum alloy or silicon carbide would be favored. While important, however, this is not really a critical issue, as the likelihood appears small that some reasonable choice will not exist where the overall performance is comparable to that envisioned in the Sombrero study.

Sombrero also had very good neutronic performance. The tritium-breeding ratio was 1.25 with 0.91 coming from ^6Li. The energy multiplication factor was 1.08, which increases the 2677 MW of fusion power to 2891 of total thermal power. The peak displacement damage rate in the carbon first wall (FW) was about 15 dpa/fpy, and the helium production rate was about 3,800 appm/fpy. The lifetime limit for radiation damage was uncertain in 1992, but based on more recent data from Oak Ridge National Laboratory, appears to be in the range of 25 dpa. This makes the Sombrero assumption, that a materials program can develop a C/C composite with a damage limit of 75 dpa, which would give a first wall life of ~5 py within a reasonable time, appear somewhat unlikely. However, given that similar, but even more circumscribed material problems exist for MFE reactor vessels, the impact of this issue depends on what further data is developed for more suitable materials.

2.3 Sombrero Power Conversion and Plant Facilities

2.3.1 Heat Transport System

The primary coolant for Sombrero is a flowing bed of Li2O particles in He gas and operates between 550 and 740 °C. The primary loop consists of four coolant circuits including one intermediate heat exchanger (IHX) in each circuit. The number of circuits

is based on the size of the heat exchangers. A state-of-the-art heat exchanger design is assumed. An intermediate loop, with lead coolant operating between 400 and 600 °C is used to isolate the Sombrero chamber from the high-pressure steam loop.

2.3.2. Power Conversion

To achieve a high efficiency power conversion, a high pressure, high temperature steam cycle, similar to the Osiris plant, was adopted for the Sombrero plant. The steam conditions as for the Osiris plant, have a peak pressure of 24.2 MPa and a peak temperature of 538°C, provide a thermal conversion efficiency of 45%. (The Sombrero analysis appears consistent with the efficiency of a fossil fuel plant employing a similar steam cycle in Monroe, MI.) However, in the case of Sombrero, 230 Mt of laser waste heat is used for feedwater heating, and this increases the cycle efficiency to 47%. It should be noted that this is may not be the most desirable situation, as high quality electricity is used to make this component of the heat; a more desirable situation would be a more efficient laser.

The steam generator arrangement is similar to that of the Osiris plant, with two steam generators, each sized for 50% of the thermal capacity (1490 MWt). Each steam generator is a state-of-the-art design consisting of a high-pressure section, an intermediate-pressure section, and two low-pressure sections arranged in a cross-compound configuration.

2.33 Reactor Building

A concept for the Sombrero reactor building has been developed. The building provides housing for the reactor, shielding of the public from fusion neutrons, and housing for the final optics. In addition, the building accommodates remote maintenance of the reactor. The concept for this building is shown in Figures 2.3 and 2.4.

The size of the reactor building is dictated by the requirements for housing the final optics of the laser driver. It accommodates 60 beam lines that offer a near-uniform illumination. All the beam lines penetrate the reactor building through a beam handling area in the basement. The building vacuum boundary is located at the building floor where the beam lines penetrate the floor through windows.

The layout of the final optics in Sombrero was determined by the requirements for reasonable lifetimes of the final optics, which was, and is, highly uncertain since there are almost no data on radiation damage of either metal or dielectric optics in high neutron fluences. Grazing incidence metal mirrors (GIMM) made of aluminum were used to bend the beams slightly (84° angle of incidence) so that the dielectric focusing mirrors were out of the direct line-of-sight of fusion neutrons. The GIMMs were located 30m from the center of the chamber, and the dielectric focusing mirrors were 50 m from the center of the chamber. Neutron dumps are located behind the GIMMs to further reduce the neutron flux experienced by the dielectric optics, which are expected to survive for the life of the

plant without replacement. In addition to the neutron dumps, the reactor building floor shields optics and equipment in the beam handling area.

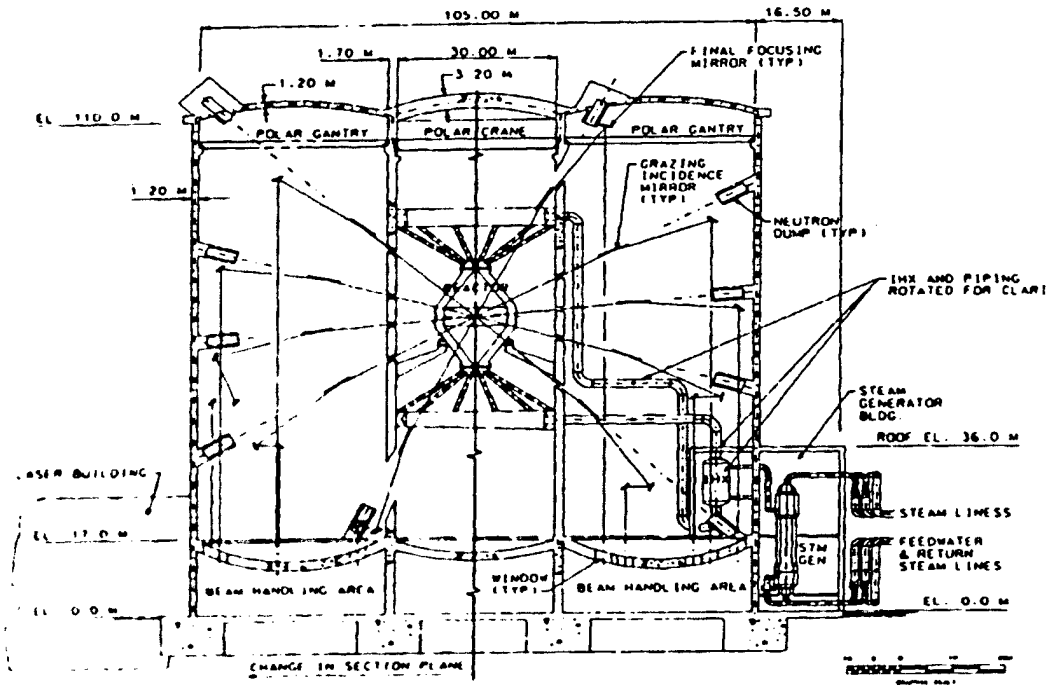

Figure 2.3 Elevation view of the sombrero reactor and steam generator buildings.

Several unique features were incorporated in the Sombrero reactor building structural concept. Since the building was required to operate in a vacuum, it is subject to an equivalent external pressure about 0.1 Mpa. For this reason, the floors and ceilings are designed as shell structures rather than as plates to reduce cost. The building has also been designed as a Seismic Category I structure and is adequately reinforced to resist buckling against external pressure.

A concept for supporting the grazing incidence and final focusing mirrors was developed. As shown in Fig. .3, each mirror was separately supported. However, for structural rigidity, some of the supports were also tied together. Each support was a combination of reinforced concrete members. The supports were also configured so that the remote maintenance equipment could access the mirrors for refurbishment or replacement.

The IHXs were located within the reactor building. However, they were housed in individual cylindrical chambers. This arrangement accommodated the 0.1 Mpa differential pressure (between the IHX chambers and the rest of the reactor building) and at the same time allowed limited access to the IHX chambers during normal power operation. The steam generators were located in a separate building outside the reactor building.

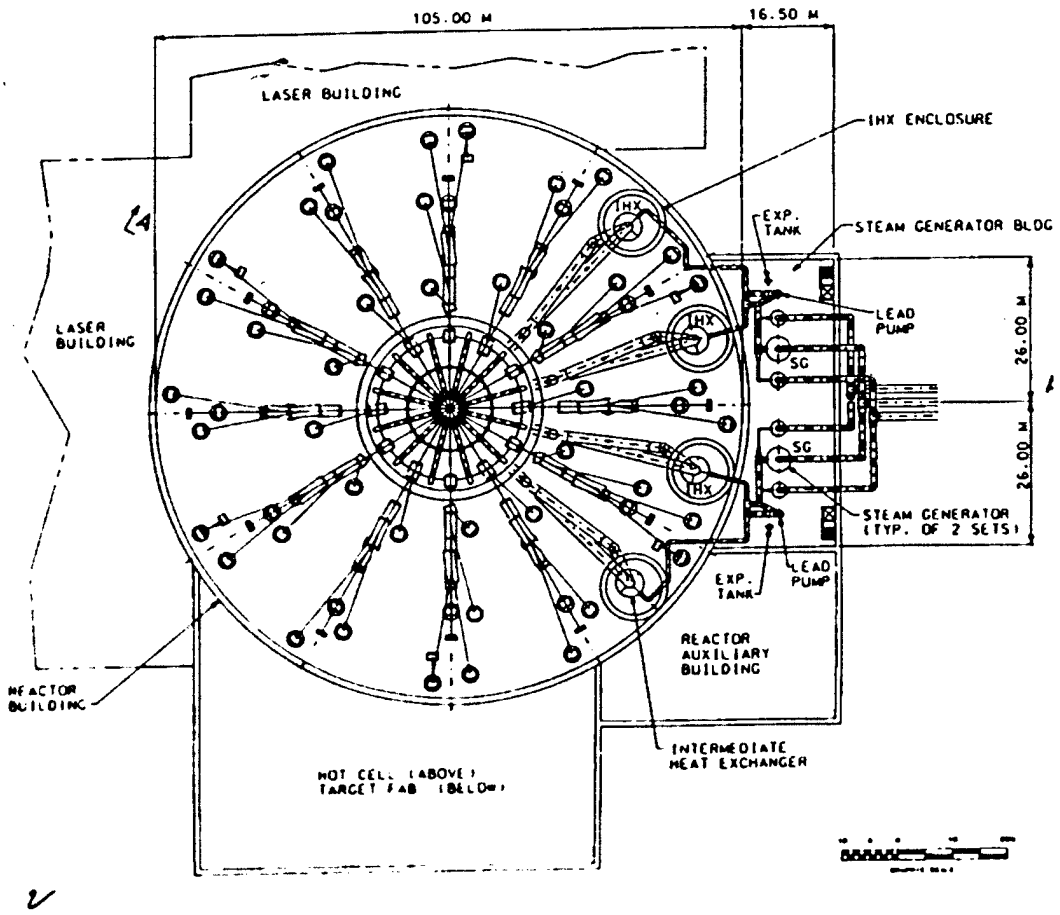

FIGURE 2.4 PLAN VIEW OF THE SOMBRERO REACTOR AND STEAM GENERATOR BUILDINGS.

As discussed further under the optics section, the Sombrero study's approach to the optical system may have underestimated the importance of positive control of the tritium. It was assumed that tritium would be recovered by pumping on the gases present in the reaction chamber. No passive methods, such as optical windows on the chamber, were incorporated to ensure this result. Additionally, it was assumed that the entire reactor building would be operated in a vacuum. On re-evaluating the optics issues, it appears that one could incorporate pressure windows on the chamber, at a location that would be outside of the neutron-irradiated volume. Additionally, the use of a low-pressure (~ 1 torr) aerodynamic window between the focusing and grazing incidence optics would greatly enhance tritium recapture in the central region of the target chamber, as well as allow for better protection of optics. Potentially, this could considerably relax the design requirements on the reactor building. The layout of this optical scheme is shown as Figure 2.5 below. A solid window is used which is located in the beam leg for each laser beam, but far enough away from the hot interior of the reactor that it can be temperature controlled at a low enough temperature that it would remain a barrier for tritium. This leg is separated from the interior of the chamber by an aerodynamic window located at a focus of the beam (Both interior regions are at low pressure, ~ 1 torr, with the

outer region slightly positive with respect to the inner.). After the focus, the beam is directed by grazing incidence mirrors that are the only optics directly exposed to the target radiation and debris.

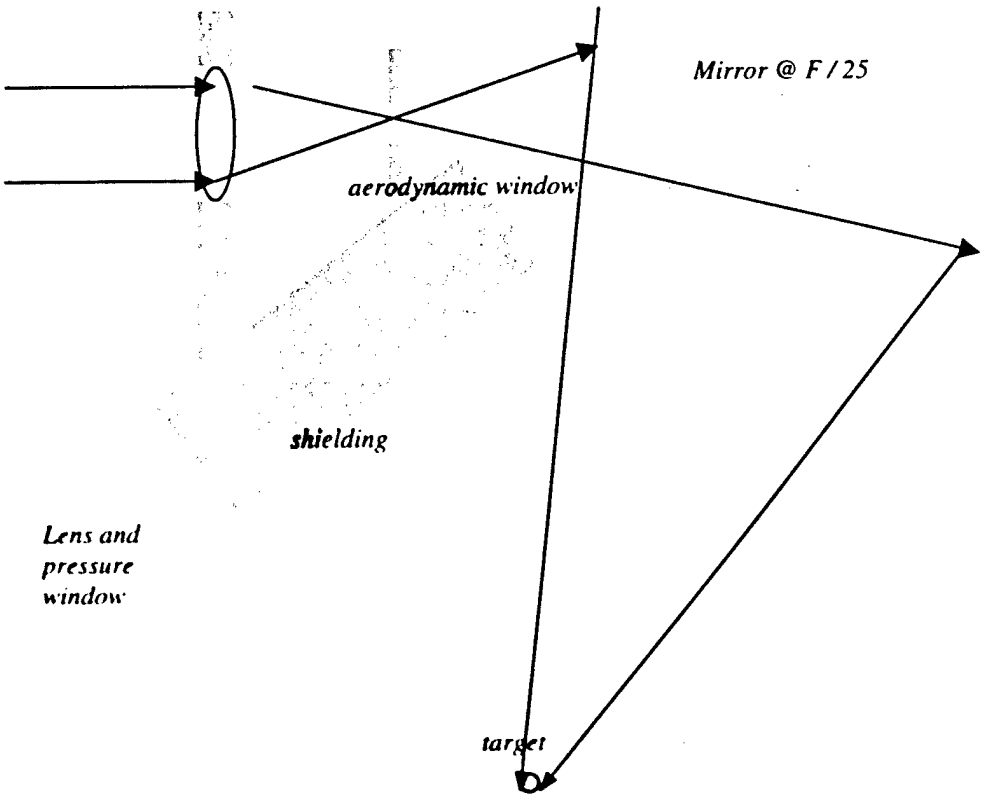

Figure 2.5 Conceptual layout for final optics train

2.4. KrF Driver Design

2.4.2 Design Overview

There are several goals in the design of a KrF driver system for IFE: 1) high operating efficiency, 2) low capital cost, 3) technical credibility, 4) high availability / reliability, and 5) low operating costs. In the Sombrero study, the authors assumed a tenth-of-a-kind plant with technology that could be mature in the year 2040 (This was common with most other recent fusion reactor studies, and allows some reasonable amortization of specific development costs.). In creating such a design, the focus was on how to optimize operating efficiency.

A point design was carried out for a 3.6 MJ (on target) KrF laser. This is slightly higher than the 3.4 MJ used as the reference design for the Sombrero power plant, but allows some margin. To scale the design to the lower energy, the volume of the final amplifiers described in this section would be reduced in proportion to the laser energy

(i.e., by 5.6%). The design parameters for the 3.6 MJ point design are given in Table 2.4-I

TABLE 2.4-I KRF DRIVER AND AMPLIFIER DESIGN PARAMETERS
[FOR A 3.6 MJ POINT DESIGN]

OVERALL DRIVER:	
Total energy on Target (MJ)	3.6
Number of Beam Clusters	60
Beamlets per Cluster	100
Final Pulse Width (ns)	6
Efficiency (%)	7.5
ULTIMATE AMPLIFIER	
Final Amp Energy (kJ)	60
Ar in Kr (%)	50
Pressure (atm)	1
Initial Temperature (C)	500
Pumping (kW/cm^3)	400
Extraction time (ns)	600
Amplifier Gain	16
Rep-Rate (Hz)	6.7
Length in Optical Direction (m)	1
Length in Flow Direction (m)	2
Length in E-Beam Direction (m)	1
Flush Factor	1.3
Fluence (J/cm^2)	5
E-Beam Voltage (kV)	610
Diode Current (A/cm^2)	40.6
Diode Impedance (ohms)	0.6
Inductance (nH)	23
Applied Field (kG)	6
Intrinsic Efficiency (%)	14.5

The KrF driver system consists of 1) a front-end which produces a pulse of the desired band width and temporal and spatial intensity characteristics, 2) several stages of intermediate amplification and progressive temporal/angular multiplexing, 3) final amplification by large e-beam pumped 2-pass amplifiers, and 4) demultiplexing and beam delivery to the reactor building. In the reactor building the beams are brought through a mirror system that provides neutron protection to the laser stages and brings equal amounts of KrF illumination to the target from 60 uniformly placed directions by way of grazing incidence metal mirrors, which are the only optical element subjected to direct neutron flux. The ultimate amplifiers (UA") in our system operate with a two-pass gain of 16, so the penultimate amplifiers (PA's) only supply ~ 6% of the total energy. From this, it is clear that the efficiency and capital cost of the laser driver system are dominated by the UA's. Because of this, our design discussion at the conceptual stage focuses on considerations of these amplifiers, how their efficiency may be optimized, and how they may most efficiently be assembled into an architecture that satisfies the target requirements.

2.4.2 KEY FEATURES ASSUMED FOR THE DRIVER SYSTEM INCLUDE:

- Direct Drive with Indirect Drive Brightness Capability;
- E-beam Pumping with High Efficiency;
- Angular Multiplexing for Pulse Compression;
- Final Amplifier Trade-offs: Total Efficiency Optimization and Waste Heat Utilization

2.5 CONCEPT VALIDATION

In support of the Sombrero concept, some technical activities have been already executed. The key ones are as follows:

- In 1995, NRL completed the Nike KrF gas laser, and demonstrated non-uniformity at the focus of each laser beam of only 1%. With beam overlap, this non-uniformity dropped to about 0.15%.
- In 1996, NRL used Nike to accelerate flat plastic targets, and demonstrated with new diagnostic techniques that the laser produced a non-uniformity on the target equivalent to only about 100 Angstroms of surface modulation (about 100 atoms). The experiment was in reasonable agreement with the computer simulations. This resolved the fundamental problem of producing sufficiently uniform laser beams to implode direct-drive targets, and provided a foundation for using the computer simulations to design high gain pellets.
- In 1997, NRL used its computer codes to design two new targets that would have thermonuclear energy gains of approximately 100. The predicted energy gain meets the minimum requirement for a fusion reactor. These target designs are still under evaluation.
- In 1997, LLNL using internal discretionary funds began the "Mercury" project, to develop a diode pumped solid state laser with 10% overall efficiency, as an alternate candidate for a fusion reactor using direct drive pellets.
- In 1998, the University of Rochester will use their Omega laser to determine if the overlap of multiple laser beams raises the threshold for laser-plasma instabilities, as has been hypothesized and as is necessary for success with direct drive target designs. NRL will optimize its target designs using its 2D codes, and will begin experimental validation by accelerating cryogenic foil targets using the same materials and laser pulse shaping as the fusion targets. LLNL will begin 3D modeling of these targets, to better determine the safety factors that will be necessary for their success.

3.0 ECONOMICS

Fusion, as would any new technology, must provide a cost which is attractive to the energy industry. This cost is made up of several factors that include both recurring and non-recurring costs. Some of the key factors include fuel target costs, operation and maintenance costs, fixed (administrative, environmental, regulatory, etc.) costs, charge costs and availability factors. Other cost factors exist but are not clearly defined, at this time. While it is easy to develop a technical program that empathizes the maximization of technical parameters, this can lead to a concept that sub-optimizes systems performance

and thus system economics. Therefore, the IFE program through its systems studies has developed a first cut at concepts which can lead to a final system, which is an economically acceptable solution. These technologies are all feasible, however, not all of these need to be incorporated into a first demonstration plant, i.e. it may be most practical to use the fact that the elements of an IFE power plant are reasonably separable. Thus, one could develop a demonstration plant, which empathizes the key technical aspects to demonstrate fusion but for the capital cost and integration risk issues, one could defer some aspects of the systems optimization. Thus the plan can also be made cost-effective while addressing key technical issues. The system and economic studies are the methodology for tracking the impact of technical performance on system economic feasibility.

The concept, to which we are working, even though it may still have some undeveloped areas at this point, can be the basis for a realistic development plan. At the most global level, we can define the regime in which the plant must operate in order to be useful. S. E. Bodner has produced an analysis of the top-level issues in the June 19,1998 note *"How cost of electricity varies with driver efficiency and target gain"*. In this analysis, the following points are made:

- The Cost of Electricity [COE] will be an all-important factor to the utilities, and it can be written as:

  $COE = \frac{C}{fEn}$, Where *C includes* all costs of building and operating the power plant, i.e. its capital and fixed costs, operation and maintenance, pellet fabrication, availability factor, etc.;
  f is the repetition rate of the system; and,
  En is the net electrical power delivered to the grid per shot.

- The net electrical power per laser shot can be derived from the following model:

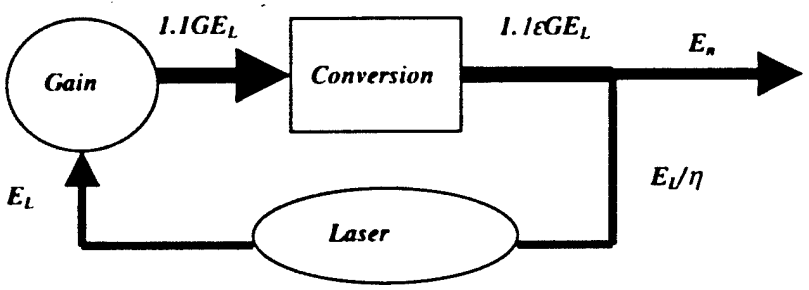

- The net electrical power can be written as:

$$En = EL\left[1.1\,\varepsilon G - \frac{1}{\eta}\right]$$

From this formula an expression for the relative Cost of Electricity [COE], as a function of laser and pellet efficiencies, can be derived as:

$$\frac{COE(\eta, G)}{COE(.07, G)} = \frac{\left[1.1\varepsilon - \frac{1}{0.07\,G}\right]}{1.1\varepsilon - \frac{1}{\eta G}}$$, Where the efficiency of thermal recovery for the reactor is taken as $\varepsilon = 0.47$ for a KrF laser-driven reactor from the Sombrero study, which assumes recovery of the waste heat in the laser process. If we plot his result against pellet gain, G, it is clear that the Cost of Electricity will only slowly change as pellet gains or laser efficiencies are varied.

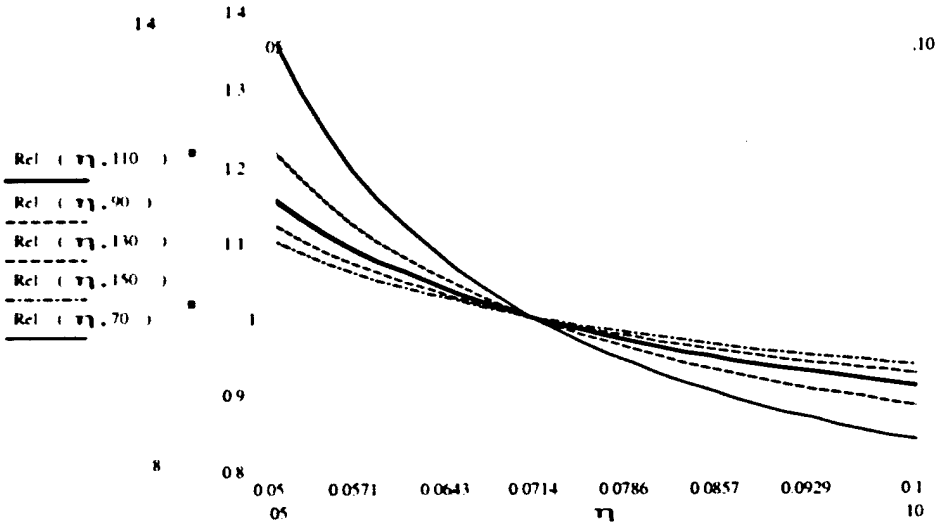

Plotting this on a linear scale over the most probable range of laser efficiencies, 5 % to 10 %, rather than on semi-log paper, shows the variations in clearer fashion.

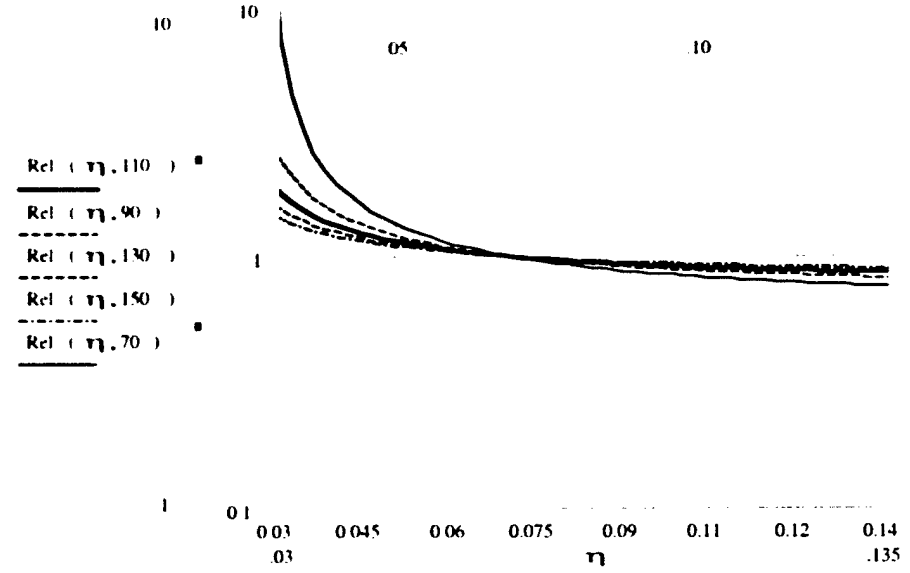

While the COE does change with higher or lower efficiencies, it is a gradual change, and the COE is certainly sub-linear in the range of likely laser performance.
From these curves, one can draw several conclusions: the COE is less than linearly influenced by the laser efficiency, and the pellet gain has a considerably stronger effect than the laser efficiency. This is because the characteristic product in the COE equation is εG, not ηG. Physically, εG is the fraction of fusion pellet output available as electricity, so it sets the scale for the reactor design problem.

Based on these and other considerations from previous studies one can specify the following top level requirements for an IFE power plant:

TABLE 3.0-I PLANT REQUIREMENTS FOR IFE

• Attractive/ Competitive COE	< $0.10 per kwh
• Moderate plant size	< 2 Gw
• Moderate plant Cost	< $ 2B
• Environmental Effects	minimal

This leads to physics goals that fall into acceptable ranges, rather than point designs:

TABLE 3.0-II PHYSICS GOALS

• Target Gain	50-200	higher is better
• Drive Efficiency	5%-20%	higher is better
• ηG	5-20	higher is better
• Beam smoothness	0.3%-3%	lower is better
• Beam Brightness	5-50x diff. Limit	lower is better
• Laser Reliability	10^8-10^{10} shots	higher is better

These earlier analyses and these technical parameter ranges need to be re-validated during the concept validation phase of the program. During this phase, the concept will be refined to include technical results and assure that the goal to develop a cost-effective concept is maintained.

4.0 KEY TECHNOLOGY AREAS:

In this section we will discuss the status of the key elements of a laser fusion reactor, the issues that have to be addressed in this phase of the program, and a top-level description of how they will be addressed. The issues which this Phase I effort will address will not be to refine the concept down to the last nut and bolt but rather will be to:

a) Determine where the required extension of previous engineering practice is great enough that a solution cannot be a prioi be assumed. These are the issues, which can legitimately be termed key issues. If a technical solution is not found, then the Phase II activity should not proceed, let alone later phases.
b) Refine and document the evolution of the overall reactor system/engineering concept. By updating the systems studies.This is represented by extensions, as appropriate, of earlier fusion reactor studies, such as the Sombrero design study. Determine which issues appear major, but where risks can be reduced, as a matter of good engineering practice, by using technology which has previously been applied to problems similar in scope, if not application, or by using sub-scale tests and analysis.
d) Identify materials development issues where the evolution of the required materials science efforts to the necessary scale and reasonable cost may be lengthy processes, or the materials impact demonstrations of engineering performance.

4.1 TARGET DEVELOPMENT

Target design and fabrication are key development and engineering issues for several reasons. First, as we saw from the global analysis, without a target design with a gain between 50-200, not only is it very difficult to achieve a reasonable cost of electricity (COE), but the only way to make up such a problem would be by postulating high laser efficiency, and possibly total energy per pulse. On the four year time scale of the Phase I activity, there will not be a definitive experimental demonstration on a single pulse basis of the successful operation of a full scale target for the fundamental reason that no laser facility will exist capable of driving the target on that time scale. As much as we would like to have a positive answer, we will have to be content with numerical simulation and limited experiments on the available smaller direct drive facilities, Nike at NRL and Omega at the University of Rochester. Assuming that these results are favorable along with the other Phase I efforts, there might be an opportunity to use the NIF at LLNL for direct drive implosions late in Phase II. It appears to be advantageous to an IFE demonstration that the capability to do symmetric implosions on the NIF not be compromised by whatever financial exigencies may occur during its implementation.

4.1.1. TARGET DESIGN

4.1.1.1 STATUS

4.1.1.1.1 TARGET DESIGN CONCEPTS The 1992 Sombrero laser fusion power plant design assumed a direct-drive target with a gain of 118 (thermonuclear yield divided by total incident laser energy), using a 3.4 MJ KrF laser. This target gain led to an attractive

cost of electricity. The target gain however was just an estimate of future design possibilities; in 1992 there were no specific target design concepts with gains in the range of 100 that could also satisfy all of the known physics constraints. Then in 1997 NRL scientists proposed two new direct-drive target designs with predicted yields of 100 – 110, using laser energies in the range of 2.5 – 3.5 MJ. These targets were based upon the technique of enhanced heating of the ablator relative to the DT fuel, via shocks or radiation. The heating of the ablator provided the necessary control of the hydrodynamic instabilities. These targets should also have minimal laser-plasma instabilities. The 1997 status of the designs is described in two articles in the May 1998 issue of Physics of Plasmas, by S. Bodner et al[i], and by J. Gardner et al[ii].

In addition to direct-drive targets, the fusion community is evaluating a more speculative laser fusion design concept[iii] for a fusion power plant called the "fast igniter" that combines the above symmetric direct-drive implosion with extra lasers to ignite the DT fuel at a higher density. If this fast igniter concept proves viable it would reduce the laser energy requirements to 1-2 MJ, and raise the energy gain to the range of 200-300. The improved target performance would lower the cost of electricity. However the fast igniter concept requires very high laser intensities, and there is a substantial risk of various deleterious laser-plasma phenomena. For the standard direct-drive target concept, the peak laser intensity is less than 10^{15} W/cm^2, while for the fast igniter concept the peak laser intensity approaches 10^{19} W/cm^2. It is the hope of the fast igniter advocates that they will be able to harness and utilize the various laser-plasma instabilities that occur at this high laser intensity. The experimental results so far have been mixed, and the evaluation is continuing. Although it is appropriate for fast igniter research to continue at its current level of effort, the concept does not yet provide the basis for an enhanced laser fusion energy program. Our proposed program is thus based upon the more conservative purely symmetric implosion of direct-drive targets, for which there is now a sufficient theoretical, calculational, and experimental data base to proceed with an enhanced research effort.

The two direct-drive target designs that now have the potential for fusion energy applications are illustrated below in Figure 4.1-1, labeled "b" and "c". There was an earlier and simpler DT target labeled "a" that may be tested on the NIF (proposed by C. Verdon [iii]); this target may reach ignition but would not produce sufficient energy gain for a power plant because the DT fuel is preheated along with the DT ablator.

Target (b) consists of a frozen DT fuel shell surrounded by a low density plastic foam, approximately 0.05 g/cc. Target (c) consists of a frozen DT shell surrounded by a low-density foam that is filled with liquid or frozen DT, and in turn is surrounded by a very thin layer of solid plastic doped with a high-Z material such as gold, tungsten, or mercury.

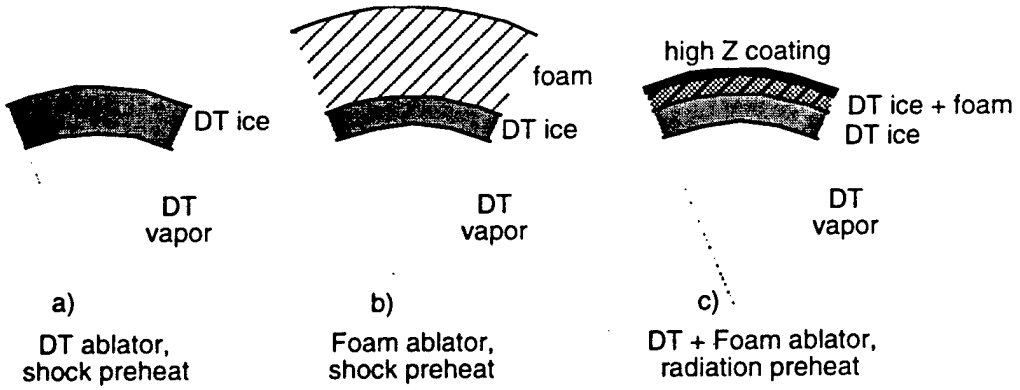

FIGURE 4.1-1 DIRECT DRIVE TARGET DESIGNS

4.1.1.1.2 SIMULATIONS OF TARGETS. Using the NRL one-dimensional spherical implosion code FAST1D, the foam ablator target "b" has been calculated to produce an energy gain of about 110, using UV light (1/4 μm) from a KrF laser, with a laser bandwidth of 2 THz, and with "zooming" of the laser beam so that the laser spot size decreases while the pellet is imploding. The NRL 2D spherical implosion code FAST2D, including ISI optical smoothing, predicts that the hydrodynamic instabilities will not destroy the fuel layer, so that the DT should burn and produce high yield.

Target "c" is predicted to produce target gains of about 110 using the NRL 1D spherical implosion code, even without laser zooming. This target does not have any significant density jump at the ablator/DT interface and thus the interface will be stable. However there have been difficulties in the 2D simulation associated with the complex radiation transport, and the 2D analysis of this target is incomplete. There is however hope that a successful implosion will soon be calculated for target "c".

There have not yet been studies of how either of these two targets will behave with 1/3 rather than 1/4 micron laser light, and using SSD rather than ISI smoothing, as would be available from a solid state laser such as the National Ignition Facility (NIF) or a diode pumped solid state laser (DPSSL) IFE driver. Recent research has instead concentrated on resolving the remaining numerical and physics uncertainties in the two target designs. However based upon previous studies, it is expected that the 1/3 micron light will have a reduced rocket efficiency and a reduced target gain. The targets would also have increased hydrodynamic distortions due to the increased laser beam nonuniformity of 2D-SSD.

Designs for inertial fusion targets have a different scientific foundation than designs for magnetic fusion devices. In the magnetic fusion program, the design of the fusion core has been based upon a combination of scaling laws, analytic theory, and numerical simulations. In inertial fusion, the detailed design of a target and the predictions of its performance are based primarily upon numerical simulations, using large and complex radiation/hydrodynamics codes. The inertial confinement fusion program does not utilize scaling laws to predict performance, and laser-target experiments have been used primarily to evaluate and improve the computer modeling.

However it is worth noting that one can never completely validate any complex hydrodynamic code; one can only test it within limited regimes.

The FAST codes at NRL contain detailed physics and numerics that has been especially optimized for direct-drive laser fusion. The code can follow the nonlinear evolution of the hydrodynamic instabilities, and it contains highly sophisticated atomic opacity physics. Gardner et al describes the code in detail in the reference. Here we wish to emphasize the uncertainties in the numerical analysis of target "b". (1) There are numerical resolution limitations at the foam/DT interface. NRL scientists are attempting to improve the resolution at the interface, but have not yet fully succeeded. (2) The 2D version of the implosion code does not have a "burn" package. The burn is only calculated from the 1D code. (3) The 2D code does not properly evaluate the 3D-laser incoherence, nor can it calculate the 3D evolution of the hydrodynamic instabilities during the implosion. Future research will address these limitations.

Direct-drive target designs must satisfy two types of laser-target physics constraints: (1) control of the various laser-plasma instabilities in the under dense laser-plasma coupling region, and (2) control of the various hydrodynamic instabilities that can arise in the higher density plasma. The status of these two effects is summarized below.

4.1.1.1.2.1 LASER-PLASMA INSTABILITIES. There are approximately half dozen distinct laser-plasma instabilities, (depending upon how one categorizes them). During the past 25 years the community has developed a very large base of experimental, theoretical, and computational research on these laser-plasma instabilities. It has been demonstrated that the combination of a short laser wavelength and incoherent laser light can reduce the scattered light and the supra-thermal electron generation by orders of magnitude, in rough agreement with theory. For direct-drive targets, the major remaining limitation in our knowledge is the effect of multiple laser beam overlap. There is an expectation, and some preliminary evidence, that the incoherence of multiple beam overlap will provide some additional stabilization.

Targets "b" and "c" are predicted to be above the effective threshold for some of the laser-plasma instabilities by a factor of only 2-3 in laser intensity. The current theories do not adequately include the effects of beam overlap, which should provide additional stabilization. There is thus some reason to believe that the high gain targets will not be destroyed by laser-plasma instabilities, provided that: (1) the laser light has a short wavelength such as the 1/4 micron of KrF lasers or the 1/3 micron of solid state lasers; (2) the laser intensity is limited to less than 10^{15} W/cm^2; (3) the light has optical smoothing with a bandwidth of a few-tenths terahertz; (4) the spherical target is illuminated by several beams incident from several angles.

4.1.1.1.2.2 RAYLEIGH-TAYLOR HYDRODYNAMIC INSTABILITY There is also now a very large theoretical and experimental data base on the hydrodynamic instabilities in laser fusion, beginning with the 1975 NRL proposal to use ablative stabilization, followed by the early 1980s NRL experimental use of optically smoothed laser beams to accelerate plastic foil targets in the early 1980's, followed by several advances in

experimental diagnostic techniques at LLNL. However until recently there were have been severe limitations in the optical quality of the laser beams in these experiments. The community was thus uncertain as to how smoothly one could accelerate a target using a good laser beam. With the 1995 completion of Nike and Omega Upgrade, the community had laser beams of sufficient bandwidth and uniformity. Experiments at both of these labs in 1996-1997 have demonstrated relatively good agreement between the experimentally measured mass nonuniformities and the predictions from the computer models. This added to the community's confidence that these codes could also be used to design high gain targets. There are still several limitations in the experiments, primarily the use of CH plastic targets, rather than the foam and DT targets designed for ignition and high gain.

4.1.1.2 TARGET DESIGN GUIDANCE FOR LASER AND TARGET DEVELOPMENTS. Based on the above, one can provide a set of target specifications for different target types. Below are the latest ones of interest. Since the targets must match the laser specification, they are included as well.

	Foam Ablator	**DT/Foam Ablator**
Inner/outer radii of DT fuel	~ 1800/2077 μm	~1800/2077 μm
Thickness of ablator	~ 870 μm	~ 170 μm
Ablator density & material	0.05 g/cc CH	0.05 g/cc CH 0.24 g/cc DT ?% Au
Inner DT surface finish	~ 5000 Å	~ 5000 Å
Outer ablator surface finish	~200 Å	?

Target Specifications, as of August, 1998

	Foam Ablator	**DT/Foam Ablator**
Number of beam directions	~ 60	~ 60
Laser wavelength	1/4 – 1/3 μm	1/4 – 1/3 μm
Peak laser intensity	~ 5×10^{14} W/cm^2	~ 5×10^{14} W/cm^2
Laser bandwidth, foot pulse	~ 2 THz	?
Laser bandwidth, main pulse	?	?
Laser nonuniformity, modes <50	< 1%	< 1%
Laser nonuniformity, modes 50-200	~ 0.2%	?
Power contrast (with zooming)	~ 120:1	~ 120:1
Zooming in focal spot size	~ 2×	~ 2×

Laser Specifications, as of August, 1998

4.1.1.3 PLANS FOR TARGET DESIGN DEVELOPMENT AND EVALUATION:

1. High Gain Target Design:
   - Improve 2D gridding at ablator/fuel interface of foam ablator target (DP funded)
   - Complete high gain 2D design of DT/foam ablator target (DP funded)

- Add burn physics to 2D implosion code (DP funded)
- Independently evaluate target designs with Lasnex codes (DP funded)
- 3D analysis of hydrodynamic instability growth in imploding targets with ISI imprinting (OFES funded, this proposal)

2. Laser-Plasma Instabilities:
   - Experimentally (on OMEGA) and theoretically evaluate effect upon two plasmon decay mode and Stimulated Brillouin scatter of overlap of incoherent laser beams (DP funded)
   - Evaluate on Nike, if necessary, the role of enhanced laser bandwidth on laser-plasma instability thresholds (DP funded)

3. Hydrodynamic Instabilities
   - Use Nike to accelerate foil targets with cryogenic DD and foams, to better simulate high gain target designs (DP funded)
   - Use OMEGA to implode cryogenic targets with significant thermonuclear burn, to study effects such as low-mode asymmetries (DP funded)

Notes: 1.DP proposal for targets should be included as an Appendix.
2.Is there any work on "Fast Ignitor" under this program?

4.1.2 TARGET FABRICATION AND HANDLING

4.1.2.1 STATUS Target designs for the laser fusion driver (LFD) require the development of new materials and fabrication techniques that are not part of the baseline ICF Program or on the critical path for ignition on the National Ignition Facility (NIF). Two of the three proposed target designs [1] (see Figure 1) for the power plant incorporate low density (40-50mg/cc), small cell size (< 200 nm), carbon/hydrogen foams of which only a few candidates are currently available [2,3]. None of these, however, have been fabricated into targets with suitable properties, geometries, and the low cost needed for power plant applications. Materials with the correct combination of composition (or opacity), density, surface smoothness, and ease of fabrication into pellets are not available with any current technology. Target fabrication may thus be the limiting constraint on the success of some of the more promising pellet designs for this program.

The three target designs for the laser pellets that have been proposed for a direct-drive fusion reactor are [1]:

(a) a DT ablator, shock preheat design;
(b) a foam ablator, shock preheat design; and,
(c) a DT + foam ablator, radiation preheat design.

(These are illustrated in figure 4.1-1, previous section.)

All three designs require the formation of a smooth, spherical deuterium-tritium (D-T) ice layer for a high gain inertial confinement fusion target. The designs also require

confinement of the fuel during and after the layering process. These pellet designs each incorporates some kind of barrier layer to contain the fuel. The barrier must allow DT gas to fill the target and after layering prevent the escape of the DT from the target by sublimation. In addition to the barrier layer, the foam ablator/shock preheat pellet and the DT+foam ablator radiation preheat pellet incorporate low density foams into their designs to provide ablative forces during the implosion which are needed to reach high convergence ratios. These foams must be cryogenically stable, easily formed to the precise dimensions, have a low density (ρ = 0.25 mg/cc) compared to DT ice, and be composed of only low Z elements, ideally just carbon and hydrogen. The foams must also be open celled for filling applications, have small pores (< 200 μm), and have an areal mass variation of less than 1% over a few microns. The two designs incorporating foam are the most promising of the three designs, producing the highest gains. The development of polymeric foams meeting the requirements for this program is essential to its success.

Polymeric foams are most often prepared by blowing, phase separation, emulsion polymerization, or sol-gel techniques. Each of these techniques produces foam materials with unique morphologies and associated limitations. The strength of the foam produced by any given technique decreases with decreasing density (increasing porosity). At the density required for fuel pellet design, very few materials have enough strength to be machined or handled without damage to the foam. The cell size of the foam is governed by the method of preparation. Of the techniques used to prepare foams, sol-gel chemistries alone have produced materials with suitable cell sizes and densities. Sol-gel produced foams have however proven very sensitive to exposure to solvents and to physical handling. Solvent substitution and supercritical extraction are required during the preparation of these foams in order to avoid the formation of zerogels (higher density foams). This extraction step places some limitations on target fabrication, since a barrier layer is involved. Carbonization of these and other foams has led to less sensitive materials with good physical properties, but with some densification. Newer techniques to produce foam materials including nanoscale templating [4] and hyper-crosslinking [5] have not been evaluated for these purposes, yet. These newer materials could meet the requirements of the LFD program.

4.1.2.2. Proposed Work Plan

This section outlines a relatively modest research effort to identify and investigate candidate foam materials and processes for the fabrication of high gain pellets (the fuel container for direct drive laser fusion) for a fusion energy power plant. The technical path proposed focuses first on the composition, pore size, and achievable surface finish of candidate foams. We would synthesize billets of the materials, characterize them, and evaluate their machinablity. This latter step might not be part of a fusion target fabrication process because of the cost limits, but we believe that the step provides two features that are worthwhile: first, machining the foams gives a reliable measure of the surface finish achievable with the material, and second, machining spherical foam parts provides a visible test of how well we are proceeding toward the specifications without having to develop mass production methods for each material. Later in the project, as we

down select from our list of candidate materials and processes, we begin development of mass production techniques for the most promising materials.

The DT ablator design requires a very thin normal density polymer layer to contain the fuel. The current likely materials for this application would include either the GDP shells produced at General Atomics or thin polyimide shells, which are currently under development at LLNL. The GDP shells are produced using microencapsulation technologies and a depolymerizable poly (α-methylstyrene) mandrel. The size, wall thickness, and surface smoothness of these shells falls within the range of materials currently used on Omega and those needed for the NIF. The development of these shells is continuing under funding for NIF and the technologies should be available for use by this program.

The foam ablator design features a thin vapor barrier separating the fuel from the foam (50-mg/cc C or CH foam). A very thin normal density polymer would be used for this barrier. GDP or polyimide would be used for fuel containment. The foam surrounding this barrier needs to be a low density CH foam with an outer surface smoothness of probably 200 nm, this sets limitations on the cell size of the foam. Assembly of such a design would require the foam ablator to be cast or formed around the vapor barrier or the vapor barrier to be formed inside the foam hemishell. This first route could involve machining foam hemishells, which could be glued together around a preformed vapor barrier. This route has already been demonstrated by LANL in its Double Shell Campaign on Nova[6], however, with a foam that did not meet the requirements for this program. The second route, to be pursued in FY01 and FY02, might involve an interfacial polymerization on the interior surface of the preformed foam shell. Possible polymeric foams for this of application would include phase-separated foams, resorcinol-formaldehyde (RF) foams, hyper-cross-linked foams, composite organic/inorganic foams and carbonized foams. The foams would have to be open-celled foams that are easy to machine and handle. Recent developments in the backfilling and machining of polystyrene foams have produced great improvements in surface finish target handling. This technology should aid in the selection and processing of new materials.

The DT + Foam Ablator design features a solid DT layer surrounded by a DT-filled open celled foam with an overcoat of a high-Z material. The development of foams and filling processes for the foam ablator design would be directly applicable to this target design. The possibility of using microencapsulation techniques to produce the foam shells would be explored as well. LLNL and Soane Technologies [7] laid some groundwork in producing shells from RF for similar applications on NIF. The size, wall thickness, density, and surface smoothness of these materials needs to tailored to our applications, however. A filling process would produce a smooth surface that could be coated very uniformly with a high Z material. Three routes to filling would be used: backfilling; the synthesis of composite organic, inorganic, and organic/inorganic materials; and, nanoscale templating.

In the initial, materials selection phase, the program will emphasize synthesis and characterization of product following machining and casting operations. Rapid screening of viable candidate materials for appropriate physical properties and ease of manufacture will focus the research. This development effort continues throughout the program but tapers off as the materials systems are down-selected and a number of suitable materials are found. The adaptation of these new materials to shell production *via* microencapsulation or other techniques would start only after finding materials that met shell requirements for density, opacity, and surface finish. The ideal foam shell material may be a compromise of physical properties and ease of production. We will provide several candidate foams whose performance can be evaluated on existing laser drivers.

4.2. Reactor Chamber

4.2.1. Status

As a result of the work on the Inertial Confinement Fusion Program, scientists are testing theories against experiment using sophisticated target designs. As larger and larger lasers drive these targets, the anticipated yield has risen to a level where the design of a chamber to hold such experiments has become a significant challenge. The NIF chamber is now being designed to hold targets with a yield of ~100 MJ and the X-1 chamber will be designed to hold 1,000 MJ yield events. On the other hand, the experimental program only requires one or two shots a day and the chamber does not have to be actively cooled to remove the thermal energy generated. Furthermore, the chambers for near term defense related ICF experiments must be designed for frequent access.

One benefit from research in the ICF area is that there is some synergism with the IFE activities. Once the performance of the targets is understood and gains near 100 are achievable, then chambers, which are appropriate to IFE, will need to be developed. These chambers will have to operate reliably over reasonable periods (on the order of a year) between scheduled maintenance intervals. Aside from developing rapid, ~5 per second, target delivery schemes and higher rep-rated lasers, the chamber's design for IFE electrical power plants must accommodate the removal of ~ 3,000 MW of thermal energy while protecting the integrity of the chamber wall. An additional function of the chamber will be to breed tritium and maintain the environment for laser beam propagation between implosions. Such severe concurrent requirements present additional challenges to IFE scientists and engineers beyond those faced in the ICF program.

It is now recognized that early identification of the critical issues facing IFE power plant chambers may allow modest experimental programs to be established to address these problem areas. Further, it is recognized that while many analysis tools exist from the ICF and other activities, there have been no systematic attempts to apply them for detailed IFE purposes, nor have experiments been performed to address these issues.

While a number of paper studies on laser fusion reactor chambers have been performed, the design data needed to completely specify such a chamber is not in hand,

but is rather evolving rather slowly over time. This means that from the point of view of 1998, studies done earlier will have some weak points. It is important to concentrate the strengths of the earlier studies, and not on what now appear to be weak points. The Sombrero (1992) study, for example, postulated a reaction chamber made up of carbon/carbon-composite sections much like the sections of a tangerine. This chamber must contain the reaction products and thermalize them to allow power generation. Recent data from Oak Ridge National Laboratory (ORNL) cast doubt on carbon as a good choice. Another look at other more appropriate materials such as aluminum alloys and silicon carbide should, of course, be done. But, the sectional chamber proposed in Sombrero remains an attractive idea.

Sombrero assumed that there would be an internal atmosphere of ~1/2 torr of xenon [or some other inert gas] to protect the wall from the x-ray flash. This atmosphere must be processed to remove the heat [part of the power cycle], as well as to recycle tritium. This idea needs to be critically evaluated, but the useful point was the idea of a low density gas for x-ray protection of first wall and optics, not necessarily only xenon.

Windows or windowless target chamber designs are also an issue and various studies have assumed all variations from no windows to fused silica windows. The major issue here is confinement of tritium to the interior of the reactor vessel. This may not be as simple as one might hope for hydrogen and its isotopes. For many years hydrogen is separated from natural gas [largely methane] by passing it through hot fused silica tubes through which the hydrogen diffuses; as an analogous process was used by Norsk Hydro for deuterium separation in the late 130's and 1940's, tritium leakage through hot fused silica might be a problem. A windowless chamber, as was assumed by Sombrero,requires that the rest of the reactor building operate in a near vacuum, which is a complication but not necessarily an insurmountable problem. The upshot of these issues would seem to be that:

- a segmented reactor vessel such as proposed in Sombrero appears very attractive, but the choice of material needs to be revisited;
- Windows on the reaction chamber probably need to be at or near room temperature rather than the neutron blanket temperature if they are to contain tritium;
- Windowless chambers appear to have problemmatic, but not insurmountable problems in terms of overall operational issues.

4.2.2 Most Critical Issues Now Facing IFE Reactor Chambers

Many critical chamber issues have evolved out of the several power plant designs conducted over the past twenty-five years. Four of the most critical issues are listed below:

1.) Protection of the first wall facing the target implosion from the intense flux of x-rays, ions, and particle debris released from the target (and the resultant shock wave) on a repetitive basis (=10^8 times/year).

2.) Maintaining an environment for the propagation of the intense laser beams to the target several times a second for continuous periods of at least a few months at a time.

3.) Protection of final focusing optical elements from the neutron fluence over the life of the plant.
4.) Protection of the structural components from the intense 14 Mev neutron fluence over the life of the chamber (=10^{23} n/cm^2)

Of course, there are other important issues related to corrosion, breeding, induced radioactivity, afterheat, etc., but the above four issues are the primary critical issues for IFE reactor chambers. It is important not to treat the above four items independently because they are usually quite interactive. One method to insure that a systems approach will be maintained is to update or develop, at a modest level, an IFE power plant study, which requires that all parameters be self-consistent. This effort is vital so that solutions can be tested in the "environment " of the rest of the reactor components. With such a study as a necessary backdrop, one can go on to consider the analyses and experiments that need to be conducted.

4.2.3 PROPOSED ACTIVITIES. In the time period from FY-99 to FY-02, there will not be any large scale ICF device operating and, therefore, all the experiments will have to be done outside such facilities. The following descriptions of experiments and/or analysis that can be performed are listed below as subsets of the four issues listed above.

4.2.3.1 FIRST WALL

4.2.3.1.1. DRY WALL The use of an internal low pressure (~ 1 torr) inert gas (He, Ne, Ar, Kr, Xe) to intercept the target x-rays and ions has been proposed for dry wall designs. The design parameters needed for such a solution can be better defined by modeling the gas with the proper opacity information and shock wave analysis. Once a solution appears reasonable on "paper", experiments with intense X ray sources can be conducted as a function of gas density and gas species. The amount of energy transmission through the gas can be measured as a function of time to determine the response of the solid or liquid components of the first wall. The absorption of the ion and particle debris in the gas can generate a shock wave which will impact the first wall surface. Codes exist to calculate the magnitude and duration of the shock wave. Experiments in a shock tube can measure the effects of such a shock wave on components inside the chamber as well as the chamber wall itself.

4.2.3.1.2. WET WALL Proposals have been made to cover the first wall with thin layers of liquid metal that are replenished through porous apertures. These structures can be made from powdered metals, woven fiber structures, or by spraying a mist of liquid metals on the first wall. Dynamic analysis of the interaction of x-rays and ion debris with the thin liquid metals can be made with codes currently in use. The analysis can then predict the thickness of the liquid metal needed to provide the direct and vapor shielding of the first wall. Experimental verification of the analyses needs to be conducted for various liquid metals (Li, Pb, Pb-Li, Flibe, etc.) Shock waves will be generated in the liquid due to ablation. They can be calculated, but their effect in the adherence of the thin liquid film needs to be studied. Experiments with existing shock tubes will address these questions.

4.2.3.2. LASER PROPAGATION

There is a close coupling between the first wall protection scheme and the propagation of intense beams of photons to the target in a predictable way. The essential factors are the scattering or breakdown of laser light in an environment that might contain atoms of inert gas or liquid metals. From the driver side, data needs to be developed on the breakdown intensity of laser beams in such an environment. However, once the critical levels are known, methods for achieving those levels (dynamically) must be devised and demonstrated. Codes now exist to calculate both the vaporization and condensation rate of atoms. Once the dynamic behavior is predicted, it should be compared to well-defined experiments. Computer codes can then be calibrated for future extrapolations to other conditions.

In addition, concepts for target injection and tracking will have to be assessed. These include methods of target injection into the chamber, protecting the target during acceleration, and tracking the target to accuracies such that the multiple beams can irradiate it. A related issue is that to have an operating concept that is not stressing and has no single point failure mechanism, there must be multiple target injectors. Whether the safely redundant number off injectors is three or more remains to be seem, but clearly, the number is not one. This also implies that each injection system operates at a reasonable fraction of the overall repetition rate, and has some "surge" capability. This point does not appear to have been addressed in previous studies.

Existing gas gun technology appears, on paper, to meet the acceleration and positioning requirements of the IFE applications. The target will require a sabot to protect it from damage during the acceleration process. Laser Doppler interferometer and/or other laser tracking techniques can be used to monitor the target trajectory and can provide pointing information in enough time to actively point the beams for each shot. The tracking and pointing requirements can perhaps be met with existing technologies. The most critical issues have to do with operating the injector with cryogenic targets.

Small-scale tests should be carried out to demonstrate the integration of the technologies required for target injection, tracking, and beam pointing. The test could be conducted in a phased approach by first developing the gas gun injector, adding tracking systems, and, finally demonstrating beam pointing of a target with low energy laser beams. Operation with cryogenic targets, but not necessarily DT, will be required.

The target will be protected from physical contact with the accelerator by a sabot. Once it is appropriate, the sabot flies off. As the target travels through the chamber, it is subjected to convective and radiative heat loads. Therefore, targets for direct drive concepts may have to remain in the sabot or incorporate additional thermal protection (e.g., a sacrificial layer of frozen gas on the outer surface of the capsule), especially when used in high temperature chambers, such as those envisioned in the sombrero study. More work is needed to demonstrate the integrity of the DT fuel layer and capsule during acceleration and transit through the chamber. Experiments are needed to develop appropriate sabot designs and heat load protection that can insulate the target

during acceleration. The integrity of cryogenic hydrogen layers should also be examined to determine acceleration limits for targets.

4.2.3.3. FINAL OPTIC

The development of final optics capable of functioning at an economically acceptable cost is crucial to the success of IFE. The threat comes from multiple areas: x-rays, ions and debris, and neutrons. In the case of laser beams, the ion and particle debris can be shielded against by fast acting valves, rotating shutters, or aerodynamic windows. The x-rays and neutrons travel much too fast to be removed by mechanical devices, although an inert gas absorber might be effective with x-rays. The neutrons present a special problem. They are too penetrating to be stopped by gas and they can, by multiple scattering, bounce. Therefore, other solution, such as grazing incidence mirrors, and neutron traps will be necessary. Sophisticated codes exist to calculate the neutron transport and energy deposition profiles. Isochoric heating of grazing incidence may disturb the surface finish needed for the next shot. Dynamic temperature profiles and surface deformations of such optics need to be calculated by codes yet to be constructed. Experiments to verify these analyses are also critical and need to be designed as soon as possible. Some candidate experiments are:

- Experiments on long-term damage of optical materials,: sapphire, quartz, CaF2, etc. , with short wave-length light and thermal neutrons; quantify the extent of thermal annealing possible and expected lifetime for top candidates;
- Experiments on the effect of neutron fluences on the surface quality of metal mirrors; quantify expected lifetime;
- Experiments to determine the best achievable surface quality of liquid metal mirrors, the reflection coefficient, and the time after a pulse required to re-establish a high quality surface.

In addition, IFE should investigate the advances made in UV optics on other programs, most notably the lithography activities that may not have the reactor environment, but clearly have long operating lifetime as a goal.

Another issue, which may mainly be an issue of inadequate discussion in the community, is the arrangement and choice of optics in the final leg of the laser beams. The problem with the final focusing optics for the laser is protection from the flux of x-rays and neutrons from the target. X-ray damage, if not ameliorated by a low pressure gas background could be a real concern for optics as the short absorption length for target x-rays in optical media and the short –ray pulse expected from a fusion pellet (~ 10's of nanoseconds) could lead to very high instantaneous heating of the surfaces with resultant mechanical failure. In microsecond pulsed DF laser irradiation of BK-7, an analogous case in the optical region of the spectrum, the out-of-band failure levels was very low compared to in-band failure levels (~ 1 joule/cm^2 compared to 100's of joules/cm^2).

Providing a long standoff distance can help reduce neutron dose rates and distances of up to 50 meters are consistent with the brightness of the laser beams and the

somewhat relaxed focal spot dimensions for a reactor. The type of optical arrangement used in current laser fusion experiments, which is illustrated below, will simply not work for the high ambient fluxes present in a working reactor. This means that it will be necessary to devise some other arrangement to protect the focus optics and allow them to have a reasonable lifetime. Standard practice in laser fusion experiments, including Nova, is clearly not good enough. This is shown below and consists of a thin glass debris shield, a focusing lens and a vacuum window on the chamber.

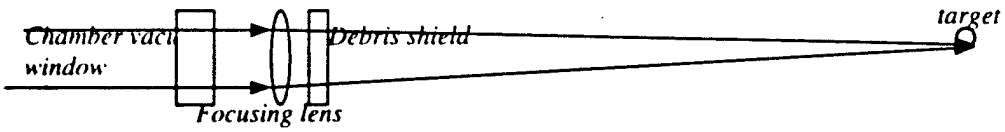

This sort of arrangement would suffer from radiation damage to all of the optical components. This leads one into a discussion of what are realistic alternatives. There are several possibilities, of varying desirability:

- A geometry with the final optical element being a near grazing incidence mirror [or mirrors] rather than a lens might mitigate the radiation problem in transparent optical materials and substitute the possibly less stressing problem of the durability of a mirror surface exposed to strong radiation fluxes.

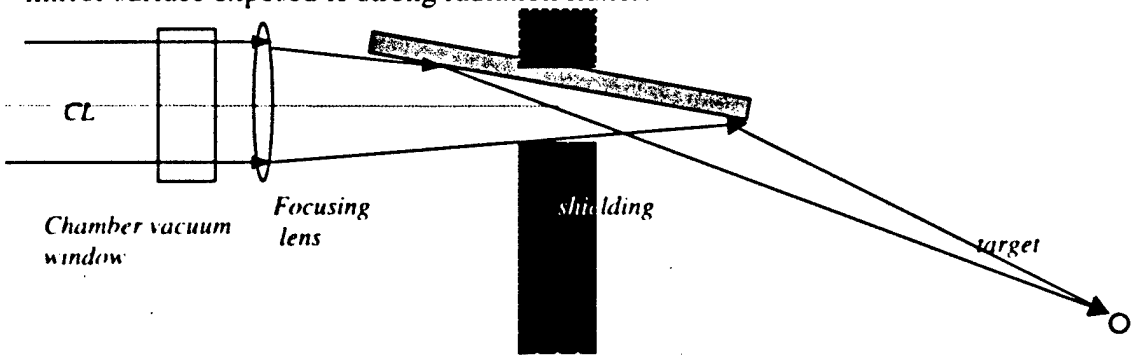

A difficulty with this approach is that the reflective surface must be closer to the target than any of the transparent elements in the previous example to avoid direct radiation paths to the transparent optics. The figure exaggerates this issue; with F/50 optics, the flux enhancement is not as severe as shown. While the window is beyond the neutron blanket, the radiative heating from the backside of the blanket may make it difficult to keep it at a low enough temperature to ensure no tritium leakage.

- A windowless approach could allow the mirror to move back to the position of the lens, but would either require large aperture upstream aerodynamic windows, which would be power hungry, or would require the reactor building to be operable at a very low pressure which would require even more special construction than other alternatives. (This latter approach was followed in the Sombrero study.) Additionally,

the tritium-handling problem now becomes an even bigger question mark, as now we must inhibit tritium transport in the gas phase as well as diffusion through solids.

- It appears that there is another choice which has not been proposed in earlier studies, but which may be worthy of further investigation. In this approach, a near grazing incidence mirror is used as the final optic in the chamber, but the beam is focused twice on its way into the chamber. After the entrance window, it is focused through a small aerodynamic window and then focused again by the final grazing incidence mirror inside the chamber. The inner and outer regions of the chamber can both be at low , ~1/2 torr to 1 torr pressures, with the outer region slightly higher than the core of the reactor. This should not be an expensive aerodynamic window to run and it should do a good job of confining the tritium in the core. Small leakage, or an accident, is not too serious here as the solid window is now easily thermally shielded from the blanket as a tritium barrier.

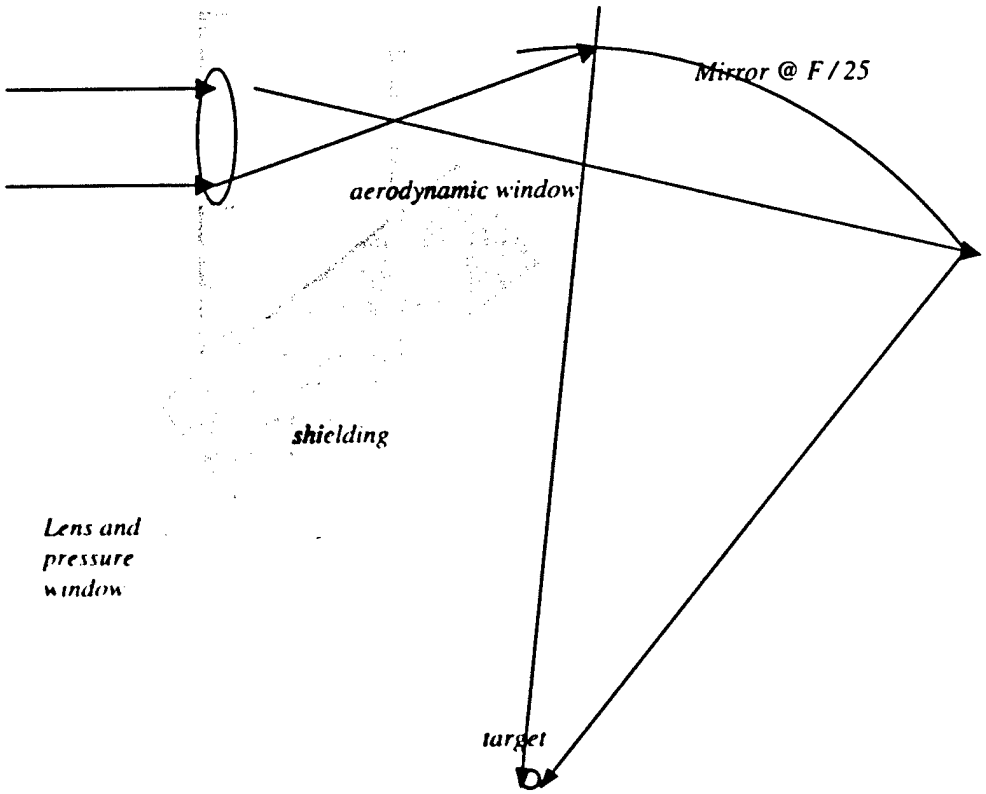

- In this latter arrangement, at the f/25 focusing condition, a grazing incidence geometry can be arranged. An advantage of this with shallow focusing is that a nominally round or square beam can have a footprint on the grazing incidence optic which has a much more elliptical or rectangular footprint than the beam at the lens; hence, even if the optic is nearer the beam focus, the laser intensity on the razing incidence element is adjustable.

- LLNL has identified a very attractive optics suite for the 1/3 micron region. Apparently the neutron induced color centering for some types of fused silica can be annealed out for this spectral region if the piece of fused silica is held at 300-500°C. They have suggested implementing this by using one or more optical wedges with a few degree apex angle to take the more sensitive optics out of the neutron line-of-flight. It is clearly worth looking for analogous effects in the ¼ micron region as the simplicity of the idea would be attractive.

4.2.3.4 Neutron Fluence

4.2.3.4.1 Liquid Metal Blanket Concepts The area, which has captured the most attention in IFE cavity design, is the use of thick streams of liquid metal to moderate and adsorb 14 MeV neutrons from the target. The idea is not new and has formed the basis of reactor designs for many years. The early work has detailed the first order effect of reducing radiation damage and activation. What is needed now is accurate isochoric heating calculations and a description of the disassembly dynamics of the free falling liquid metal streams or liquid metals in porous tubes. There is also significant room for improving the design of the flow patterns and the ability to re-establish the flow patterns on a 3-5 Hz frequency. Experiments to demonstrate successful flow patterns also need to be performed. Another issue is the extent to which isolated droplets and aerosols of the liquid metal will interfere with laser propagation to the target, and should be addressed either in this area, or in the activity under 4.2.2.2.

4.2.3.4.2 Dry Wall Concepts The use of flowing solid particles to capture the heat, breed the tritium, and/or protect the first wall has been used in several power plant designs and is part of Sombrero. This concept has much merit, but has issues. One of the critical issues yet to be adequately studied is the method of maintaining proper vacuum control as well as the design of solid to gas/steam/liquid heat exchangers. Compatibility with structural materials also needs to be addressed. Computational tools for the above analyses exist, for the most part. Experiments illustrating the ability to capture and transport heat to working fluids are required before the idea will gain acceptance from the more conservative heat transfer community. Granule breakup and wall erosion may also be issues over the useful life of the plant. The Sombrero study assumed, based on the best data then available that a carbon or carbon-composite first wall structure could survive for a usefully long time in a fusion power plant. More recent data makes it questionable whether a carbon structure could survive and maintain structural integrity for the required total dose; alternate materials such as some aluminum alloys and silicon carbide need to be evaluated for suitability in the role of first wall material in order to maintain the attractive features of a dry first wall for a laser fusion power reactor.

4.3 THE KRYPTON FLUORIDE LASER

4.3.1. BACKGROUND

The krypton fluoride (KrF) laser is one of a class of rare gas halide excimer lasers that were discovered in the early to mid-1970's. An excimer is an ion that has an unstable ground state, but may have one or more stable excited states. Various combinations of rare gas (He, Ne, Ar, Xe, Kr, Ra) atoms plus a halogen (Cl, F, Br) atom have been found to meet this prescription, i.e. a bound upper energy level, but an unbound (repulsive potential) ground state. It was realized very quickly that these excimers might make attractive lasers as they would be de facto four-level lasers since any ground state population resulting from lasing (or fluorescent) processes would rapidly be destroyed by collisions with other ions or atoms in the gas. Another feature of many excimer lasers is a relatively short wavelength, in the blue to ultraviolet region of the optical spectrum, where most other stable ion gas lasers are not particularly robust lasing candidates. They have attracted considerable attention from laser developers as good success has been obtained in pumping them with either electron beams or with gas discharges.

Krypton fluoride that lases at 0.248 microns drew considerable attention soon after its discovery because of its potential for a laser fusion driver. In addition to the short wavelength, it's high intrinsic efficiency and scalability to high energy were recognized as advantages for this application. Additionally, the rather broad lasing bandwidth (4THz), and the fact that it is a gas laser (versus solid-state) make it relatively simple to implement a variety of techniques for smoothing and averaging the laser intensity on a target to achieve highly uniform pellet illumination and manage thermal issues. The latest and, currently, the best realization of these advantages are embodied in the NRL Nike laser system. Nike and several other excimer facilities have demonstrated reliable operation of e-beam pumped excimer lasers at high energy. However, to carry these results forward and meet the challenging environment of a fusion power reactor will require substantial additional development to meet the average power capability, as well as to simultaneously extend reliability and overall efficiency. In particular, it is necessary to achieve the following extensions of KrF laser technology from what has been demonstrated so far on the ICF program:

- To be viable as a power reactor, the laser driver in a fusion power plant should have as high an efficiency as is possible consistent with cost constraints. While efficiencies as low as 5-7% appear adequate to support attractive costs of electricity, this high an overall efficiency has never been demonstrated on a reasonably large KrF laser. The Nike laser, which was not optimized for efficiency, operates at an efficiency far below this range. An objective of this program has to be to carry out a series of developments and experiments to demonstrate that such efficiencies are, in fact, reasonable for a reactor-scale KrF excimer laser.

- Excimer lasers on the scale necessary for a fusion reactor will be excited by high energy pulsed electron beam sources, at least if they are to be based on known technology. There are some practical issues of both efficiency and reliability for such sources. Typically, electron beam sources operate at relatively low overall efficiency, on the order of or less than 50%, and with rather poor reliability, a few hundreds to a few thousands of shots before failures occur. Both of these characteristics need to be radically improved for this technology to support high laser efficiency and reliability. As we will discuss later, there is some technology, which may point the way to simultaneous success in both areas.

- Another issue which has not received much attention in earlier studies is that one path to improving cost and maybe efficiency is to design the large excimer laser amplifiers for a power reactor to operate at much longer electrical pulse duration than amplifiers such as Nike (250 nsec). As a power reactor site will be large for safety and environmental reasons, ~ 0.5 to 1 square mile, the real estate will be in hand to delay optical beams for much longer periods than was possible on Nike. This could beneficially impact the electron beam power supply efficiency and cost as long pulses will require fewer magnetic compression stages than short pulses. From the point of view of a power plant designer, it may be desirable to operate the laser amplifiers with gain pulses as long as 10 microseconds, if this is possible. Compared to a system using 2 microsecond pulses, one needs only one-quarter of the number of laser amplifiers. There will be more optics in beam relays, but this is relatively inexpensive and reliable. An issue that the program will address is the extent to which excimer laser technology and pulsed power technology supports such a long pulse laser strategy and what are the impacts (thermal, materials, etc.) of such a strategy.

    - Some issues clearly scale without any real problem. Laser beam quality should not be affected by lengthening the pulse as the duration, in either case is very short compared to the acoustic transit time across the aperture, 1.2-3 milliseconds for a meter aperture [depending on gas mixture and temperature]. This means that there is no time for any non-uniformity in electron beam deposition to be reflected in changes in local gas density or index of refraction. Similarly longer pulse electrical operation of the pulsed power is always simpler and tends towards higher efficiency.

    - An area of concern is the electron gun itself. The Nike electron guns use a carbon felt cathode, which would not be suitable in any case for rep-rated operation because of rapid degradation and debris. A better long-lived cathode needs to be developed as part of this program in any case. Longer pulses will be more stressing than shorter pulses. The only cathodes which have been reported to operate at high currents, > 1 ampere/cm^2, for long times, ~ 100 microseconds, are the carbon needle cathodes developed by the Efremov Institute in Russia for large CO_2 lasers. Whether this type of

cathode, or some other choice, is in fact adequately reliable, is a critical path issue in obtaining usable KrF lasers for a fusion reactor scenario.

- Another area of concern involves the chemistry of strongly excited KrF laser mixtures. If all of the many reactions going on in the excitation of this laser are reversible and rapid, then one can arbitrarily lengthen the pulse. If, this is not completely the case, as the excitation proceeds, one may deplete some critical species and see gain fall-off as a result. This issue needs to be addressed for KrF as in going from sub-microsecond time scales to tens of microseconds, you enter a regime where ions may be used more than once in a single laser pulse. Some degree of non-ideal behavior can be tolerated and, in fact, could be compensated for by varying the input power of the e-beam source in time slightly. The key issue is to determine what is going on in typical discharges and to determine the amount of control, which can be exercised by simple expedients such as operation at higher or lower total pressures.

- Optics for the KrF laser amplifiers is another area where the technology used on Nike, fused silica windows, is not suitable for use at higher repetition rates, powers, etc. A non-degrading window technology or a repetition rated laser needs to be developed. The best candidate materials from the point of view of fluorine compatibility, sapphire, calcium fluoride and magnesium fluoride are not available now in single pieces large enough for a full-scale fusion amplifier. A fusion-bonding process may be the best way to proceed, in at least the near term, to show the required performance.

4.3.1.1. Commercial Krypton Fluoride Technology

Commercial application of KrF (and other excimer) lasers now and in the near future will be mainly in the semiconductor fabrication area for high-density (0.25 micron and smaller feature size) microcircuits. This is a major market in the U.S. and internationally and the semiconductor industry (Sematech) "road-map" for optical lithography through 2002 projects a commercial U.S. market for lithography equipment (lasers, masks, mask and wafer positioners, etc.) of ~$400M, of which 1/3 to ¼ will be laser sources. Industry has risen to this challenge and is making discharge pumped excimer laser sources specially designed to work as part of a semiconductor foundry operation. An example of the performance particulars of one of the more successful entrants in this field from Cymer, Inc. is shown below.

From this picture it is clear that this type of laser represents a substantial investment in

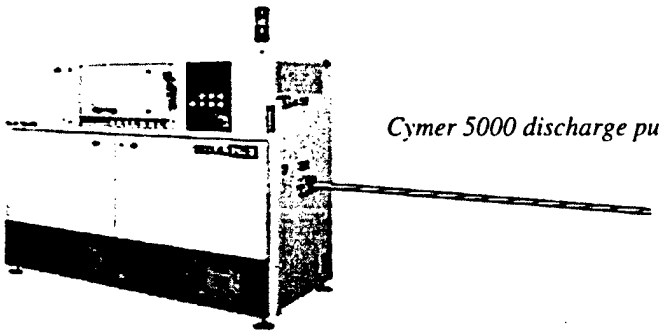

Cymer 5000 discharge pumped KrF laser

engineering this type of laser beyond the "breadboard" level to where it becomes an industrial component capable of sustained operation in a semiconductor "foundry". The table of specifications for the Cymer laser does not dispel this impression.

PERFORMANCE SPECIFICATIONS

	ELS-5000	EX-5000
Wavelength:	248 nm	248 nm
Repetition Rate:	1000 Hz	1000 Hz
Pulse Energy:	10 mJ	15 mJ
Average Output Power:	10 W	15 W
Spectral Bandwidth (FWHM)	< 0.8 pm	< 100 pm
Integrated Energy Stability: (50 pulse window)	< ± 0.8%	< ± 0.8%
Gas Life:	100 million pulses or 5 days	
Window Service Interval:	1 billion pulses	
Expected Pulse Power Module Life:	> 10 billion pulses	
Expected Chamber Life:	> 3 billion pulses	

Note: Specifications listed are typical.
Actual specifications vary depending on the exact configuration order.

Several points are noteworthy about this type of laser. Because this is a commercial laser, designed for use in a production application, some care has been taken to understand system availability. At 1,000Hz, the number of shots adds up very rapidly. Five days of continuous operation amounts to 432,000,000 shots; apparently, the typical user will operate the laser less than 23% of the time. In fact, for lithography, most of the time is consumed by inserting, extracting and aligning masks and wafers. Additionally, most users will measure exposures by counting the number of pulses to make a simple energy gauge. The minimum expected exposure is apparently typically 50 pulses. It also appears that even here with very low energies per pulse, the window lifetime of 50 days is the pacing item, in terms of one where one must physically interfere with the laser operation for an extended interval. (Gas changes could be automated where no real interruption worse than those for aligning masks or wafers would result.) The next

component expected to fail is the discharge chamber in the laser, at about 150 day intervals. The discharge power supply is expected to last about 500 days.

For photo-lithography, one major difference with the fusion case is apparent if one notes the very narrow line-width of the laser. A spectral bandwidth of 0.8 pm (the Cymer ELS-5000) corresponds to a bandwidth of ~100 kHz at 248 nm, the KrF wavelength. This is a very narrow line-width, essentially a single longitudinal mode laser. In contrast, for fusion one wants a very broad bandwidth laser. An advantage of KrF is that the gain line is so broad that a bandwidth of 4 THz is obtainable. The reason why narrow line-width is so important for lithography is to minimize color dispersion in the optical system for exposing the wafers. Calcium Fluoride transmissive optical components are preferred over fused silica because they have less color dispersion.

In short, while discharge pumped commercial excimer lasers may be an important commercial laser, the extent to which, and how, this community addresses lifetime, optics, efficiency and maintenance issues will be in terms of what is needed for optical lithography, not in terms of what is needed for fusion. Therefore, while there will be some synergism with commercial KrF developments, this may be more fortuitous than planned. However, it will be of some benefit where there is overlap since photolithography is a major laser market. That this should be so for KrF lasers is not any more surprising than the limited extent to which neodymium glass lasers for fusion impact commercial solid state lasers, which are mainly neodymium doped yttrium aluminum garnet (Nd: $Y_3Al_5O_{12}$, or Nd: YAG).

4.3.1.2. High Energy Research KrF Lasers

The most well developed excimer amplifier configurations for high energy per pulse lasers have used direct excitation and formation of the excimers using relativistic electron beams, rather than the discharge technology used in the low energy per pulse, high repetition rate commercial lasers. The highest energy per pulse ever achieved from a discharge laser was ~75 joules from the NRL KARL 20 cm aperture discharge laser test-bed in the early 1980's. Scaling a discharge to appreciably larger apertures suffers from two problems, both of a rather fundamental nature with negative practical consequences. (1) As a discharge is scaled up, the minimum inductance of the current loop formed by the discharge electrodes and the conductors increases proportionally to the loop area or aperture width squared. This head inductance will limit the current rise time of the discharge. As excimers are not storage lasers, the power dissipated during the rise and fall of the discharge current is essentially wasted. (2) As the aperture is increased, the voltage necessary for the discharge to have optimal coupling to the plasma increases as the aperture width. This again makes large discharges less than optimal. Both problems encourage one to "solve" them by raising the voltage even higher, which then makes surface flashover a third problem. As a practical matter, discharges are well suited to apertures of 10 cm or less, but become increasingly marginal at larger aperture sizes.

For fusion, where energies of as much as 50 kJ's are required per aperture, relativistic electron beam excitation, in short, is the only scalable approach. Excimer

amplifiers (typically KrF, but sometimes XeCl (305.1nm)) have been built which have produced single pulse energies of 5-10 kilojoules. Almost all of these lasers have been built for very low repetition rates, 1-2 shots/hour or less for laser proof-of-concept or laser fusion target experiments. There was some effort in the 1980's to produce high repetition rate, ~100 Hz, lasers for the Defense Department, but at considerably lower energy per pulse, typically less than 100 joules per pulse. The most successful of the DOE fusion related facilities is the Nike facility at the Naval Research Laboratory, which was designed for very uniform laser irradiation of planar targets at energies in the range of 2,000 to 5,000 joules. This facility uses 56 beams to sequentially extract up to 5,000 joules from a large (60-cmx60cmx100cm) KrF amplifier. Technological successes with Nike include the following:

a) Reliable target facility with more than 600 shots per year for target experiments:
b) Laser energies is in good agreement with Monte Carlo e-beam deposition and laser extraction codes;
c) Development of closed-loop computerized systems to handle large number of laser beams;
d) Achievement of the best target illumination uniformity of any large laser;
e) Achieved small enough intensity imprints in target momentum distribution for target implosions in laser fusion application.

4.3.1.2.1. NIKE LASER DESCRIPTION

Large electron-beam pumped KrF amplifiers must be pumped for greater than 100 nanoseconds to obtain high energy; but the excited state KrF laser transitions have lifetimes as short as the nanosecond regime. This means that the excited state KrF molecules do not actually store any energy, at least on time scales of the pump duration. Therefore, to efficiently operate, the KrF amplifier needs a probing pulse as long as its pump pulse. That really says that KrF, even on sub-microsecond time scales, is a laser that operates in an essentially continuous lasing mode. This presents a technical complication for IFE since the pulse lengths needed for fusion have much shorter duration than the pump duration. The best resolution of this mismatch, which has been demonstrated on Nike and the earlier Los Alamos Aurora lasers, is angular multiplexing where sequential beams are sent through the amplifier at slightly different angles. The amplifier sees itself as uniformly loaded as first one pulse, then successor pulses are amplified. At a sufficient distance from the amplifier, the beams separate as they propagate. Nike uses a computerized scheme where CCD cameras view the position of large groups of beams. This system allows the alignment of 56 beams in parallel. A photograph of the Nike propagation bay that contains the computer-controlled optics that accomplishes the angular multiplexing is shown in figure 4.1. Precise temperature control of the bay assures that once the beams are aligned that there is little angular drift.

Figure 4.2 shows a photograph of the Nike laser final amplifier that is typical for electron beam pumped systems. Two cathodes are located on either side of the gas cell containing the laser gas. Pulse charged coaxial lines using water as the dielectric provide the voltage to drive the cathode. Electrons are generated at the cathode surface, and are accelerated

through a thin foil from vacuum to gas. External electromagnets prevent pinch of the electron beam and help guide it through the laser gas.

Figure 4.1 The Nike propagation bay

This amplifier has demonstrated 5 kJ output distributed in 56 beams and produces 3-4 kJ routinely for target experiments. Approximately 75% of this laser energy is transported to target for experiments.

Figure 4.2 the Nike 60cm aperture amplifier

Direct drive laser fusion requires ultra-uniform illumination of the target to obtain symmetric implosions. The only schemes to achieve this uniform illumination have involved using controlled levels of coherence. Figure 4.3 shows the scheme used with Nike to obtain uniform illumination. Output from a multi-mode, broadband KrF oscillator diffusely illuminates an aperture. The aperture is imaged through the amplifier system to

target. If the image is not distorted one obtains uniform illumination of the target. This scheme requires broad laser bandwidth. Nike has achieved 3 THz bandwidths. The scheme also requires that there not be appreciable distortion due to the nonlinear index in the high power laser beam's path. The gaseous media and the low saturation fluences help ensure that this distortion is low. Figure 4.4 shows the excellent beam quality achieved after the final amplifier with Nike. In target experiments where we overlap 37 beams onto targets, we have demonstrated very low levels of laser imprint, equivalent to 100 Angstroms surface finish. Our target calculations pellets show that with some control of hydrodynamic instability, this illumination uniformity is adequate for high gain fusion.

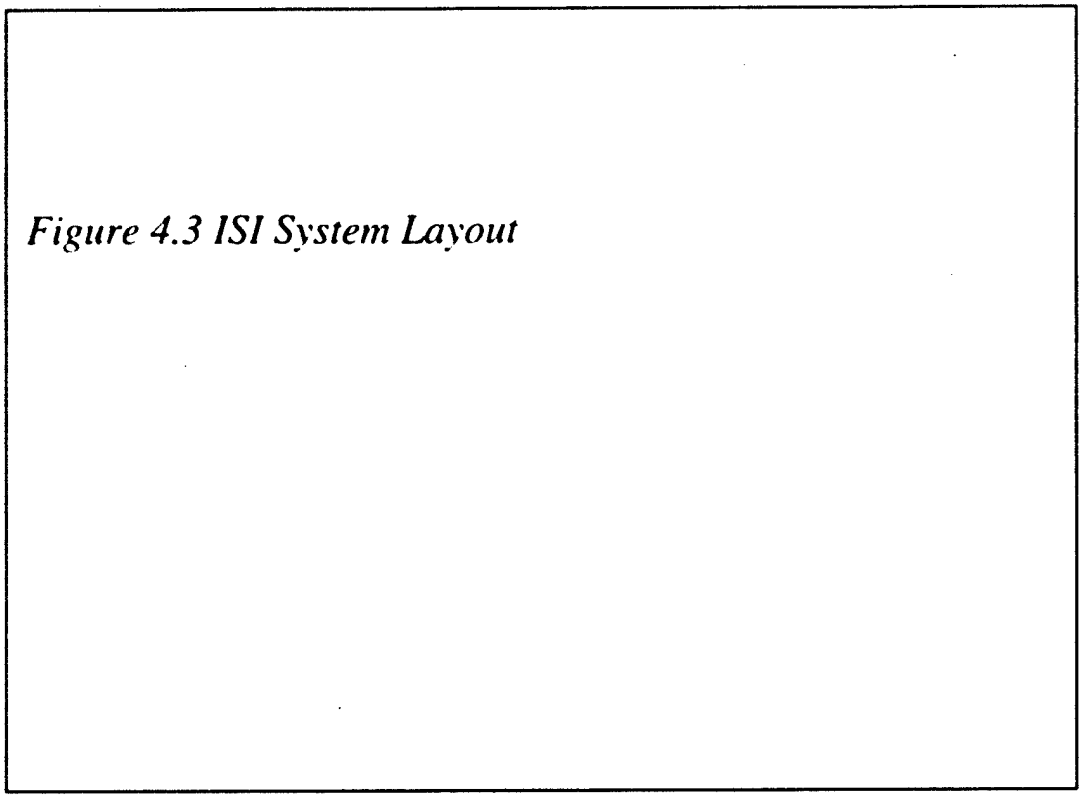

Figure 4.3 ISI System Layout

Figure 4.3 Induced spatial incoherence (ISI) layout , showing image-relayed amplifiers placed near the Fourier plane of the object. The instantaneous and time-averaged focal profiles are illustrated for the case of a flattop object envelope.

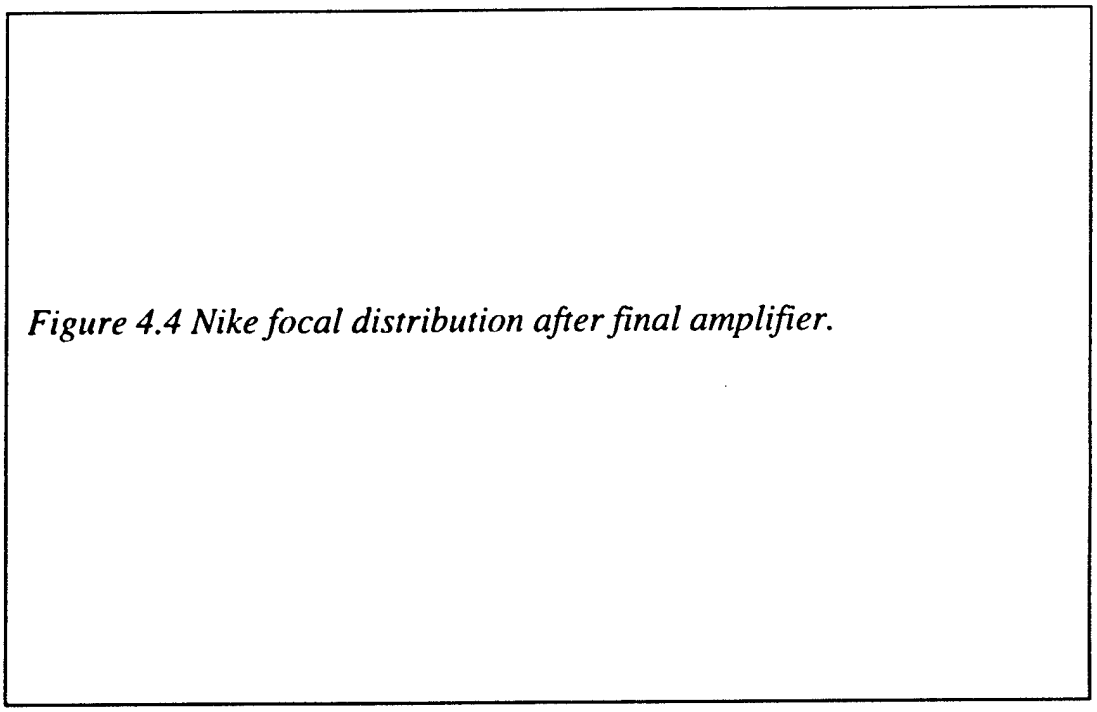

Figure 4.4 Nike focal distribution after final amplifier

4.3.2. AREAS NEEDING FURTHER DEVELOPMENT

A number of areas of KrF laser technology need considerable development before they would support the laser performance, efficiency and reliability required for a fusion reactor driver. These include:

- REACTOR ENERGY SYSTEMS. Reactors need about 3 MJ laser energies. The largest KrF lasers are 5-10 kJ. This appears to be a large jump. However, existing amplifiers are within a factor of ~10 of that thought to be required for a reactor. High energy can be achieved by using 50-100 modest energy amplifiers in parallel. The Sombrero reactor study used 50 kJ amplifiers. A 2 MJ design study by NRL used 34 kJ modules. The amplifiers in the NRL study used a segmented cathode scheme. Each segmented cathode was about the same size as used in the NRL Nike 60-cm final amplifier. We do not think that extrapolation of existing technology to the amplifier size, and energy required for fusion energy is a serious problem. As noted earlier in this section, an issue which was not addressed fully in the Sombrero study was the potential for effective use of longer, ~ 10 microsecond, gain pulses in the laser amplifiers. A Nike-sized amplifier operating for 10 microseconds rather than the 250 nanoseconds of Nike could produce 40 times the energy or 200,000 joules. While this may be an oversimplification, we think that the issues of achieving long run time, high repetition rate, high wallplug efficiency and reactor grade reliability are the more pressing issues to be resolved in the near term. Once the technology is fully developed, scaling to systems capable of

driving a fusion reactor appears possible. Care will be taken in this program to pursue only amplifier technologies that readily scale to reactor size.

- **COST/RISK TRADEOFF FOR LONGER PULSE LASER OPERATION.** Most of the single pulse electron beam excited excimer lasers which have been demonstrated to date have operated with electrical and laser gain pulse widths of 0.25 to 0.5 microseconds. This has resulted from a convenient coincidence of the pulsed power technology developed in the 1970's through 1980's for (largely) Defense Nuclear Agency generators and the amount of optical multiplexing which can be accommodated in typical laboratory spaces. This doesn't represent an intrinsic limitation on KrF laser technology, and, in fact, longer, i.e. microsecond pulse operation, appears to be a desirable mode of operation for the next generation of higher efficiency devices. A thrust of this program will be to determine how long a gain pulse is consistent with high efficiency, reliable laser amplifier operation, and how cost and risk trade off with pulse-width.

- **HIGH EFFICIENCY SYSTEMS.** Simulation codes and experiments have indicated that intrinsic efficiencies of 12-15% can be achieved with KrF. Intrinsic efficiency is defined as the ratio of the electron beam power deposited in thee gas to power out. With target gains of 100, one needs minimum laser efficiencies of about 6 % for an economically viable reactor. The net efficiency of the amplifier is reduced from the intrinsic efficiency by inefficiency in generating the electron beam, and transporting it to the laser gas; by losses in transporting the laser to the target; by the power to run the magnets in order to and cooling of the amplifiers. On balance, it appears that overall efficiencies of 6-8% can be achieved with KrF. But no system has been constructed with this mandate. The highest reported net efficiency with KrF is 3%. Developing amplifier technology that will allow such high efficiencies to be obtained on reactor scale devices will be a primary objective of this proposal.

- **HIGH REPETITION RATE. HIGH RELIABILITY SYSTEMS.** As mentioned earlier, the only readily available commercial systems are discharge pumped systems. While these are low energy systems, the gas processing technology and research into long lifetime optics is directly applicable to larger e-beam pumped systems. A few high repetition rate e-beam pumped systems have been constructed and operated by the DoD. The largest of these was the 10-cm aperture 10J, 100 Hz XeF (351 nm) EMRLD laser system developed for DARPA. Difficulties with utilities available at the White Sands Missile Range when the laser was being tested restricted operation to a few tests with 10 second bursts of 1,000 pulses or less. Nominally the laser was designed for true long-term continuous operation. A full demonstration of a laser amplifier module with representative repetition rate, true continuous operation and high reliability is critical for fusion application, and is a primary focus of this research effort.

- **OPTICAL MATERIALS AND COATINGS.** Currently available optical materials are not suitable for certain critical locations in a KrF reactor system. The windows in the laser amplifier must function in a stressful environment. We present in detail the status of amplifier window technology later in the proposal. The optics after the final amplifier will be exposed to high fluxes of laser light. The final focusing and beam handling optics will be exposed to radiation from the target chamber. Testing and developing suitable optics is critical for evaluating the feasibility of a KrF laser fusion reactor.

- **DESIGN TOOLS FOR LARGE SYSTEMS.** A number of laser design codes have been developed and used to predict KrF laser performance. Kinetics codes have been written where the researchers attempted to predict the output of e-beam pumped amplifiers based on simulations of the complex reactions in the laser gas that lead to the lasing transition. Potentially this route could allow accurate predictions of laser energy, intrinsic efficiency and laser pulse shapes. This work was primarily accomplished in the 1980's and there is virtually no current effort in code development. There is a need to resurrect and expand this work. In order to be useful in the design of KrF and to accurately predict the laser output parameters, the code needs to account for the complicated 3D geometry in angularly multiplexed amplifiers.

  So far, detailed calculations of electron transport into KrF amplifiers have not been accomplished. The design work in current systems has for the most part involved simple analytic estimates of electron transport from cathode to gas. Some work using a particle-in-cell (PIC) code in simplified geometry was accomplished by Los Alamos National Laboratory. However, this code predicted an e-beam instability that was not observed experimentally in the Nike 60-cm amplifier.

  We believe that with the availability of cheap large scale computing, it would be cost-effective to develop electron transport codes. This tool could aid greatly in the design of systems with efficient transport into the gas. This is particularly critical in making accurate predictions of performance for the larger amplifiers in a reactor system. It is worth noting in passing that much of the early computational work was done on computers much less powerful than current workstations.

4.3.3. PROPOSED LASER DEVELOPMENT TASKS.

The proposals in this section address the proposed approach to resolve the major issues with the maturity of the KrF laser technology for a fusion reactor driver.

The **first element** and center-piece of the KrF effort is the development of a 30-cm aperture 5 Hz amplifier module. This amplifier will utilize electron-beam pumping and its development will address most of the issues involved in scaling this technology to a reactor. The proposed amplifier is approximately the size and performance of the next to last amplifier in a reactor system.

The **second element** is the development of an advanced laser front end that will provide the pulse shaping and uniform laser focal profiles needed for a reactor system. This effort builds on the front-end development for the Nike laser, but will be oriented towards performance parameters required for a reactor. The advanced front end will have sufficient energy and repetition rate to drive the 30-cm amplifier. It will be combined with the 30-cm amplifier and the resulting system used to develop and demonstrate pulse shaping and focal profile control at high energy and repetition rates.

The **third element**, development of materials and coatings, is critical for both the proposed KrF development and extension of this development to reactors. The KrF amplifier environment is hostile to optics with high fluxes of x-rays, laser light and a hot laser gas mixture that contains fluorine. This effort will center on developing window materials and coatings that have longevity in this environment. Optical materials and coatings at other high-stress locations in the system will also be evaluated. This includes the high damage threshold mirrors for transporting beams to target and the final reactor-exposed optics. This KrF laser-optic development at 248 nm wavelength will benefit somewhat from and be coordinated with the synergistic development at 337 nm for diode pumped solid state lasers.

The **fourth element** in the KrF development will provide the engineering tools needed to design and evaluate reactor class KrF lasers. This will include two laser simulation codes. The first will be an advanced kinetics code that includes beam propagation through the laser system. This work will be based on a code now used to simulate NIKE. The second code will simulate electron beam propagation from cathode into the amplifier. This code will guide the development of high efficiency beam transport and deposition in the laser gas. The physics that underpins the development of the two codes will be tested with the Nike laser system as well as the newly developed 30-cm amplifier. These tools will allow much more rapid and accurate evaluation of design choices for reactor class KrF amplifiers and systems. The resulting analysis may point towards more efficient, lower cost operating regimes for KrF than present understanding of KrF technology allows. The tools will be applied to develop a cost/performance optimized conceptual design for the KrF component of a reactor system.

Together, these four elements will provide a comprehensive, rigorous basis for expanding KrF into the regime required for reactor operation. In the following sections we discuss the plans for each of these elements.

4.3.3.1 30-CM APERTURE REP-RATE KRF LASER AMPLIFIER

4.3.3.1.1. INTRODUCTION

Direct drive with a krypton-fluoride (KrF) laser is an attractive candidate for a inertial fusion energy (IFE) because of its potential for outstanding beam quality and its short wavelength. The recently completed Nike laser facility was built to study the

physics of direct drive ICF by ablatively accelerating planar targets. Nike is a multi-kilo-joule KrF laser with a very high beam uniformity ($\Delta I/I < 0.2\%$ for all overlapped beams), and the unique capability to accelerate relatively thick targets on a low adiabat under conditions scalable to direct drive ICF[1]. Experiments with Nike have demonstrated that KrF has achieved the beam smoothing required to reduce the effects of the laser non-uniformity to very low levels; the mass modulations "imprinted" by the laser are approximately 100 Angstroms [2]. Based on these experiments, our models show that an implosion driven by a laser with the established smoothness of KrF could likely achieve ignition, if not moderate gain. As shown elsewhere in this proposal, current research will help us identify the requirements necessary to achieve the high gain needed for inertial fusion energy. In addition to the favorable laser and target physics results, the Sombrero reactor study showed that a fusion power plant based on a KrF driver can be economically attractive [3]. However, to accurately assess the reactor potential of this approach, it is necessary to address several key engineering issues regarding this laser.

The Sombrero study was based on a 3.4 MJ KrF laser driver. We can get some idea of the layout of this 3.4 MJ laser by extrapolating our conceptual design for a 2 MJ KrF Ignition Facility[4]. The reactor could consist of an array of parallel beam lines, configured to illuminate the target with 60 laser beams. Each beam line is composed of a set of identical amplifiers, each having an output energy in the range of 30-100 kJ. These amplifiers are about 6-20 times larger than the 60-cm amplifier of the Nike laser[5]. But this is not as large a step over the Nike as it would first seem, as each of these amplifiers are composed of eight e-beam modules that are actually slightly smaller than the e-beam in the NIKE 60-cm amplifier.

An additional feature of the KrF amplifiers in a reactor driver, which is different from the Nike amplifiers is the pulse duration of the extracted pulses, the duration of the laser gain and the geographical extent of the angular multiplexing. Nike operates with a gain pulse which is ~ 250 nanoseconds in duration and produces 60 four nanosecond pulses. This design represents a reflection of the real estate available at NRL to house Nike, among other factors.

A reactor driver laser will have very different constraints. It must produce longer target irradiation pulses, 10-20 nsec in duration; additionally it must do this at maximum efficiency and minimum total plant cost. For a reactor, the amount of available real estate is considerable. Data presented during the MFE-ICF workshop on eisting conventional power plants documented site sizes of 385 to 2,500 acres for conventional, fossil fueled power plants and at least 750 acres for one 2.2 GW nuclear plant. Heavy ions designs presented were sited on 750 acre sites. It would be reasonable to expect that an ICF site would be on the order of 1-2 square miles in extent. With this much real estate available for other reasons, such as site security, personnel safety, etc., it is eminently reasonable to plan to extend angular multiplexing to a grander scale than Nike. Space for optical delay lines is not hazardous, except while the laser is on, and it need not be particularly high quality space. The main requirement is that it be at constant temperature to minimize optical gradients. Potentially, one could have delays as long as 2 x 5 microseconds and a

10 micro-second pulse-width on the gain of the large amplifiers. A single amplifier then might produce as many as 500 twenty-nanosecond target pulses.

There are two advantages in evaluating the extent to which this can be done during the proposed program. First, longer gain pulses, as we will see in the discussion on pulsed power can be produced with higher electrical efficiency because fewer stages of magnetic compression will be required. Secondly, fewer total amplifier modules will be needed at longer pulse duration, leading to both capital cost and operating cost savings.

This longer pulse mode of operation does not come totally free of development risk. The major risk area is in the cathode development area in that the new cathodes to be developed must be capable of operating for a long enough electron beam pulse to support the long pulse concept. As the current Nike carbon cloth cathode is marginal, even for single pulse operation, considerable improvement is necessary.

It is worth emphasizing that this concept of using the longest possible gain pulse is a powerful approach to optimizing the laser. Whatever result is obtained by evaluating the engineering constraints will represent a near optimum solution, both in regard to efficiency and economics.

4.3.3.1.2. TECHNICAL OBJECTIVES

The overall goal of this program is to develop and evaluate the technologies required to build a laser with the rep-rate, durability, efficiency, and beam quality required for Inertial Fusion Energy (IFE). We cannot address all these issues with a single system. To demonstrate the overall efficiency of a KrF laser driver would require a large system that would be directly scalable to a full-sized reactor beam line. Also, as noted above, a full demonstration might require a large site and facilities. Such an integrated demonstration system is too large a first step towards a rep-rate laser driver. This has led us to propose to evaluate the potential of KrF as a fusion reactor driver with two complementary programs at a more modest level of funding: one on a new 30-cm Rep-Rate Laser, the other on the existing Nike 60-cm amplifier.

The 30-cm Rep-Rate Laser will be used to develop the technologies necessary to build a suitable pulsed power driver for IFE (i.e. one that meets the IFE engineering requirements for durability, efficiency, and cost). By "pulsed power driver", we mean the entire system required to deposit the electron beam energy into the laser gas, from wall-plug to electron beam. The 30-cm Rep-Rate Laser will also be used to demonstrate that we can repetitively amplify a high quality laser beam. The size of the system was chosen to be small enough to be flexible, but large enough to be relevant for an IFE-sized amplifier

The program on the Nike 60-cm amplifier will be used to address those issues that cannot be resolved with the 30-cm Rep-Rate Laser, in particular: the intrinsic efficiency, ASE, and electron beam current flow. The 60-cm amplifier is large enough that the results obtained with it should be directly scalable to an IFE driver. Thus, the combined Rep-Rate/Nike programs should allow us to address most of the laser issues for IFE,

including the important issue of the achievable overall efficiency foe a KrF reactor driver laser.. The Rep-Rate program is discussed here, and the Nike experiments are discussed in a later section.

The scaling of KrF to longer pulses will be addressed to determine the upper limit to laser gain pulse width imposed by laser kinetics and/or practical engineering considerations for reliable, long-lived KrF laser operation.

4.3.3.1.3. REQUIREMENTS

The engineering requirements for KrF as a laser driver for Inertial Fusion Energy (IFE) as given by the Sombrero reactor study[3] were:

Overall System Efficiency:	5-7%
Rep-Rate	5 Hz
Durability (shots between major maintenance)	10^8 pulses
Cost of the Entire Driver	$180/Joule(on target)
Total Driver Energy	3.4 MJ

In addition, there are requirement on the laser beam uniformity that have been determined by our current research [2]:

Beam quality-high mode fluctuations	0.2%
Optical Bandwidth	2.0 THz
Beam quality-low mode distortions	1-2%

The Sombrero study did not explicitly address the pulse-width of the gain pulse for KrF laser amplifiers in the fusion driver. This study called for an overall laser efficiency of 6-7%. Table I gives our assessment of the efficiencies we need for the various components of an IFE driver in order to achieve this figure:

Table I: Required and Achieved Efficiencies for KrF laser driver for IFE

Component	*Required*	*Achieved*	*Needed*
Ancillaries	0.9	.90[a]	1.00x
Pulsed power-Prime to Electron Beam (100ns)	0.8	.63[b]	1.25x
Electron Beam into Gas	0.8	.50[c]	1.60x
Sub-Total(pulsed power driver efficiency)	0.58	0.27	
E-Beam into Laser	0.12	.12[d]	1.00x
Laser on Target	0.9	.75[e]	1.20x
Total	0.062	0.016	

Notes

(a) Ancillaries: based on existing technologies for gas cell cooler, hibachi cooler, command and control system, and vacuum pumps. Assumes heat in cooling water is dissipated in a cooling tower or subsurface circulation.

(b) RHEPP, Reference 6. The efficiency quoted for RHEPP is 50%, which has an 80% efficient, ten stage Linear Induction Voltage Adder to produce 2.5 MeV at the output. We only need 500eV, so the LIVA can be eliminated, and the efficiency of the entire system increases to 63% with only this change.

(c) NIKE 60-cm Amplifier, Reference 5.

(d) The NIKE 60-cm Amplifier has an intrinsic efficiency of 8%. But other experiments have reported efficiencies of 12% and higher [References 5,6]. This needs to be verified for larger (IFE size) systems.

(e) NIKE Laser, Reference 1.

4.3.3.1.4 DESCRIPTION OF THE 30-CM REP-RATE FACILITY

A generic drawing of the 30-cm Rep-Rate Facility is shown in Figure 1. The main amplifier has an optical aperture of 30 cm x 30 cm, and the system will operate at 5 Hz. The laser gas will be pumped with two opposing 500 keV, 112 kA electron beams, each one with a cross-sectional area of 100 cm x 30 cm. The amplifier will be driven by one or more commercial discharge pumped excimer lasers, although we may incorporate a more advanced front end in the later stages of the program.

The laser architecture will use similar angular multiplexing to that used in Nike, except that there will be fewer beams, to probe the saturated laser gain. We will also include the type of alignment system used in Nike [1]. Table II gives the major parameters for initial 30-cm Rep-Rate Laser operation, which will be focused mainly on developing and demonstrating candidate long-lived e-beam cathodes, cooled foil structures, and optical beam conditioning to ensure that the gain medium returns to a high quality before the next pulse. These are the three areas where Nike provides either no useful point of departure or, in the case of the carbon cloth cathodes, one known to be inadequate for the next phase. For comparison, this laser is physically about twice the size of the 20cm Amplifier in the Nike facility [9].

The truly demanding issues involving this laser are not shown in the diagram, but, in addition to the development of cooled foils, reliable cathode emitters, and beam conditioning involve the scaling of the pulse duration into the microsecond domain. Nike is a 250 nanosecond machine; for the rep-rated amplifier to be on the development path to a fusion reactor, it should demonstrate microsecond, or longer, operation, as this is where the laser fusion reactor needs to operate. The leap from 250 nanoseconds to 10 microseconds is too great a leap to take in one step. Therefore, our program plan is based on validating technology for the microsecond time scale combined with experiments to determine how far into the multi-microsecond time scale it is possible to scale reliable, long lived operation.

As noted earlier, the database for large, e-beam pumped KrF lasers is no exhaustive, by any means. In order to explore the engineering issues in scaling to long pulses in a rational fashion, it is desirable that all minor "steps" be by factors of two to three and be characterized by well-documented complete experiments. In this fashion, we will be able to quantify exactly where projected improvements will occur and why they will occur. Accordingly, the demonstration objectives for the 30-cm amplifier are as listed in Table II, both for the initial phase and the second phase:

Table II: Parameters of initial phase 30-cm Rep-Rate Laser

Laser Input	2-10 J
Laser Output (minimum)	400 J
Gain	40-200
Pulse width (total)	100 nanosecond
Main amplifier optical aperture	330 cm x 30 cm
Working flux	4.4x106 W/cm2
Window loading	0.44 J/cm2
Main amplifier E-beam Loading	500 kV
Main amplifier current	2 x 111 kA = 222 kA
main pulse length	100 nsec
e-beam energy	2 x 5.55 kJ = 11.1 kJ
diode impedance	4.5 Ω each diode
Main amplifier cathode area (per side)	100 cm x 30 cm
Main amplifier cathode current density	37 A/cm2
Hibachi transmission efficiency (goal)	80%
Deposited energy	8.88 kJ
Deposited pump rate	1.0 MW/cm3

The initial parameters are representative of what is desirable for a test bead for foils and cooled cathodes, i.e. approximately "Nike-like", but operated at a 5 Hz repetition rate. The initial pulsed power drivers will be assembled of available moderate cost and efficiency components in order to test new cathodes and cooled foil structures as rapidly as possible. As detailed below, the pulsed power will evolve to high efficiency microsecond duration modules over the first eighteen months of the program. The actual choice of final pulse duration will not occur until we determine what can be supported by experimental results. Notionally, for a one-microsecond choice the final performance numbers might look like Table III:

Table III: Microsecond duration 30-cm Rep-rated laser parameters

Laser Input*	2-10 J
Laser Output (minimum)*	400 J
Gain	40-200
Pulse width (total)	1,000 nsec
Main amplifier optical aperture	330 cm x 30 cm
Working flux	4.4x106 W/cm2
Window loading	0.44 J/cm2
Main amplifier E-beam Loading	500 kV
Main amplifier current	2 x 111 kA = 222 kA
main pulse length	100 nsec
e-beam energy	2 x 55.5 kJ = 111 kJ
diode impedance	4.5 Ω each diode
Main amplifier cathode area (per side)	100 cm x 30 cm
Main amplifier cathode current density	37 A/cm2
Hibachi transmission efficiency (goal)	80%
Deposited energy	88.8 kJ
Deposited pump rate	1.0 MW/cm3

* The assumption is that a 100 nsec long multiplexed pulse stack will be used with suitable delays to sample the full microsecond gain duration. Running as an oscillator, the amplifier would be expected to produce as much as 4,000 joules of energy in a microsecond.

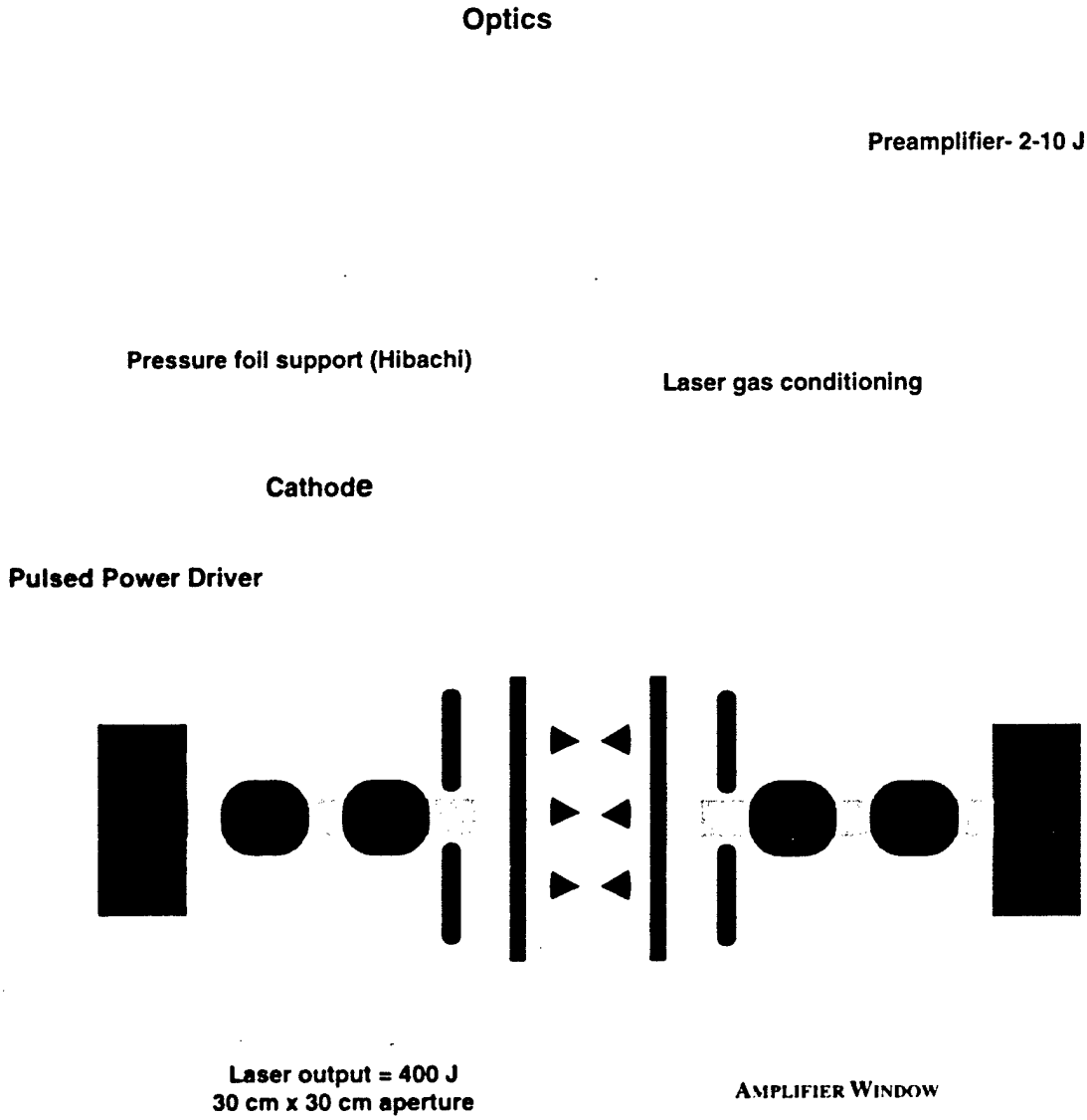

Figure 4-1: Layout of the 30-cm Rep-rate Laser and the key components that require development for IFE

4.3.3.1.5 COMPONENTS OF THE 30-CM REP-RATE LASER

Figure 4-1 shows the key components that require development for IFE: The pulsed power driver, the electron beam source (cathode), the pressure foil support structure (or hibachi). The laser gas conditioning system, and the amplifier windows and optics. In the next five sections we discuss the technologies we plan to develop for each of these components. Many of them have been developed elsewhere, but not necessarily

in a parameter range appropriate for IFE, nor have they been integrated into a single facility.

4.3.3.1.5.1. PULSED POWER

A suitable pulsed power driver for IFE must satisfy three difficult requirements simultaneously: (1) Lifetime of greater than or equal to twenty (20) years at 5 Hz repetition rate (3×10^9 pulses), (2) Efficiency of greater than or equal to eighty percent (80%), and a cost of less than or equal to $4.75 per joule of energy. (The cost figure was estimated from the Sombrero study. This study allocated 30% of the cost of the laser driver, or $55.00/ (laser joule) of $180.00/(laser joule) total, to the pulsed power. As the overall efficiency from electron beam to laser energy is 8.9% (from Table I), this equates to $4.75 per electron beam joule.)

We feel that the most promising existing technology is an approach that uses non-linear magnetic switches [10]. In this approach, a relatively low voltage "source" containing an active switch is used to pulse charge a capacitor. The capacitor has a saturable inductor at the output, with the core of the inductor chosen so that it blocks the current until the capacitor charges to peak voltage. At that point the core saturates, its permeability (and hence inductance) rapidly drops, and the capacitor discharges on a time that is much faster than the charging time. Typically this circuit can achieve about a factor of ten in pulse compression. Adding additional stages compresses the pulse further. Including a step-up transformer between stages and perhaps a linear induction voltage adder at the output obtains the required voltage, while using a pulse forming line as the last capacitor attains the required pulse shapes. The major advantage of this technology is that it uses all solid state compression and thus should have an extremely long lifetime (> 10^9 shots).

Sandia National Laboratory has built a large electron beam generator based on this concept [5]. Called RHEPP, for Repetitive High Energy Pulsed Power, this facility has parameters that are within a factor of 2 to 5 of what is required for a KrF facility. The beam voltage is 2.2 MV, the current is 25 kA, the pulse width is 60 nsec, and the cathode dimensions are 10 cm x 100 cm. RHEPP runs at 120 Hz, which is significantly faster than we require. The durability is at least 10^6 shots, with 10^9 pulses reasonably expected. The overall system efficiency is reported to be 50%. But this includes an 80% efficient 2.5 MV Inductive Voltage Adder that would not be needed for our application. So the efficiency of RHEPP, if it were to be duplicated today, would be around 63%. Also, as discussed below, the number of stages of compression could be reduced, which would increase the efficiency even further. In fact, our 80% goal may well be achievable with this technology. The concept is so successful that the RHEPP technology has been replicated in industry for materials processing.

A different variation on this approach is to use the recently developed Semiconductor Opening switch (SOS) technology [11]. The SOS can interrupt current densities of up to 60 kA/cm^2 on a timescale of a nanosecond. Thus it can be used to rapidly interrupt large currents flowing through an inductor, in order to generate large

inductive (V = Ldi/dt) voltages across a load. An SOS-based generator uses the same initial pulse compression stages as RHEEP, but achieves the high voltage and final pulse shaping with a single stage comprised of an array of silicon switches, rather than a transformer, pulse forming line and a linear voltage adder. Thus, the system is much simpler. The SOS technology has been the basis for several electron beam generators. The largest of these, called "Siberia" is capable of driving 8 kA at 800 kV for 60 nsec through an electron-beam diode at a rep-rate of 150 Hz [12]. These are comparable to our requirements. The lifetime of these systems is reported to be greater than 10^8 shots. The efficiency is in the range of 50% [13], so some improvement is necessary for the IFE applications. But it is reasonable to expect that we would achieve some significant improvements as the technology is relatively new and was not developed with efficiency in mind. Also, as in RHEPP technology, there are significant gains to be made by reducing the number of magnetic compression stages.

The present cost of both of these technologies exceeds the $4.75/ joule criteria suggested by the Sombrero study. The cost of the magnetic switch approach is dominated by the high price of the Metglas that is used in the saturable inductors. Using the most economical compression stage gain, which is around 3.1, the energy that a Metglas core can switch on each pulse is about 40J /kg. At the present small-quantity price of $ 100/kg, the cost of Metglas for every switch in a magnetic switch compressor based on RHEPP would be more than half the pulsed power budget. The cost to build an SOS-based device would be less because it has fewer saturable inductors, but it would still be too high. However, it has been estimated that the cost of Metglas could drop as low as $12/kg for large volume quantities [14]. If Metglas is being adopted by the utility industry, then it is possible that the cost will drop even further in the future.

It is clear from this discussion that a reduction in the number of stages of pulse compression in both approaches is desirable for both efficiency and cost. The most straightforward way to do this electrically is to incorporate a switch with a faster energy transfer time in the first compression stage (the source). The faster the transfer time, the fewer subsequent stages are needed.

A switch with an energy transfer time of about 10 microseconds could reduce the number of magnetic compression stages to a number between none and three, depending on final amplifier electrical pulse width. Even with a three-stage switch we could meet the IFE efficiency and cost requirements. It should be noted again here that there is also an optics and real estate trade-off. If a larger footprint and more complex optical multiplexing scheme is used, then the pulse power requirement on the amplifier may be eased in favor of a longer pulse, i.e. less compression required.

At this point in time all the data are lacking to quantify this trade exactly, other than to note that there will definitely be a trade-off in which by a capital cost trade off of less Metglas (fewer compression stages) against more optics and laser building volume (longer gain pulses on the amplifier), one can raise the plant efficiency. An objective of this program is to develop the detailed data needed to quantify this argument.

Ignoring the optics trade for the moment, there are three candidates for a fast-opening switch. The most promising from a durability standpoint, albeit the least developed, is to use solid-state switches. A number of manufacturers are testing solid state switches for pulsed power, and their published results indicate that in a few years solid state switches may have advanced sufficiently [15] to realize a three stage pulsed power driver. A second approach is to use thyratrons. These already have a rise time that is fast enough to allow us to go to a three-stage system, but their lifetime is limited to about a year. This might be acceptable, if sufficient redundancy is built into the design. The third approach is to use spark gaps. The switch lifetime can be extended by blowing high pressure gas through the gaps, as is used in the "Vortex" design [16]. Moreover, they have large current carrying capabilities, and they might allow us to eliminate another stage of magnetic compression relative to solid state switches.

If the magnetic switch based systems prove to be unworkable, then there are other pulsed power avenues to pursue. The most attractive of these is to use a step-up transformer to pulse charge a conventional water pulse forming line. Another approach would be to use a Dc supply to charge an oil/paper dielectric cable [17]. In both of these cases, the efficiency would be higher than with magnetic switches, and the cost would be less, but we would have to use high voltage spark gaps to discharge the pulse lines, and this could limit the system lifetime.

4.3.3.1.5.2. Electron Beam Source

We would prefer to use a simple field emission cathode as used in the Nike amplifiers [4], except that this exact solution would clearly not work for a reactor. In Nike the emitter material is velvet cloth and the lifetime is only a few hundred shots. In RHEPP, however, the cold cathode emitter was made of a much tougher metal-dielectric grid. The lifetime of this device was reported to be at least 10^8 shots [18]. The parameters: (area ~ 10 x100 cm^2; current density ~ 25 A/cm^2) are within a factor of 1.5x of what we require for the 30-cm Rep-Rate Laser.

We should note that we will also require a magnetic field to guide the electron beam, whereas RHEPP does not, and that the magnetic field may prevent the metal-dielectric cathode from emitting uniformly. While this may not necessarily compromise the system performance, it would probably shorten the lifetime of the foil, which serves as the vacuum barrier for the electron gun.

If uniformity is the only issue, UV illumination of the photo-cathode could solve this problem. Such devices are reported to be very durable and are used for the UV-pre-ionized discharges on the lithography lasers. The drawback is the added complexity.

There are other types of possibly suitable non-metallic field emission cathodes, which have been reported, such as the carbon needle arrays used for 80 microsecond pulses at greater than 1 A/cm^2 in large aperture, long pulse Russian High Energy CO_2 Lasers. In short, there appears to be reasonable hope that a workable technology may be available, or can be developed for a reliable, low cost, and long lived electron gun

cathode. Figure 4-2 is a schematic representation of this cathode. Thin, 200 micron diameter rods, about two centimeters in length and with a 20 micron radius "tip" are glued into a carbon block on 5mm centers. In theory, at least, when an arc attempts to form from a particular emitter, the increased resistive heating blows off the tip, causing that emitter to cease emitting.

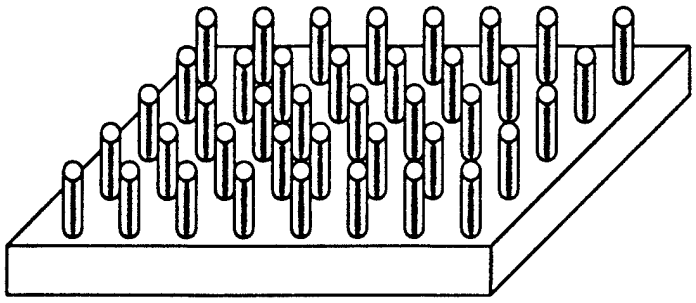

Figure 4-2 Russian Carbon Needle Cathode Structure showing 200micron diameter carbon needles on 5mm centers. Test data on devices up to 50cm x100cm (20,000 emitters) has been presented.

4.3.3.1.5.3 Pressure Foil support (The "Hibachi")

The electron beam traverses the cathode-anode gap, passes through an anode foil, through a pressure foil support structure, and through a pressure foil before going into the laser cell. The pressure foil must isolate the gas in the laser cell (typically 1.2 atmosphere pressure) from the hard vacuum of the diode (~ 5 x 10^{-5} torr). The pressure foil support structure is commonly referred to as the "hibachi". There are two issues with the hibachi/pressure foil: lifetime and electron beam transmission. Long foil lifetimes were achieved on the EMRLD laser at AVCO [19] by blowing high-pressure helium gas between the anode and pressure foils. EMRLD had a rep-rate of 125 Hz, and ran in bursts of 10 seconds. The foils did not degrade, even after 10^5 shots.

Efficiency is another matter. To achieve our requirements, the hibachi should transmit close to 80% of the electron beam energy, or about 1.6x what was achieved on the NIKE 60-cm amplifier [4]. Achieving this may be possible if we use the new type of hibachi structure that was developed and partially tested by Los Alamos National Laboratory (LANL) [20]. This uses thin rods under tension rather than the conventional deep ribs as the foil support. Preliminary experiments showed the transmission efficiency approached 90%. We plan to combine these two technologies for the 30-cm Rep-Rate Laser. Both pressure and anode foils will be made of Titanium alloy Ti 3-2.5 (3% Al plus 2.5% V) which has good high cycle fatigue strength and has excellent ductility at high temperatures (300°C). Thin tubes (instead of Los Alamos' rods) will support these foils, so the supports can be water-cooled. The foils themselves will be cooled by turbulent helium, as in the EMRLD device. We calculate that the foils will heat to about 150oC, which is well below the fatigue temperature of the titanium alloy. The total heat load to

the foils will be about 6 kW and this heat can be removed with a helium flow of 275 cfm, which corresponds to a flow velocity of about 40 m/sec.

4.3.3.1.5.4. LASER GAS CONDITIONING

On each shot the electron beam heats the laser gas. Not only must the gas be cooled down for the next shot; it also must be returned to a quiescent state to assure that the next KrF laser beam will be very uniform. It is particularly important to eliminate the short scale-length, ordered temperature variations perpendicular to the aperture. The EMRLD laser program addressed this cooling/quieting problem. High capacity blowers circulated the gas in the laser cell through a heat exchanger and a series of mixing plates and diffusers. This enabled the EMRLD laser to faithfully amplify a beam that was only 1.3 times the diffraction limit [19]. However, this impressive result was obtained from the raw data only by removing a large pulse-to-pulse "jitter" or variation in laser beam pointing which was considerably larger than the beam spread. In separate experiments AVCO established that a tip-tilt corrector could be used to remove all or at least most of this aberration. At the 100 Hz repetition rate of EMRLD, the most probable source of this pointing "jitter" may have been un-damped acoustic energy, or other sources. (EMRLD was cooling water supply-limited by the facilities at White Sands to ~100 Hz for one second, or 50 Hz for 2 seconds.) The Sombrero study capitalized on this and attempted to recover some of this waste heat in the reactor steam cycle. By operating at temperatures up to 300°C, the heat can be converted with relatively high efficiency (up to 75% of the Carnot efficiency) into electricity. In the case of the 30-cm Rep-Rate Laser, we will not convert the waste heat, but we will operate at higher temperatures to look at some engineering aspects of the system. The gas is heated to about 180°C after each shot. We calculate that with a gas flow of about 10 m/sec (flow of 4,500 cfm) we can effectively cool the gas through a water-filled heat exchanger to 50°C between shots. The heat will be removed from the water using a passive cooling tower.

4.3.3.1.5.5. AMPLIFIER WINDOWS AND LASER OPTICS

The amplifier windows operate in a rather hostile environment of fluorine, intense UV light, x-rays and energetic electrons. The Nike 60-cm amplifier has used coated or uncoated quartz windows and these tend to last only a few hundred shots. We do not know as yet what exact mechanisms are causing this degradation in the Nike windows; this program will allow us resources to pursue this issue further. A second approach will also be followed to find a superior window material. Calcium fluoride windows have been employed with considerable success in the small KrF discharge lasers used for semiconductor processing [21]. However, high quality CaF_2 windows are presently available only in sizes up to 30 cm x 30 cm, and not in the larger sizes (~100 cm x 100 cm) required for an IFE driver.

Sapphire is currently being grown commercially in sizes large enough to allow fabrication of single piece rectangular Al_2O_3 windows up to 30 cm x15 cm in size, and oriented for low birefringence. Potentially, the required full-size laser windows could be fabricated by a fusion-bonding process similar to what was done by TRW with 35 cm

long pieces of Nd: YAG on the DARPA DAPKL (Diode-Array Pumped Kilowatt Laser) Program. Successful fusion bonded elements demonstrate the same mechanical strength as single element pieces of the same material. A small company in Pleasanton, CA, Onyx Optics, Inc. owns the patents developed by Hoya, as well as their own subsequent patents and has produced laser rods and other fusion bonded components for LLNL, NRL, and a number of companies.

On this program we plan a two-phased approach: The major portion of the work will be carried out with separate off-line experiments and with experiments on the Nike laser. This program is described later in this proposal. When a successful window has been developed, it will be tested for long life durability on the 30-cm Rep-Rate Laser. In order to not delay the Rep-Rate program, we will first start with Calcium Fluoride windows as this will allow more time to develop other concepts and will leverage off the experience of the semiconductor community.

A fusion driver would also require the development of other optics (turning mirrors, final-focusing elements) with higher damage threshold than are currently available. The program to develop these is also described later in this proposal. The development of low-cost fabrication techniques for such relatively simple optics is not explicitly part of this program, but the National Ignition Facility (NIF) Program at LLNL is addressing similar damage and cost issues in a major way for the many pieces of flat, polished optics used in NIF.

4.3.3.1.6. PROGRAM PLAN

The development of a high efficiency advanced pulse power driver will take the longest time, about three years. Thus, in order to get started on the other components, our program plan is comprised of multiple parallel paths. In one path we develop the cathode, hibachi, and gas recirculator on a simple rep-pulsed power system. In a second path, we extend the pulse duration capability of these systems, in the third path, we will develop the prototype advanced pulsed power system. All the technologies are then combined in a single integrated demonstration. The elements of the two plans are:

A) Cathode, hibachi, gas recirculator development program plan

1. **Construct simple pulsed power system (12 months):** We will build a pulsed power system based on standard, well-established technology: a step-up transformer, a water dielectric pulse forming line, and repetitive spark gaps. We propose to build two identical systems. The outputs (e-beams) will face each other and leave space for the laser cell that will be incorporated later. Details of this system are given in the appendix to this section. This system could be built in about a year. It will have an applied magnetic field and will use an absorber to dump the electron beam.

2. **Develop emitter (6-12 months):** Because the two pulsed power drivers are independent at this phase, we can pursue parallel development paths

for the emitter. We will try the simple metal/dielectric cathode design of **RHEPP** first, and then go to more advanced designs, such as CsI coated graphite emitters, or a photoemission cathode, or the Russian carbon needle cathode.

3. **Develop hibachi (6-12 months):** We will add a hibachi structure and gas cell to look at pressure foil lifetime and transmission issues. The gas cell will have a rudimentary circulator to remove the heat. Again, having the two independent drivers will allow us to pursue two development paths.

4. **Add gas recirculator (6 months):** We will add a high quality gas recirculator and an input laser. The gas recirculator will be developed and built off-line, so it can be installed and tested during earlier phases. We will not add fluorine to the 30-cm laser cell at this time. The objective of this phase is to validate that the design of the recirculator is adequate that the repetitive injection of the electron beam does not distort the laser input.

5. **Amplify high quality laser beam (6 months):** We will add fluorine to the cell, use a high quality KrF input laser, and evaluate the spatial profile of an amplified high quality laser beam. This will validate our beam quality module. This data will also be used in comparisons of KrF kinetics code results and experiments. This will also allow us to assess the issues in laser gas recycling during long pulses.

6. **Optical Delay.(6 months)** We will develop an electronic delay line such that we can delay probe beams for up to a microsecond and then propagate them through the test 30-cm amplifier.

B) Advanced Pulse Power Driver Program Plan

1. **Assessment and Preliminary Experiments (18 months):** We will evaluate the various candidates identified above in terms of the lifetime, efficiency, and cost requirements for IFE. We will identify developments that are required to achieve an adequate design for the 30-cm Rep-Rate Laser, and conduct appropriate tests. Our plan is as follows:

   a. **Magnetic pulse compressor- RHEPP technology**: A good basis exists for designing magnetic pulse compressors. PSI has developed the most advanced simulation model for these systems and used it to build a successful 250 kV, 100 Hz, 70kW magnetic compressor in 1997. This model will be used to develop compressor designs with the required 80% efficiency while minimizing Metglas volume and other factors affecting cost. We will assess the likely cost of Metglas in reactor quantities. The use of spark gaps, thyratrons, or solid state devices as the first stage switch will be evaluated. We will hold

discussions with manufacturers to assess potential technology advances, and these will be evaluated with tests of developmental components. Solid state switches are one candidate for these component tests. Another candidate is a new type of Metglas core developed by one manufacturer that uses a proprietary coating rather than the standard Mylar insulation. These can handle more energy per kg, and have better thermal properties, that should lead to higher efficiency and lower cost. DoE labs with experience in magnetic compressor design (LLNL, Sandia) will be encouraged to contribute to and review our assessments of this approach.

b. **Magnetic pulse compressor- SOS technology:** The first stage switch and Metglas issues for the SOS technology are the same as for the RHEEP technology. But, there are some issues that are unique to this system. The foremost is if there is some fundamental limitation in the semiconductor-opening switch itself that prevents us from achieving the required efficiency or pulse width. A secondary issue is if the auxiliary circuits necessary to drive the SOS are inherently inefficient. We will work with the originators of this technology to address these questions. We will also acquire and test the key components and subsystems so that we can establish for ourselves the suitability of this approach. A number of SOS devices have already been purchased, and we will review their design and performance with the users. Another device is being fabricated under contract to NRL to demonstrate output pulses as long as 100 nsec.

c. **Spark gap based systems:** We will review other spark gap based systems, such as water lines or oil/paper cables, for possible "breakthrough" developments, but we will pursue them in detail only if the magnetic compression systems appear unlikely to meet the requirements. However, it should be noted that the repetitive Spark-Gap based driver that we will build to develop the emitter, hibachi and gas recirculator (see Appendix) will be operational before the assessment phase of the Advanced Driver Program is complete, and thus, we can get a better idea if this technology is extendable to an IFE reactor.

2. **Selection Review**

At the end of the assessment phase, a review will be conducted in which possible driver candidates for the 30-cm Rep-Rate Laser will be presented, along with supporting analyses and test data. A recommended pulse width and design will be presented which will include conceptual mechanical drawings and electrical simulations. We will include design extrapolations to a reactor scale driver

3. Construction of the Baseline Advanced Pulsed Power Driver

We have allocated 18-24 months for the preliminary design, final design, fabrication, and checkout of the advanced pulsed power driver. This should be sufficient time to allow for flexibility and versatility and to test sufficiently to establish reliability. The preliminary design phase will be closely coordinated with the parallel work on the emitter, hibachi, cathode and gas recirculator to ensure a proper electrical and mechanical impedance match with the final application. A key issue will be a design for a microsecond regime system which will allow testing at the 100 nanosecond level of the emitter, hibachi, cathode and gas recirculator using the conventional (spark gap) pulsed power driver . Prior to the demonstration of this device, testing will initially be done with a resistive dummy load, and then a dummy electron beam diode.

C) **Full test of integrated facility: Combine advanced pulsed power with emitter/hibachi/gas recirculator.** We will replace the two spark gap-based pulsed power drivers with the advanced pulsed power driver, and run the facility in a rep-rate mode for an extended period of time. This will give us long run time experience with a rep-rate laser. It should allow us to determine the durability and efficiency of all of the components, and evaluate the quality of the amplified laser beam on a long-term basis. We anticipate the integrated test period should last 12 months.

D) Summary

We have a program plan to build a 30-cm Rep-Rate Laser that will enable us to develop some of the key technologies required for IFE. The 30-cm Rep-Rate Laser should have a pulsed power system that can deposit the electron beam energy into the laser gas with the durability, efficiency and cost required for IFE. The 30-cm Rep-Rate Laser will also allow us to evaluate the technologies required to repetitively amplify a high quality laser beam. This system should be large enough to make a convincing demonstration of some of the technologies required for an IFE driver and it should be flexible to make a versatile test-bed. When complete this facility will significantly increase our confidence in assessing the viability of KrF as a driver for fusion energy.

E) Appendix: Description of spark gap-based pulsed power driver:

In order to allow us to start addressing the emitter/hibachi and gas recirculator issues as soon as possible, we have elected to first build a low-risk spark gap based driver that uses well-established technology. The design is based on the same technology, and same performance, as the DAHRT injector that was developed by Pulse Sciences, Inc. [1]. The same technology has been used in the Airex system, as well [2]. One side of the system is shown in Figure A1.

(We will build both sides.) A 100kV power supply is used to charge a 2.4μF capacitor bank to 93 kV. The capacitor bank is then discharged through a single spark gap switch into a 1:13 step-up transformer, and then into two 4.4 Ω coaxial water-dielectric pulse-forming lines. The lines are discharged through SF_6 -insulated laser triggered switches into a common cathode. The output parameters of the system are 500kV, 112 kA/side = 222kA total, 100 nsec flat top. The operating voltage of this is about 66% of that of the DAHRT injector. The step-up ratio of the transformer is less, as is the charge transfer. We calculate that the lines are operating at about 65% of their breakdown voltage [2] and that the switches should last at least 10^6 shots [3,4]. We have also included powered divertors to minimize any post-pulse ringing. Thus, we expect this to be a fairly reliable system. We anticipate that it will be operational at the end of the first year of the program.

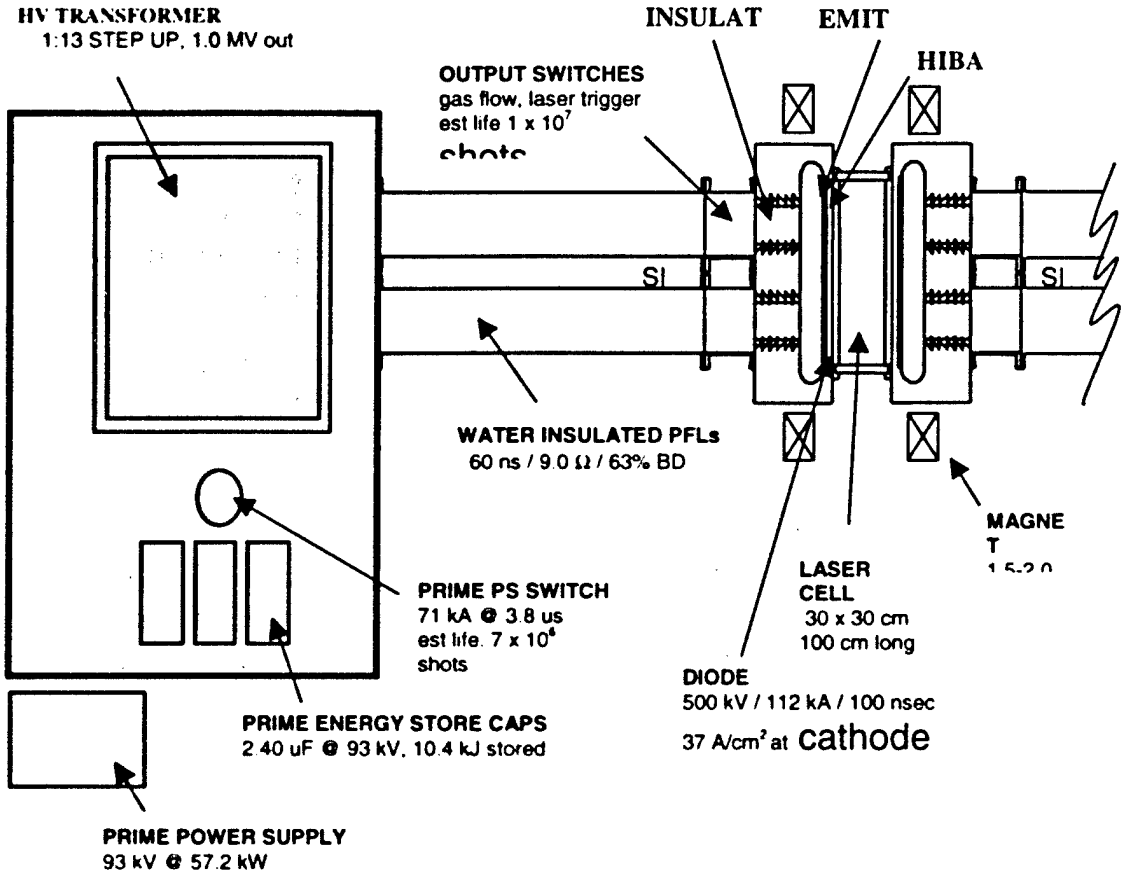

Figure A1: Spark gap based pulsed power system to develop emitter, hibachi and gas circulator technologies.

4.3.4 ADVANCED FRONT END

4.3.4.1 INTRODUCTION

The front end of the laser system provides the initial temporal pulse shaping, tailored focal profiles, and amplification to the energies required for the power amplifiers. The Nike front end is currently an all discharge pumped system that has successfully met the needs of that facility. The oscillator and first two preamplifiers are commercial devices that use UV pre-ionized discharge pumping. These amplifiers have built in gas circulation and pulse power that allow repetition rates up to 10 Hz. These commercial lasers have 20 ns FWHM gain pulse lengths and up to 0.5 J output. Following these are two stages of amplification by higher energy x-ray pre-ionized discharge-pumped amplifiers developed at NRL. These amplifiers do not have the built in repetition rate of the commercial amplifiers and can operate only at about 0.1 Hz. Four of these amplifiers in parallel provide the energy needed to drive the first e-beam pumped amplifier.

The beam smoothing is achieved by diffusely illuminating an aperture with broadband multi-mode radiation from the oscillator. [See Figure 4.3.4.1-1 for an optical schematic.] This aperture is ultimately imaged through the amplifiers onto the target. Telescopes arrange that the Fourier pupil (far field) of the aperture is relayed to the center of the discharge pumped amplifiers. Gain non-uniformity near the Fourier plane of the aperture does not imprint onto the focal distribution. However, the small commercial discharge pumped amplifiers in the Nike front end have a large length to width ratio (80 cm/ 1 cm), and there is appreciable amplification at distances well removed from the Fourier plane. There is also some imprinting of tilt on the focal distribution. This effect is removed by the tilt removing optics shown in the figure. In the following larger aperture amplifiers, we do not observe a significant imprint due to gain non-uniformity. This is because, at the larger apertures, the divergence of the laser beam is smaller, and the effective depth of the Fourier plane is longer than the amplifier.

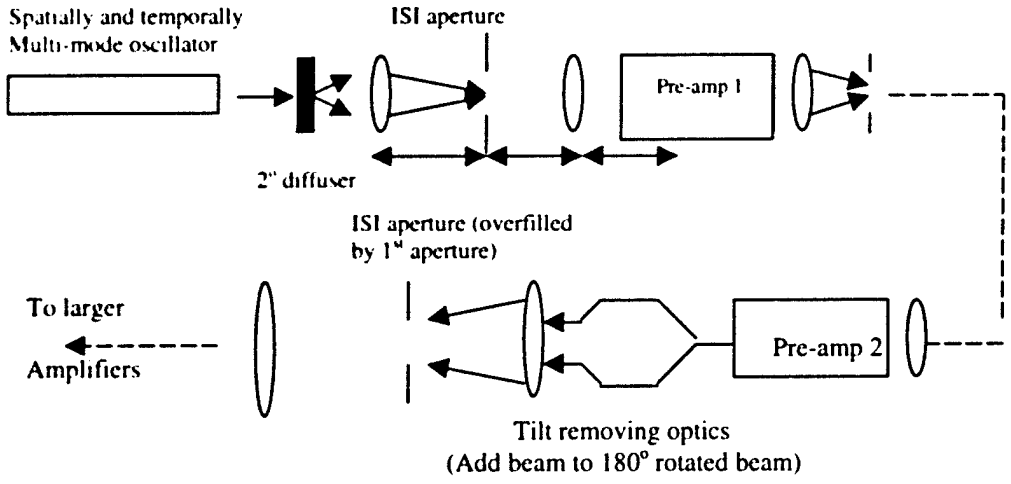

Figure 4.3.4.1.1 NIKE laser front-end beam shaping optical schematic

The pulse shaping is accomplished with Nike by Pockels cells located after the first and second preamplifiers. The pulse shape is polarization and angle encoded into the pulse from the oscillator. This strategy ensures that the amplifiers see nearly continuous loading. The pulse shape is thereby not distorted by variation in gain saturation during the pulse. After the final discharge pumped amplifier, the pulse is recovered by means of polarizers and spatial filters that reject the co-propagating control beam. Table 4.3.4.1.I shows the characteristics of the Nike front end.

Table 4.4.1.1.I NIKE LASER FRONT END PROPERTIES

Parameter	Value
Energy Output:	2 J
Repetition Rate:	0.1 Hz at full energy
focal profiles:	30 to 100 times Diff. Limit flat top profiles; 1% RMS uniformity
pulse contrast:	2000x via Pockels cells $> 10^7$ due to gain switching of pre-amps
pulse shaping:	up to 8 ns pulse with arbitrary shape

The Nike front end has demonstrated that it is a practical solution for low-repetition rate target irradiation of flat targets, but significant enhancement will be necessary for the Rep-Rate Laser front end.

4.3.4.2 Front End Improvements Needed for Rep-Rated Laser

The Rep-Rate Laser will be a technology demonstrator for scaling of KrF laser technology to the requirements of a reactor driver. The front end needed to drive this amplifier will need to incorporate several changes from the Nike front-end laser. These include:

- More energy: about 10 J to extract full energy and suppress ASE in the following amplifiers;
- Higher repetition rate: 5-10 Hz at full energy;
- Higher beam spread: ~200 x D.L. needed to create laser profiles suitable for pellet illumination;
- Longer pulses: 20-30 ns for pellet implosions.

The Nike front end was created to illuminate flat targets at a low repetition rate. While it has been very successful in demonstrating how to create very smooth illumination profiles on flat targets, the Rep-Rate laser will require a different realization of the same technology. Beams with more incoherence and divergence will be needed to illuminate 0.5-cm diameter pellets with reasonable F-number optics. Happily, this will also allow the Rep-Rate Laser to be less sensitive to optical aberrations, which is a cost benefit in that it will allow a reactor to use poorer quality, cheaper optics than were used on Nike. It

would be difficult to amplify such pulses in the narrow initial pre-amplifiers of Nike without imprinting. These amplifiers also do not support the need for longer pulses. The standard cylindrical-ring electrode Pockels cells used on Nike would have very poor contrast ratio with higher divergence beams.

None of these problems represent insurmountable technical difficulties but will require some directed development. Most, and perhaps all, of the current discharge pumped pre-amplifiers could be replaced with small electron beam pumped units. A review of currently available discharge laser technology, which was not available when Nike was designed, will be done. Electron beam pumped KrF amplifiers would have about twice the gain per unit of physical length of discharge pumped devices. Electron beam pumping would also readily allow for longer gain pulses and might allow temporal pulse shaping by structuring the pulse shape of the electron beam. The Pockels cell issue can be resolved by using thin crystal Pockels cells such as LLNL is using on the NIF.

4.3.4.3. MILESTONES

a) Develop small e-beam pumped and/or new discharge pumped amplifier modules for front end;
b) Develop pulse shaping needed for a reactor via advanced Pockels cells and gain control of amplifiers;
c) Develop means to produce the 200x DL focal profiles needed to illuminate pellets;
d) Design and construct a front end with beam smoothing and sufficient energy output to drive the 30-cm Rep-Rate Laser at 5 Hz;
e) Integrate with 30-cm Rep-Rate Laser and demonstrate full power operation while maintaining illumination uniformity and pulse shaping.

4.3.5. ADVANCED KRF WINDOW DEVELOPMENT

4.3.5.1. INTRODUCTION

The large amplifiers in the laser system require large, high quality windows to separate the laser gas from the surrounding environment. Typically, these windows have been made from UV quality synthetic fused silica (SiO_2). The lifetime of the laser windows in the harsh laser environment is a significant issue, which has not been successfully resolved to date.

A number of environmental factors affect the lifetime of the windows. The most important of these is the fluorine gas used in the laser mixture. Fluorine is the most reactive of the halogen elements and readily combines with any available hydrogen (from residual atmospheric water of any hydrocarbon residues) to form hydrofluoric acid (HF). Hydrofluoric acid is used industrially to etch glasses and fused silica. Over time, HF and fluorine destroy the inner surface of quartz amplifier windows. The intense UV laser fluences may exacerbate this problem. UV light has been shown to act as a catalyst for

etching glass with fluorine [1]. By activating the surface of the glass with UV light, fluorine could be made to etch glass without the introduction of hydrogen. Additionally, the high laser fluence may be near the laser induced damage threshold (LIDT) of typical optical coatings used to reduce window reflections. Coating damage, of course, is another mode of rapid window degradation. In lithography, it has been found that long duration, high average intensity exposure to KrF laser radiation can also cause density changes in some varieties of fused silica, affecting the optical path length and, potentially, leading to a degradation of transmitted wave-front quality.

Another issue which may be important for repetitive operation in the UV is laser treatment or conditioning of the coatings on optical windows. For lasers operating at longer wavelengths, experience in the commercial and industrial laser world indicates that there is benefit to exposing coated optics to repeated irradiation at power and energy density levels of ~ 20% to 50% of the expected damage levels for several hours of run time. The observation that this results in improved coating durability is much more compelling than the reasons offered as to why this procedure is so effective. The most likely explanation would appear to be some variety of laser annealing is taking place which reduces stresses and strains in the coating stack.

Successful, long duration rep-rated laser operation will require large high quality UV windows, which do not degrade because of any of these effects. Additionally, the amplifier windows will be exposed to significant fluences of high-energy electrons and x-rays from the electron beam pump sources. The windows must also have sufficient mechanical strength to withstand the static and dynamic pressures and stresses caused by repeated laser operations, including occasional malfunctions.

The choice of window materials for UV laser operation is limited by the required optical properties to fused silica (SiO_2), magnesium fluoride (MgF_2), calcium fluoride (CaF_2), and sapphire (Al_2O_3). Of these, only fused silica is presently available in sizes larger than 30-cm diameter. Both sapphire and calcium fluoride have been used successfully as windows for fluorine-rich chemical DF and HF lasers in DoD programs. Calcium fluoride or Magnesium fluoride windows are used in smaller discharge pumped lasers because of their excellent resistance to HF and fluorine attack. Additionally, the low index of refraction of calcium fluoride and magnesium fluoride allows laser operation without an anti-reflection coating. However, MgF_2 probably does not scale to meter-size optics, while CaF_2 might. Currently there are efforts to grow 36" diameter CaF_2 windows in industry for lithography [ref]. Tests at NRL in a fluorine cell have shown that magnesium fluoride resists chemical attack better than calcium fluoride. The lifetime of calcium fluoride in the amplifier environment requires further evaluation. As mentioned above, sapphire is also available and demonstrates excellent mechanical strength, as well as a resistance to chemical attack as good as that of MgF_2. Currently, non-birefringent sapphire windows up to 30 cm x 15 cm can be fabricated from 90° boules grown by a Heat Exchanger Method (HEM) process by Crystal Systems, Inc. Production of larger elements as single crystals is technically possible, but commercially unmotivated. Since sapphire has a high index of refraction, 1.78, uncoated windows would have a very high surface reflection of ~ 8% per surface. Sapphire would almost

certainly require anti-reflection coatings. Fortunately, a single quarter wave layer of MgF2 on sapphire will reduce the reflectivity to less than 0.1% at 0.25 micron.

An additional plus for sapphire is that there is some successful experience in fusion bonding sapphire crystals together to make bonded structures larger than can be grown at present. Diffusion bonding is a process in which two material surfaces are optically polished to be very flat such that if they are placed together for an appropriate time and under sufficient pressure, van der Waal's forces cause the surfaces to bond together with a bond strength equivalent to the mechanical strength of the basic material. This has been used successfully for a number of solid state laser materials to create large or unusual shapes, which cannot be formed from monolithic pieces of as-grown crystals [ref-onyx Optics]. Bonds as long as 35 cm in length have been successfully made in $Y_3Al_5O_{12}$ (YAG). Bonds also have been formed between YAG and sapphire to form laser sandwich slabs in which the center Yb:YAG layer is the laser and the sapphire is for heat removal. In mechanical and optical testing, the optical and mechanical damage strengths of the bonded regions were equal to or superior to the surrounding bulk material. Potentially, one could make a window of arbitrary size by bonding m x n pieces of sapphire , each ~ 15cm x 30cm. As sapphire grows stoichiometrically, which really only means there is a unique, well-defined crystal structure, the index of refraction variance from sample to sample should be small, on the order of 1-2 x 10^{-6} per cm of optical path length. A multi-element one inch thick window might then show an index jump of the order of $\lambda/10$ at 248 nm, if no selection of the panes were used. By making the joint at an oblique angle, the index jump from pane to pane could be made to occur more gradually. In a reactor scenario, where ~ 2 x 60 x 9 x2 = 2160 panes were necessary for one meter aperture windows for 60 amplifiers, pre-selection could reduce this jump to ~ $\lambda/50$ on average.

To the best of our knowledge, no fusion bonding experience exists for calcium fluoride or magnesium fluoride, although there is no reason to expect that this could not be done. The issue of index jumps between panes would be worse, however, as the window thickness would have to be much greater.

An AR coating that could resist corrosive attack and reduce the surface reflectivity will be required for sapphire and might be required for other fluorine-durable materials. In the simplest of all worlds, a coating for fused silica that was fluorine-impervious could allow its use for even the largest windows. The simplest coating structure to reduce reflectivity is a single layer of the material $\lambda/4$ at 248 nm thick in optical path. Such a layer of MgF_2 is commonly used in the optical industry. For sapphire, this is close to an optimal solution and the reflectivity is reduced to less than 0.1% per surface. For fused silica, the reflectivity is reduced from 4% per surface to 1.5% per surface. This single layer coating will be best when the index of the coating material (n_{MgF2} = 1.38) is the square root of the material index and that of the atmosphere (n~1). As a further plus, one might expect MgF_2 coatings to resist chemical attack, similar to the bulk material. However, these coatings on fused silica have not proven durable on the Nike optics. There may be several factors at work in this case. Deposited coatings are not as dense as bulk material and HF may be diffusing through to attack the underlying substrate. The chemical composition of the coating may not be purely magnesium

fluoride, leaving residual $MgF_xOH_{(2-x)}$ in the coating, where HF can attack it [ref]. A number of different processes and coating designs have been evaluated at NRL with only modest success in improving coating durability [ref].

Windows for the Nike 60-cm amplifier were originally coated with a fluorine resistant AR developed for the Aurora Laser at Los Alamos National Laboratory, in collaboration with Spectra-Physics. It consisted of multiple alternating layers of Al_2O_3 and aluminum fluoride (AlF_3). Operational results with this coating have varied. It has on occasion outlasted an uncoated window, while at other times it has deteriorated faster than the uncoated window. The reasons are not well understood. Laboratory tests show that the coating survives chemical attack better than fused silica, except in the presence of hydrocarbons.

For these and other tests, samples to be tested are placed in a small stainless steel vacuum chamber. This is evacuated to rough vacuum and then filled with an atmospheric pressure with a gas mixture of 95% neon and 5% F_2. UV transmission of the samples is monitored with a spectrophotometer before testing, and at intervals during the test. Initially, the chamber was evacuated and baked at high temperature to drive off any residual water vapor. Under these conditions, the coatings and bare SiO_2 samples survived for several days. A small amount of H_2O was then introduced into the chamber. The bare fused silica etched in less than two hours, while the coatings typically lasted two to four times longer before any drop in transmission was noted.

To date, the only materials that have survived this test indefinitely (greater than four months) are MgF_2 and Al_2O_3, both in bulk form. Calcium fluoride begins to degrade after several weeks, while SiO_2 lasts only hours.

The only improvement in coating performance over the LANL/Spectra Physics design has been to increase the number of layers, and hence the physical thickness in the coating. A variety of coating materials, substrates and coating processes have been tried without significant improvement in coating durability.

Windows on Nike typically last about 6 months or 300 shots. For windows to last the several billion shots envisioned for future systems, the corrosion resistance of the inner (exposed to the laser gas) surface must be greatly improved. Also, the effects of high radiation fluences, both electrons and x-rays, need to be evaluated, and possibly improved.

One method that has not been investigated because of the probable greater cost is the use of a flowing gas curtain inside the window to protect it from the fluorine in the laser gas. This has been used successfully on the Navy repetitive-pulsed chemical laser (RPCL) to protect the windows of a laser running significantly stronger F_2 concentrations than a KrF laser mixture.

4.3.5.2. Optical Window Improvement Program

Because there is already a lifetime problem with laser windows for electron-beam pumped large aperture amplifiers; the first priority is a development program to solve the corrosion problem for laser windows, such that the lifetime needs of the Rep-Rate Laser can be met. The issue of larger windows for reactor drivers will be deferred until successful development directions become well enough defined that the considerable expenditures required to demonstrate full-scale windows are justifiable. The work will focus on the three areas of: optical substrates advanced coatings and alternate window designs. Table 4.3.5.2.I summarizes some of the areas of concern for each of these. For all program components, resistances to chemical attack and radiation resistance are critical issues.

The goals of this optics development program are threefold. First, to develop substrates and anti-reflection coatings that can resist corrosion in the hostile laser environment. This proof-of-principle demonstration will be performed on small optical components (typically 1 " in diameter). The optics will be tested both statically and in use on the rep-rated lasers developed for the work described elsewhere in this proposal. The substrate coating should survive one million shots in a laser at a working fluence of over 2 J/cm^2. Second, these optics will be tested for resistance to radiation darkening. Again the goal will be to produce an optic that is not significantly degraded by a x-ray and electron fluence similar to that expected in an actual laser over a one million shot lifetime. The third program goal will be to work with vendors to demonstrate that the required substrates and coatings can be fabricated in sizes of 30 cm aperture. The final deliverable will be a pair of windows that could survive one million shots in an electron beam pumped KrF amplifier.

Table 4.3.5.2.I Optics Development Issues

Substrates	Coatings	Alternate Concepts
Materials	Materials	Engineering feasibility
Large size fabrication	Coating design	
Effect of uncoated window on amplifier performance	coating process	
High temperature operation	High temperature operation	High temperature operation
Strength of Material		

For substrate development, we will work with existing component manufacturers to extend and improve current technology. The materials of choice are MgF_2, Al_2O_3, and CaF_2. Current state of the art in MgF_2 is 10-cm diameter, and there are poor prospects for scaling significantly larger. It is thus not a good prospect for scaling to meter size optics, but may be useful as a substrate in evaluating coatings, especially ones, which are supposed to act as a barrier to protect the substrate. CaF_2 and Al_2O_3 are both currently available up to 30-cm aperture; there is also commercial effort underway to scale to larger sizes for the lithography industry [.]. Optical quality of these materials at large sizes

will be an issue, for lithography even more strongly than for IFE. Demonstrating adequate lifetime on AR coatings for sapphire will be a key issue because of the high index of refraction.

Substrate performance may be affected by radiation darkening by x-rays, UV, and high- energy electrons. A great deal of work in ongoing to characterize these issues for space applications and lithography [...]. We need to assess the impact of these factors at the moderately high operating temperatures expected for an IFE amplifier, 500-600°C. In passing it is worth noting that high temperature operation is not necessarily detrimental; it could in fact prove beneficial in protecting against cumulative effects of radiation exposure.

We need to expand the effort begun under the Nike program to evaluate and improve the corrosion resistance of UV anti-reflection coatings. One obvious extension of prior testing procedures will be to use MgF_2 or sapphire substrates to reduce the risk of sub-surface damage to the substrate contaminating apparent coating performance results. We will continue to involve coating vendors in the development process, as well as outside consultants expert in optical coatings.

Alternate window designs will be explored. One concept is to protect the optic with a thin optical membrane, which could be rapidly and inexpensively replaced. Pellicle membranes developed or the lithography industry are currently available in sizes up to 30-cm diameter, which transmit more than 99% of the UV light. If a suitable design could be developed to minimize pressure stresses on this window, it might provide chemical protection for the main amplifier window. Radiation effects and/or high temperature operation may be fatal flaws for this concept. The level of effort here will be critically dependent on the quality of the concepts, as well as the success of the more conventional approaches.

4.3.6. Design Tools For KrF

4.3.6.1. Introduction

An issue of some concern in proposing a KrF laser driver for IFE is that the most efficient and economical operating regime for an IFE reactor driver laser may, or may not, be the best and most efficient regime in which to operate large electron beam pumped KrF amplifiers, which will largely determine the laser efficiency. There is considerable experience in operating small discharge pumped KrF lasers in a continuous repetitive mode, some experience in operating large electron beam pumped KrF amplifiers in a single pulse mode at or near room temperature, but very little experience in operating strongly excited electron beam pumped amplifiers in a repetitive pulsed mode. An issue in the latter case is that it is desirable from an operating efficiency standpoint to let the gas temperature in the recirculating loop rapidly equilibrate at a temperature of 500-600°C, but there is only limited experience [from EMRLD burst mode operation] in operating KrF in this mode.

It is also worth noting that the EMRLD designers expected from their code modeling of KrF kinetics to see the laser output increase considerably at elevated temperatures, but experimentally this did not occur. Some reports in the literature appear to give support to the concept that krypton-rich mixtures may be capable of achieving intrinsic efficiencies of 15% or greater, even near room temperature. Once again, as with elevated temperature operation, there is little reason for confidence in our current ability to scale these results into different operating regimes.

The situation is not any more resolved with regard to codes to predict the propagation and absorption of the electron beams in the laser gases. Simulation calculations performed at Los Alamos prior to the design, fabrication and testing of the Nike 60-cm amplifier predicted not only the need for a larger applied magnetic field to avoid "pinching" of the electron beams by a factor of approximately two, but predicted a beam instability at or near full beam current which did not occur at all.

This rather unsatisfactory situation is not a reason to postpone the 30-cm Rep-Rate Laser, as conditions can be accessed which will allow it to operate in a meaningful way for developing a design basis for larger amplifiers. Interpolation is always a more certain procedure than extrapolation, after all. It does, however, point out clearly that further work is merited to ensure that the conclusions which will be drawn from the results on the 30-cm Rep-Rate Laser for the large meter-aperture amplifiers for an IFE driver, will be based as soundly as possible on experiment, calculation and simulation.

4.3.6.2 Modeling and Analysis Tasks

4.3.6.2.1. KrF Laser Kinetics Models

It might be expected that the kinetics of KrF lasers is well understood. This, while a desirable situation, is far from a certainty. There are several reasons for this situation:

- The laser kinetics are quite complicated as they involve not just excitation of KrF molecules, but the actual dissociation of fluorine and the formation of KrF excimers in an excited state, with considerable complication from the diluent and unexcited gases. The short upper level lifetime also means that the KrF is actively participating in the process on a time scale short compared to the duration of the pumping pulse. Most models, which have been developed to date, are forced to estimate many unmeasured rate coefficients by gas kinetic models.

- Additionally, in most small experiments it is difficult to measure the fraction of the electron beam, which is absorbed by the laser mixture, as opposed to the walls of the cell, or other structural members such as the foil support structure. This leads to most such experiments generating relative data with gaps in the description of the actual conditions.

- As noted earlier, the gas in an e-beam pumped amplifier may be heated 50 to 100°C, or more, during a single e-beam excitation pulse. The temperature resolution of even well controlled experiments is thus poor.

In order to quantify the status of the laser kinetics models and modeling, we intend to access the best available models and exercise them fully on the best available data sets and in comparison to each other on the same data sets. One non-US source, which seems worthy of note, is a Russian code for predicting excimer laser kinetics. Schafer Corporation obtained the corresponding XeCl rate package for this code last year and found that it included considerable cross-section data, which has not been reported in the open literature by the Russian laboratories. It seems prudent to obtain the KrF analog of this code, as well as various US, and Western models.

4.3.6.2.2. Development and Testing of Advanced Kinetics-Based Beam Propagation Code

Once confidence has been attained that the physics is correct in the KrF kinetics modeling, a serious issue which should be addressed is to model the detailed propagation dynamics for the pumping beams and laser extraction in angularly multiplexed amplifiers with the pulse shaping necessary to implode fusion pellets. The code must include three spatial dimensions to properly account for "dead" spaces in the angularly multiplexed amplifiers, and be realistic in the time dimension to include the effects of pulse shaping and long gain pulses. This will be a valuable tool for evaluating the relative merits of various pulse shaping and multiplexing configurations. The results will be bench marked to experiments on the Nike 60-cm amplifier and the 30-cm Rep-Rate Laser.

4.3.6.2.3. Electron Beam Propagation Code

Amplifier apertures in the 1-meter class are projected for the IFE application. The design of efficient electron beam transport is more difficult with large apertures because, even with segmentation the cathode is very large and the current per cathode is high, well beyond the pinch limit. The self-field of the electron beam is large and it becomes crucial that one accounts for the beam deflection by the self-field. The design of foil support structures that do not intercept the beam becomes more difficult with large spans and the large magnetic fields. We propose to develop codes that simulate the electron beam in geometry that realistically models that of KrF amplifiers. The development will build upon the PIC (Particle-in-cell) codes that have already been developed in the microwave, plasma physics, and pulsed power communities. The testing of the code predictions will be primarily performed using the Nike 60-cm amplifier. The high currents and large sizes of the components of this device should allow testing near the regimes required for reactor-class KrF amplifiers.

REFERENCES

Section 4.1.1

i. Bodner Phys plasmas

[ii] Gardner, phys plasmas
[iii] Tabak, fast ignitor

SECTION 4.1.2

1. Bodner, S. E.; *et al.* **Direct -Drive Laser Fusion: Status and Prospects.** Physics of Plasmas, 5(5), 1901-1918.

2. Williams, Joel M., Jr.; Nyitray, Alice M.; Wilkerson, Mark H. **Manufacture of plastic composite foams having tailorable properties.** U.S. Patent 4,966,919 A., 1991.

3. Glembocki, O. J.; Rebbert, M. L.; Prokes, S. M.; Sethian, J. D.; Marrian, C. R. K.; Chan, L. Y. **Optical properties of low-density foams considered as targets for inertial confinement fusion.** J. Vac. Sci. Technol., A (1998), 16(1), 50-56.

4. Holland, B. T., Blanford, C. F., Stein, A. **Synthesis of Macroporous Minerals with Highly Ordered Three-Dimensional Arrays of Spheriodal Voids.** Science (1998), 281, 538.

5. Steckle, W. P. Jr.; Apen, P. G.; Mitchell, M. A. **Highly Crosslinked Nanoporous Polymers.** U.S. Patent 5,629,353 A, 1997.

6. Duke, J. R.; *et al.* **The Fabrication of Double Shell Targets for Nova.** (Submitted to Fusion Technology June 1998).

7. Lambert, Stephen M.; Overturf, George E., III; Wilemski, Gerald; Letts, Stephan A.; Schroen-Carey, Diana; Cook, Robert C. **Fabrication of low-density foam shells from resorcinol-formaldehyde aerogel.** J. Appl. Polym. Sci. (1997), 65(11), 2111-2122.

Section 4.3.3.

1. S. P. Obenschain, S. E. Bodner, Y. Chan, D. Columbant, K. Gerber, R. H. Lehmberg, E. A. McLean, A. N. Mostovych, M. S. Pronko, C. J. Pawley, A. J. Schmitt, J. D. Sethian, V. Serlin, J. A. Stamper, C. A. Sullivan, J. P. Dahlberg, J. h. Gardener, A. V. Deniz, J. Hardgrove, T. Lehecka, M. Klapish, "The Nike Laser facility: Performance And Initial Target Experiments", *Physics of Plasmas*, **3**, 2098 (1996).

2. C. J. Pawley, et al., "Measurements of laser imprinted perturbations and Rayleigh-Taylor growth with the Nike KrF Laser" *Physics of Plasmas*, **4**, pp. 1969-1979, (997).

3. I. V. Sviatoslavsky, et al., "A KrF laser driven inertial fusion reactor, Sombrero", *Fusion Technology*, **21**, 1470 (1992)

4. M. W. McGeoch, S. E. Bodner, S. P. Obenschain, J. D. Sethian, I. D. Smith, P. A. Corcoran, and R. A. Altes, "A conceptual design of a 2 MJ KrF Laser Facility", *Fusion Technology*, **32**, (1997).

5. J. D. Sethian, S. P. Obenschain, K. A. Gerber, C. J. Pawley, V. Serlin, C. A. Sullivan, W. Webster, A. V. Deniz, T. Lehecka, M. W. McGeoch, R. A. Altes, P. A. Corcoran, I. D. Smith, O. C. Barr," A large area electron beam pumped Krypton Fluoride laser amplifier", *Rev. Sci. Instrum.*, **68**, pp. 2357-2366, (1997).

6. L. X. Schneider, K. W. Reed, R. J. Kaye, "Repetitive High energy Pulsed Power Technology Development for Industrial applications," Proceedings of the fourteenth International Conference on the applications of Accelerators in /Industry and Research, Nov. 6-9,1996, Denton, Texas, *Sandia National Laboratory Report #* SAND 96-2350C.

7. A. Mandl, D. Klimek, and E. Salesky, "KrF laser studies at high density", *Fusion Technology*, **11**, pp. 542-547, (1987).

8. Y. Lee, f. Kannari, and M. Obara, "Power extraction study of an e-beam pumped atmospheric pressure Kr-rich KrF laser amplifier", *J. Appl. Phys.*, **65**, pp. 4532-4541, (1989).

9. D. Sethian, C. J. Pawley, S. P. Obenschain, K. A. Gerber, V. Serlin, C. A. Sullivan, T. Lehecka, W. D. Webster, M. W. McGeoch, I. D. Smith, P. A. Corcoran, and R. A. Altes, "The Nike electron beam-pumped KrF laser amplifiers", *IEEE Trans. On Plasma Science*, **25**, pp. 221-228, (1998).

10. W. S. Melville, "The us of saturable inductors as discharge devices for pulsed generators", *Proc. IRE*, **98**, 185 (1951).

11. Yu. A. Kotov, G. A. Mesyats, S. N. Rukin, and A. L. Filatov, " A novel semiconductor opening switch for megavolt repetitive pulsed power technology: experiment and applications", *Digest of Technical Papers, Ninth IEEE Pulsed Power Conference*, Albuquerque, NM, June 21-23, 1993, IEEE, New York , NY, pp.134-139.

12. Yu. A. Kotov, G. A. Mesyats, S. N. Rukin, V. A. Telnov, B. g. Slovikovskii, S. P. Timoshenkov, and A. I. Bushiyakov, "Megavolt nanosecond 50 kW average power all solid state driver for commercial applications", *Digest of Technical Papers, Tenth IEEE Pulsed Power Conference* Albuquerque, NM, July 3-6, 1995, IEEE, New York, NY, pp. 1227-1230.

13. S. N. Rukio, private communication.

14. Pulse Sciences, Inc. for their "Feasibility study for the advanced hydrotest facility advanced radiographic machine" obtained this information.

15. *Proceedings 1998 International Power Modulator Symposium*, Westin Hills Resort, Rancho Mirage, CA, June 23-25, 1998. See particularly the papers: (a)"Sub-microsecond pulse switching characteristics of a 4500 V IGET", K. Okamura, M. Souda, F. Endo, M. Matsuda, and E. Kaneko; (b)"Improved semiconductor switches for pulsed power applications", F. J. Wakeman and B. k. Green: (c)"Improved turn-on characteristics of fast high current thrystors", L. Ducimetiere, g. Schroder and E. Vossenberg.

16. R Limpaecher and R Litte, "An application of a high energy spark gap in a repetitive mode", *Digest of Technical Papers, Fifth IEEE Pulsed Power Conference*, Arlington, VA, June 10-12, 1985, IEEE, New York, NY, pp. 477-480.

17. R Limpaecher, R Litte, and S. Ghosroy, "High voltage cable PFL test results", *Proceedings Seventeenth International Power Modulator Symposium*, Seattle, WA, June 23-25, 1996, III, New York, NY, (1986), pp. 264-270.

18. S. D. Korovin, " Long lifetime metal-dielectric cathodes", Contract report AF-0416, High Current Electronics Institute, Tomsk, Russia,(1993)

19. J. Moran, Textron Defense Systems, Everett, MA private communication.

20. J. P. Brucker and E. A. Rose, "Foil Support Structure for Large Area Electron Guns", *Digest of Technical Papers, Ninth IEEE Pulsed Power Conference*, Albuquerque, NM, June 21-23, 1993, IEEE, Piscataway, NJ, (1993), pp.747-750.

21. Cymer, Inc. brochure for 5000 Series laser, dated 1996.

Appendix:

1. J. Fockler, B. Bowen, V. Carboni, J. Kishi, and R. Kuenning, "A 4 MV Flat-top Electron Diode Driver" *Digest of Technical Papers, Eighth Pulsed Power Conference*, San Diego, CA, June 16-19, 1991, IEEE, New York, NY, pp.177-182.

2. J. Launspach, C. Bonnatond, J. de Mascureau, D. Villate, P. Allison, L. Bulita, T. Kauppila, D. Moir, B. Taylor, S. Watson, J. Fockler, B. Bowen, J. Kishi, and D. Morton, " Recent result on the DAHRT and AIREX 4 MV +/- 1%, 3.5 kA electron beam injectors" *Proceedings of the Tenth International Conference on High Power Particle Beams*, San Diego, CA, June 20-24, 1994, p. 515.

3. *J. C. Martin on Pulsed Power*, T.H. Martin, A. H. Guenther and M. Kristiansen, editors, Plenum Press, NY, (1996), p.179.

4. A. L. Donaldson, M. O. Hagler, M. Kristiansen, G. Jackson, and L. Hatfield, "Electrode erosion phenomena in a high energy pulsed discharge", *IEEE Transaction on Plasma Science*, **PS-12**, (1984), pp.28-38.

5. R Limpaecher and R Litte, "Heat dissipation measurement in a high power repetitively pulsed spark gap", *Conference Record of the 1986 International Power Modulator Symposium*, IEEE, New York, NY, pp. 149-154.

Appendix 2: Simplified Model of IFE Power Plants

Abstract

This model allows calculation of allowable laser system cost as a function of: (1) laser system efficiency; (2) grid cost of electricity (COE); and (3) BOP thermal efficiency.

The starting premise is that the grid will determine the COE, not by the plant. Although this is an unconventional view of power plant economics, it has no effect on the conclusions of allowable costs. However, it leads to an interesting simplification of the plant, in the following sense: IFE plants have the unusual property of being substantial users of electrical power. In a conventional plant the internal usage of the product (electrical power) may be from a fraction of a percent to perhaps 10 percent if very low efficiency electrostatic precipitators are used. A laser-driven IFE plant, in contrast, is projected to use 20 to 30 percent of the gross production for powering just the lasers. This is usually viewed as an internal feedback loop within the plant, and the plant optimization is juggled to hold constant net production.

The alternative view used herein is to unroll this internal feedback loop; to buy the power for the lasers from the grid, then to sell the gross production back to the grid. In doing this we fix the gross production of electricity, so the net varies slowly with laser efficiency. With the gross production fixed, many plant variables either become constants, or become sufficiently weak variables that they can be adequately approximated by constants. This considerable simplification makes the power plant analysis considerably more transparent.

By unrolling the laser electrical supply, the equipment needed to support this large power flow appears explicitly. Thus, the power comes in through a dedicated switchyard, with its associated costs. These very real costs, which scale strongly with laser efficiency, tend to be relatively hidden in many IFE plant studies.

Another variable that appears is the recovery of laser waste heat. This is usually treated very simplistically as a reduction in the amount of fusion energy required supplying the steam generators. However, real life is much more complex, in that how this waste heat is utilized dramatically affects the steam flow through the plant, including through the low-pressure turbine stages and the main condenser. Both of these have substantial costs associated with them. We include two extreme cases: (1) all laser waste heat recovered, or (2) no laser waste heat recovered. We approximate these conditions by assuming two discrete values for the BOP thermal efficiency: 47 percent and 45 percent, respectively.

In neither case do we include the cost of heat exchangers to get the heat out of the laser system. That is presumed to be a laser system cost. Also, we assume the recovered waste heat replaces BTU-for-BTU regeneration steam. This is slightly optimistic in that steam regeneration is highly optimized to conserve entropy, while it is likely waste heat recovery will not be able to reheat the feedwater at constant entropy.

Many plant costs are simply taken as fixed, using the values from the Sombrero plant study, from the Prometheus-L plant study, or from rather arbitrary assumptions. Greater complexity can be added in the future, but with insignificant effect upon the conclusions.

One unrealistic artifact is that the plant repetition rate varies with other design variations. Reality should be that that the repetition rate is an independent parameter, determined by best estimates of the chamber clearing time. However, at present we have only one "certified" direct-drive target design point. Thus the absorbed laser energy and the resultant target yield can not be varied to accommodate laser efficiency changes, so the repetition rate must change, at least for now.

The display of the results, on page 3, was the suggestion of Michael Monsler of Schafer Corporation. What is plotted is a family of curves, each curve being the allowable laser system total direct cost as a function of laser system efficiency. The family of curves is built up by varying the COE. And each curve is split into two by the two laser waste-heat recovery assumptions. The derivation and assumptions are as follows.

The allowable laser system direct capital cost varies from a low of -$200 million for a 5-percent efficient laser and a 5c/kWh COE up to +$4 billion for a 15-percent efficient laser and a 12 c/kWh COE. If we assume the laser costs $1 billion, then it must be between about 7.5 percent efficient to 14 percent efficient for COEs of 7 to 6 c/kWh.

A second conclusion is that the recovery of waste laser heat does not translate into a significant increase in the funds available for the laser. The savings are eaten up by the additional costs of the turbine and main condenser. In a conventional plant the condensate return is heated at constant entropy until, as high-pressure feedwater, it enters the boiler at very near the boiling temperature, the steam generator adds the heat of vaporization, and the superheater subsequently provides additional temperature rise for the vapor phase. This counter-intuitive process, called regeneration, maximizes the plant thermal efficiency, and diverts about one-third of the total steam flow around the low-pressure turbine stages and condenser. Replacing a substantial fraction of the regenerative steam with laser waste heat dramatically alters the plant steam flow and equipment.

What we will do below is the following:

(1) Follow the power flow through the plant;
(2) Derive a gross budget;
(3) Estimate operating cost from the power flow;
(4) Convert the remainder to a total direct capital cost;
(5) Deduct the Sombrero estimates of reactor cost;
(6) Deduct BOP costs using Sombrero and Prometheus scaling from the power flow;
(7) Deduct other capital costs using Sombrero estimates; and,
(8) Allocate the remainder to the laser system.

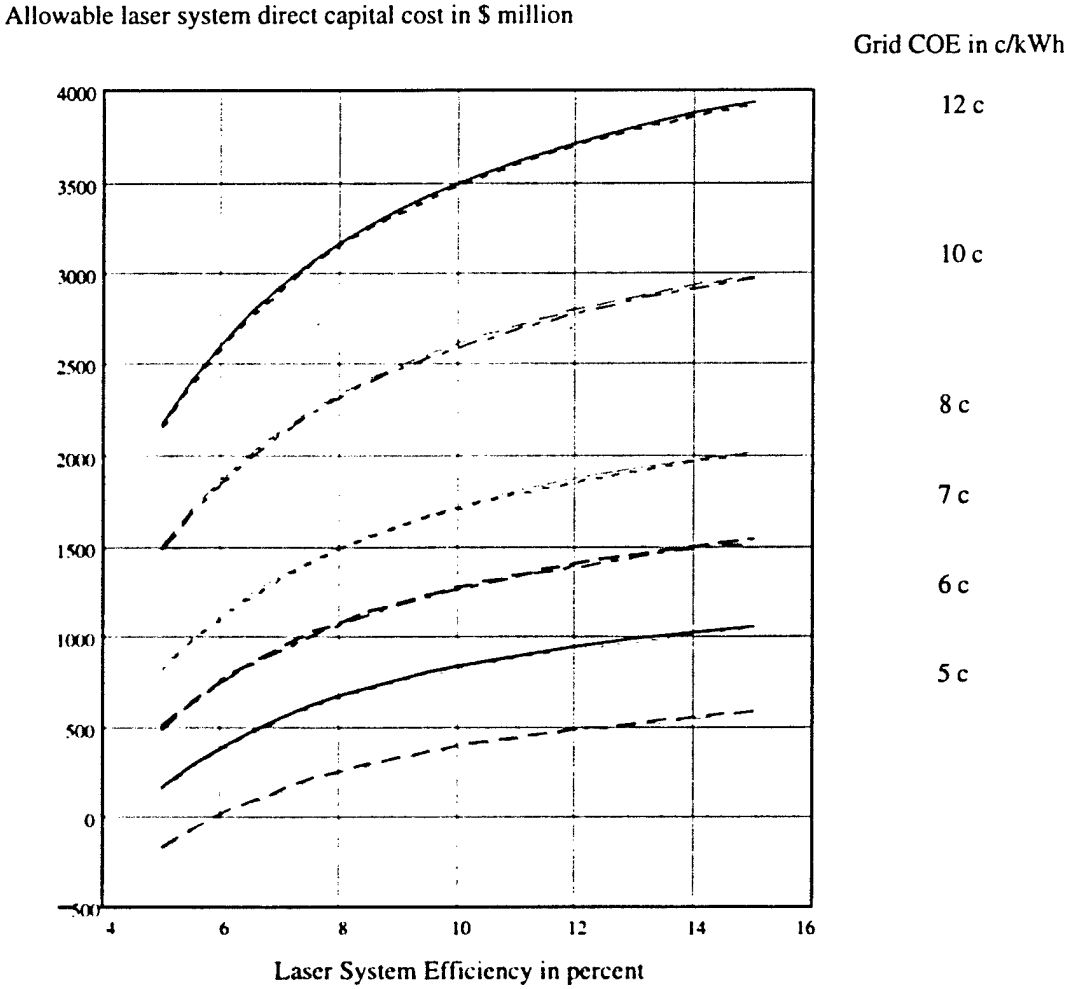

(Upper curve of each pair is for BOP efficiency of 47 percent, lower curve for 45 percent.)

As mentioned, one measure of significant simplification, compared to Sombrero, is that we fix the nameplate rating of the alternator, rather than fix the net electrical production. Although this means the net electrical production varies slightly as the laser efficiency varies, it also means that many variables in the Sombrero analysis become either constants or have such weak functional relationships that they can be assumed to be constants without adversely affecting the conclusions.

The following discussion walks you through the logic:

(1) The plant buys enough electrical power from the grid, at the prevailing COE, to power the laser system. That power comes in through a switchyard and transformer bank.

(2) That electrical power is converted to optical power with an efficiency that varies from 5 to 15 percent.

(3) Either none or all of the laser waste heat is used to replace regeneration steam in the feedwater heaters.

(4) The laser optical power is transmitted to the target with an efficiency assumed to be 0.90.

(5) The target is assumed to absorb 0.70 of the incident energy.

(6) The absorbed energy is fixed at 2.4 MJ.

(7) Energy flow, on a per-pulse basis, prior to this point can be back calculated from the absorbed energy, all they way back to the laser electrical switchyard feed. Below we will get the repetition rate so that these can be converted to power flows from per-pulse energy flows.

(8) The target gain is fixed at 110 and the yield at 110 times the absorbed energy. The absorbed energy and gain are a fixed design point from NRL. Eventually one wants to select the target performance from a gain versus absorbed energy curve, to maximize plant profitability at the highest repetition rate consistent with chamber clearing and consistent with the target net electrical production. It is critical that qualified authorities in IFE target design bless the assumed yield versus absorption curve. Currently we have not a curve, but only a single point. Thus we must vary either the rep rate or the plant output as the laser efficiency changes. Fixing the plant gross output, as we have done, significantly simplifies the calculations.

(9) The coolant is assumed to be solid lithium oxide, as in Sombrero, and the fusion energy multiplication in the blanket is assumed to be 1.08. The tritium-breeding ratio is presumed adequate to support plant requirements and is not considered further. The efficiency of heat transfer from the blanket to the steam generator is assumed to be 1.00.

(10) Rather than consider the details of regeneration and debates over the shape of the left vertical edge of the Rankine s-T curve, we assume a steam cycle efficiency of 0.45 if no laser waste heat is recycled, and 0.47 if the entire laser waste heat is recycled.

(11) The alternator is assumed to have an efficiency of 0.987.

(12) The nameplate rating of the turbine is fixed at 1305 MWe.

(13) The power flow from the target to the turbine can now be back calculated.

The plant repetition rate is calculated from the target fusion power and per-shot energy. The laser power flow (optical output, electrical input, and waste heat) are now back calculated from the fusion target absorbed energy and the repetition rate.

For our assumptions of gross electrical production, target absorbed energy, target gain, and fusion multiplication ratio; the plant repetition rates are 7.21 pps and 6.91 pps for thermal efficiencies of 0.45 and 0.47, respectively. It is likely that both of these values are too high to be consistent with intra-pulse chamber clearing, but that data must await both detailed chamber design and experimental studies, such as proposed by the University of Wisconsin. And, as mentioned, the two values differ because we have only one target design point at present.

The balance-of-plant electrical requirement is assumed to be 55 MWe from Sombrero. This includes everything except the laser system pulse power, magnets, and gas circulation and cooling.

The gross electrical output is the nameplate rating minus the BOP requirement, or 1250 MWe, fixed. The useful net electrical output thus is 1250 MWe minus the laser electrical power input, which varies with the laser efficiency.

The plant is assumed to operate at full power 0.75 of each year during its lifetime. The value of the gross electrical production is 1250 MWe times the COE times 0.75 times the number of hours in a year. This is $82.125 million/yr. for each one cent per kWh COE.

The plant lifetime is assumed to be 30 years. The lifetime total gross value of the plant product is the annual value times the lifetime.

From the annual gross sales value, we must deduct the operating costs and certain capital costs that scale with operating costs. These are discussed in the following section.

Plant Operating Costs

Operating costs are calculated on an operating hourly basis and on an annualized basis.

Cost of laser electricity. In this model the cost of laser electricity has two components: (1) Buying the power from the grid at the COE; plus (2) amortization of the cost of the switchyard that feeds the lasers.

The input power to the lasers can be calculated from the repetition rate of the plant, the absorbed energy at the target, the target absorption fraction, the optical transmission efficiency, and the laser efficiency. This can then be converted to an annual energy requirement by multiplying by 0.75 times the number of hours in a year. And this is converted to a cost by multiplying by the COE.

The capital cost of the switchyard and transformers required to feed the laser pulse power system is a capital cost associated with this power flow which is outside the laser system proper. This cost was scaled from the Sombrero switchyard cost using the "kW to the 0.4 power" scaling rule used in Sombrero. This gives an estimated direct capital cost for the laser switchyard, which can be converted to a total capital cost estimate by

multiplying by (1.0 + 0.93), where 0.93 is the capital cost adder from Bechtel in the Sombrero study. The capital cost adder covers indirect capital costs (design) and estimated cost of money during construction.

Annualized Charge. The next task is to convert this total capital cost into an annualized charge. A constant 6.5 percent cost of money and a 30-year lifetime were assumed. Under these assumptions, the net present value of $1 per year is $13.06. Thus, for every $13.06 of total capital cost of the laser switchyard, an annualized charge of $1.00 is incurred to pay for it. This enters explicitly since it is a strong function of assumed laser efficiency. Applying the capital cost adder of 0.93 for indirect capital costs, then $1.00 of annual cash flow will buy $13.06/(1.0 + 0.93) = $7.05 of direct capital cost. This yields an hourly charge for amortization of the laser electrical switchyard of the estimated direct capital cost divided by $7.05 per dollar and further divided by the number of operating hour per year (24 x 365 x 0.75 = 6570 op hrs/yr.).

The cost of power is X times (COE in cents per kWh / laser efficiency in percent) where X is $16.25 million and $15.56 million for thermal efficiencies of 0.45 and 0.47 respectively. Thus, for a plant with a thermal efficiency of 0.47, a laser efficiency of 7.5 percent, and a COE of 6 c/kWh, the annual power bill for the lasers is 15.56 x 6 / 7.5 = $12.45 million/yr. or $1,895 per operating hour.

In addition, the laser draw is 330 MWe and the switchyard is estimated to cost 70 x $(330/1360)^{.4}$ = $39.7 million direct capital cost. Dividing by $7.05 per dollar gives an annual cost of $5.63 million, or $857 per operating hour.

Cost of Staff. A second operating cost is staff. A staff of 100 was assumed at an annual cost of $120,000 each. This is probably a somewhat high estimate for a 10th of a kind plant, at $12 million per year, or $1,826 per operating hour.

Cost of Consumables. The plant requires routine supplies of gases. An arbitrary value of $500 per operating hour for gases for the laser and $50 per operating hour for chamber gases were assumed. Additionally, $2,000 per day (operating or not) for helium liquefaction and $1,000 for liquid nitrogen every day, whether up or down were assumed. It was assumed that the plant uses $1 million of coolant ceramic and lead per year. The cost of consumables is thus $5.7 million per year, or $869 per operating hour. All of these numbers are arbitrary guesses.

Targets. Previous studies have included the capital cost of the targets as a factor in the plant cost. This complicates the plant capital cost estimate. Further, it is reasonable to assume that the target factory may be replaced or redesigned several times during the lifetime of the plant. The target factory was taken out of the cost plant estimate and viewed as a vendor selling the plant targets on a per-each basis. At $0.25 each, which is an upper limit estimated in the Prometheus study. As with all costs, this can vary, if savings can be effected elsewhere. Since the task here is primarily to define the challenge for the laser designers, the target factory problem has been simply off-loaded to the target fabrication people by allocating them this fixed price per target. The plant uses

24,876 or 25,956 targets per operating hour at 6.91 or 7.21 pps, respectively. At the arbitrary charge of $0.25 each this is $40.9 million or $42.6 million per year, respectively, equal to $6,220 to $6,500 per operating hour.

Maintenance. In addition to gases and targets, things have to be repaired. We allocate funds on an annual basis for several routine maintenance tasks. It was assumed that foils last 1,000 hours, cost $50 each, and there are 4 per amplifier in 65 amplifiers. That is about $13 per hour. Other high voltage equipment was assumed to cost about $1 million per year in spare parts. Optics maintenance was assumed to cost $10 million per year. The chamber was assumed to require $10 million of maintenance every 5 years, annualized to $2 million per year. Maintenance parts total are $13.1 million per year or $1,992 per operating hour. Again, these numbers are arbitrary guesses

Total operating cost is the sum of the following: (1) Cost of laser electricity (including amortization of the switchyard); (2) Cost of staff ; (3) Cost of consumables ; (4) Cost of targets; plus, (5) Cost of maintenance parts. It is also necessary to allocate a decommissioning cost. A fixed charge of $100 million was assumed and allocated as $3.33 million per year or $507 per operating hour.

The allowable total capital cost of the plant is the present value of a dollar per year ($13.06 per assumptions given previously) times the following: (1) Gross value of annual production; less (2) Annual operating costs; less (3) Annual allocation for decommissioning

The allowable direct capital cost of the plant is the allowable total capital cost divided by the total direct cost factor (1 + 0.93 from earlier)

Fixed Costs. From this cost some slight fixed, or nearly fixed, costs must be deducted. From Sombrero: (1) The cost of the reactor was taken as $592.1 million; (2) The cost of land and buildings were taken as $289.6 million; and, (3) The cost of the main turbine and its auxiliaries were taken as $326.3 million. The cost of the main condenser and cooling towers is scaled from Sombrero from the fusion power minus the gross electrical output.

What is left is the allowable direct capital cost of the laser system, which is a function of the laser efficiency, and of the plant thermal efficiency (reflected in waste heat recovery), and of the COE. All of this is what appears in the plot on page 3.

APPENDIX 3

MANAGEMENT PLAN

OCTOBER 26, 1998

Management of the Direct Drive (Laser) Inertial Fusion Energy Program will require coordinating the laser activities of both the krypton fluoride (KrF) and Diode Pumped Solid State Laser (DPSSL) driver programs, as well as answering those technology questions related to chamber development, target design, target manufacture, and target injection. This management function needs to be performed such that the technical activities are focused to answer the critical scientific issues that allow the IFE community to demonstrate to the Department of Energy (DoE) that we are on a path that can lead to an eventual power plant whose cost of energy and cost of electricity (COE) will be acceptable to the power industry. Thus, while developing the best purely technical answer (i.e. highest efficiency) is the goal of a purely scientific endeavor; this program needs to balance pure scientific goals with the economic realities of eventual industrial participants.

It is the latter issue that can complicate the management issue. Scientists are good at criticizing science, but not necessarily, assessing science's ability to promote industrial advances. Therefore, to aid in managing the program a model will be developed which is appropriate for an IFE plant using a DPSSL as a driver, and another model for a plant using a KrF laser as a driver. These models will be used to relate technical characteristics (pulse energy, beam uniformity, laser efficiency, thermal conversion efficiency, plant availability, etc.) to COE for each concept. Thus, the models can help in setting task goals and priorities, as well as, in reviewing progress against agreed milestones. This will help in identifying the need for changes in program strategy, where necessary, i.e. increased resources for critical issues, and in descoping activities that have adequately answered issues, even if the detailed goals have yet to have been met. These models will also be able to assist program managers in best use new information from other programs to assess program progress and to assess the priorities for funding changes, both increases and decreases. The key point to make is that the models can be used to ensure that the KrF and DPSSL programs are both focused on their key issues relative to an IFE fusion reactor, which may be quite different at this phase of development. These models can also be used in an unbiased way to provide oversight to the efforts.

To assure focus, both an oversight panel and an executing technical panel will be established. The oversight panel will be chaired by Gerry (Schafer/LSI), and the membership will consist of Stregack and Monsler (Schafer), a TRW representative, Meier or Logan (LLNL), R. Hunter, Powell (LLNL, D. Hammer (MFE representative), the program managers; S. Bodner and M. Campbell as ex officio members, and a DoE representative. This panel will meet at nominal intervals of four months and can task any and/or all of the other panels for input on particular issues. Either co-chair of the technical panel can bring an issue to the oversight panel for assistance in responding for IFE program to requests for reviews and updates by DoE, various review panels and outside requests from the larger National community.

The executing technical panel will be chaired by the Program Managers, S. Bodner (NRL) and M. Campbell (LLNL). Assisting the technical panel will be the System Modeling Leads, Monsler and Meier. Under the technical panel are also a KrF Team, chaired by S.

Obenschain (NRL) and a DPSSL Team, chaired by S. Payne (LLNL). The present membership of these teams is:

	KrF Team (S. Obenschain-chair)	DPSSL Team (S.Payne-chair)
Lasers	Sethian(NRL) McMahon(Schafer)	Marshall (LLNL) McMahon (Schafer)
Large optics	Lehecka (NRL)	Wallerstein(LLNL)
Physics/modeling	Walters (Schafer)	Krupke (LLNL)

Both teams will be assisted by an independent team which is tasked to address reactor critical technology areas.

Fusion Reactor Team J. Stregack (Schafer/ Chairman)		
Chamber	Barr(Schafer) Logan (LLNL)	Sviatoslavisky(Wisconsin) ? (ORNL)
Pellets	Duke (LANL)	Hendricks (Schafer)
System modeling	Monsler (Schafer)	Meier (LLNL)

By using these panels effectively, we can keep track of both requirements and of the impact of results, in real time and use this mechanism to reformat the program as it evolves to ensure that resources are concentrated on the most pressing and highest impact issues.

Appendix 4

Preliminary Design of Electra 30-cm Amplifier Guide Magnet

1/28/99

Introduction

The Electra amplifier uses an active medium of krypton-fluoride excimer gas lasing at 248 nm. The gas is pumped by two opposing 500 keV electron beams, each of rectangular cross section of 1000 mm wide by 300 mm high. The current density in each beam is 38 amperes per square cm; the pulse top duration is 100 ns and the rise and fall times are about 10 ns.

Each electron beam generates a self-induced magnetic field due to the current flow. If propagating in free space, the spatial peak of these self-fields would be approximately 750 oersteds. The self-fields are modified by return current flows, an effect that is difficult to calculate. Further, the self-fields of the two counter-propagating beams cancel, with varying efficiencies at differing planes within the laser gas cell.

The effect of the self-field upon a single electron beam propagating in free space is to induce the beam to collapse into filaments where the electrostatic repulsion balances the magnetic pinching. Such self-pinching may occur in the cathode-to-anode gap of the electron gun, in the drift space occupied by the hibachi between the anode foil and the pressure foil, and to a lesser extent in the gas cell. The reason for the latter statement is that as the pump beams propagate into the laser gas, the electron paths are increasingly dominated by collisions with the gas molecules (called "blooming") and are less and less affected by the beam self-fields, as the self- fields more and more cancel each other as the beams approach the center plane of the laser gas cell.

There are two well-known techniques for eliminating the self-pinching of the electron beams due to their self fields: the use of non-uniform beams with high current densities in their edges, and the imposition of an external guide field that dominates the self field.

Beams with high edge current densities have been extensively utilized in pumping KrF amplifiers. Despite the elimination of the guide magnetic field, they have not enjoyed wide popularity. This benefit is not free of cost, because the non-uniform beam intensity is created using fast-pulse, high-voltage electrons, an expensive commodity. Secondly, the high edge current densities significantly limit the choice of cathode designs and materials.

External guide fields are usually imposed at one to a few times the peak self-field of the

beams. Because the guide field is orthogonal to the self-field, it is equally effective for inhibiting self-pinching of both counter-propagating electron beams in the amplifier.

The Nike 20-cm amplifier operates at approximately the same beam self field and pulse width as the Electra 30-cm amplifier. The Nike 60-cm amplifier operation has been very stable with a guide field of approximately twice the self-field, or about 1500 oersteds. It has a higher e-beam self-field than Electra will have and operates best with a guide field closer to one times the self-field.

For Electra we anticipate use of a guide field, aligned with B parallel and anti-parallel with the electron trajectories. The anticipated operating field strength is 750 to 800 oersteds and the design maximum value is 1500 oersteds. In all cases the field intensity is characterized at the spatial location corresponding to the peak of the free-space self-field of the electron beam. For rectangular beams of uniform intensity, this is at two points along the extreme edge of the beam. These two points are the midpoints of the short (usually vertical) edges of the beam.

Objectives

The objectives are to design a magnet system with the following properties:
(1) Clearance between the coils for the beam and rear mirror;
(2) A clear aperture within each coil to surround the electron gun box with at least one inch of clearance;
(3) Fit within the clearances available around the gas circulator without redesign;
(4) Compatible with NRL's available cooling water;
(5) Cost, including coils, power supply, and installation, within a fixed budget;
(6) Continuous operation at 1,500 gauss in the region of peak self fields;
(7) Field lines normal to the cathode surface well within 5 degrees;
(8) nominal field uniformity and minimal field bowing;
(9) 10 year service lifetime; and,
(10) An eye-pleasing appearance.

Design: Winding Method

The preliminary design described here is identified as Electra 036S3. This is a variant of Electra 036, the 36th coil design examined for the Electra laser. The "S" designates a "short" variant of design 036 in which the straight coil legs are reduced to 1600 mm from 1700 mm. "S3" indicates the third variant of the 1600-mm short design derived from the basic version 036 design. Three variants were examined for design case 036. Base case 036 is a 1500 Oe magnet with 1700-mm straight legs. Case 036H2000 is a high field variant, at 2000 Oe. 036S3 is a 1600 mm leg-length variant of the 1500 Oe base case.

The design chosen consists of two racetrack oval coils, each with straight legs of 1600

mm, semicircular arc ends, and a vertical clearance between the straight legs of the coils of 950 mm. This length clears the 1550-mm length of the electron gun boxes. These coils are each enclosed in non-ferritic metal cans for protection and support. The cans support the coils so that the faces of the coils are 400 mm apart. This clears the 30-cm optical beam and the rear mirror mount.

Each coil consists of 126 turns of conductor, laid up as seven turns radially and 18 turns longitudinally (in the direction of B and the common axis of the two coils).

There are two common multi-layer coil-winding configurations: solenoid and pancake. A single-layer solenoidal coil is a coil whose length is great compared to its radial thickness. The conductor is wound in a long, thin layer spiraling in the longitudinal direction. Additional layers may be added, forming concentric single-layer solenoids, thereby increasing the inductance and the field strength. Solenoidal coils are characterized by long conductor lengths, very uniform fields, and relatively low labor costs in fabrication.

The alternative is to wind like a watch spring, in a pancake. Practical designs use double pancakes, in which the conductor spirals inward radially to the center of the spiral, transitions to an adjacent plane, and spirals back outward radially to the outside again. Double pancake designs are characterized by relatively shorter conductor lengths, better cooling, and substantially more labor required in winding. The layer-to-layer transitions distort the field so the uniformity is not as good as for solenoid winding. Multiple double pancakes can be stacked up in the longitudinal direction to increase the inductance and field strength.

Another case of the double pancake configuration is a foil-wound coil. In these coils the conductor is a wide, thin foil, which spirals in, jumps over, and spirals out. Foil-wound coils achieve extremely high uniformity on iron-poled magnets, but are difficult to cool. In our design 036 each double pancake has 14 turns, seven radially in each pancake. Each coil has nine double pancakes stacked longitudinally, giving the final configuration of 7 by 18 turns.

Design: Conductor

We chose 0.625-inch square OFHC copper conductor, with a 0.375-inch round diameter center hole for cooling. The outside corners have 0.060 nominal radii, and the resistance is 29.90 micro-ohms per foot. There are several tradeoffs here.

First, it is a standard die size available from a US vendor. This reduces the time delay considerably, both by eliminating the time and cost of making new dies, and saving the shipping delays (or airfreight costs) of shipment from Europe.

Second, we chose a round ID wire. This tends to be more available than square ID wire, and has a lower resistance per foot. However, it is somewhat harder to wind.

The corner radii make installation of insulating tape easier and reduce the risk of epoxy cracking due to stress concentrations at the conductor corners. However, the corner radii increase the coil resistance and decrease the percentage of the coil volume that is useful conductor.

The 3/8-inch ID provides for substantial coolant flow and channels large enough to resist blockage. Conversely, it takes away copper, both increasing the coil resistance and the thermal heat capacity. (The latter is important only in pulsed service.)

Having a large ID dictates a large outside dimension. Using 5/8-inch square conductor provided for adequate conductor area around the cooling bore while keeping the conductor weight to a manageable 1.06 pounds per foot. Small conductor would be too inefficient in use of the coil volume, and larger conductor would be much more labor intensive to wind. Also, as will be discussed below, this conductor size is convenient for winding the coil with no internal splices, which both eliminates potential failure points and substantially reduces winding labor.

There is one downside to the large conductor. For conductors up to approximately 0.45 inches square, the conductor can be fabricated with a ceramic insulation already applied, eliminating one taping step in coil winding. The larger conductor comes bare and requires two independent tape layers be added.

Larger conductor also increases the field distortion caused by the layer-to-layer transition in each double pancake. It also requires fewer turns at higher current per turn. This increases power supply cost, which minimizes at about one ohm load resistance. In this case we have achieved a total load resistance of the order of 0.2 ohms, which isn't too bad. Smaller wire obviously raises the resistance, but it rapidly diminishes the fraction of the total available volume filled with copper, degrading the efficiency of the coil and increasing the cost of insulation.

Each double pancake is wound with not one, but two, conductors. The two are interleaved so each makes three and one-half turns in to the center and an equal number back out in the second layer. This has three effects: (1) it doubles the coolant flow per double pancake, halving the temperature rise; (2) it halves the weight of each individual conductor, so each can be a complete, single piece from the mill, obviating the need for splices inside the coils; and, (3) it at least doubles the field distortion from the layer jumps.
This form of winding is commonly termed "two in hand" since the winder must work conductors in pairs that are wound at the same time.

Adjacent double pancakes are laid into the coil in alternating senses, such that the field distortions from the layer-to-layer transitions tend to cancel each other. The effect is far from perfect, but it helps. This makes the electrical connection of the conductors somewhat more complex, since the current flow through adjacent double pancakes now must be in opposite directions. However, there are standard techniques for handling this.

The length of each conductor is 152 feet, the weight 161 pounds, and the resistance 4.45 milliohms. Double these numbers for each double pancake, and there are 18 conductors (nine double pancakes) per coil. The total weight of each coil is approximately 1500 kg.

Design: Insulation

The 1500 Oe field strength is achieved at 1010 amperes per turn. With all turns wired in electrical series, the voltage is approximately 90 volts. The highest voltage between adjacent turns is 15 volts, taking into account the two-in-hand winding and the alternating sense of adjacent double pancakes.

Each conductor is taped twice. The inner tape has adhesive and bonds to the conductor surface, completely covering it. This tape has high dielectric strength and provides the basic turn-to-turn and turn-to-case insulation of a few kV. Each conductor is then spirally wound with fiberglass tape. This tape serves three functions: (1) It protects the insulating tape during winding; (2) It spaces the turns apart to allow epoxy impregnation between turns; and, (3) And it reinforces the epoxy.

A typical lay-up like this has a spacing of 0.038 to 0.040 inches between adjacent turns radially and between adjacent layers axially within each double pancake.

Additional tape, called "skip tape," binds the turns and layers of each double pancake together, allowing them to be moved from the winding machine to the potting mold. The skip tape does not form a continuous layer. It provides an additional approximately 0.016 to 0.020 inches of spacing between adjacent double pancakes, which improves the penetration of the epoxy into the windings. Around the exterior of the coil the epoxy layer is approximately 0.10 inches thick, providing mechanical protection for the conductors and taping.

Finally, each coil is vacuum impregnated with a compatible, long-life epoxy. The epoxy wets the fiberglass tapes and rigidly holds the conductors in place, preventing them from moving and eventually abrading through the tape insulation. The potting is done in a sealed, vacuum-tight mold. The mold is evacuated and the epoxy is separately degassed under vacuum. Then the epoxy is introduced and flows between the turns, wetting the fiberglass tape. The "vacuum" used is crude, perhaps 10 torr. The result leaves some small voids and bubbles. But at 15 volts per turn, and a peak magnetic pressure of a few pounds per square inch, this is no matter. At higher voltages and/or higher fields, potting becomes much more important.

Design: Terminations

95

Normal practice is to braze together the series connections between conductors inside the coils. These reduce the coil resistance and hence power dissipation. However, we have elected to not do that for the following reasons: (1) Only about two thirds of the connections could be internal with the alternating senses of double pancakes; (2) The lack of internal connections increases the user's confidence; (3) there is adequate space for external electrical connections; (4) in the remote chance of a failure, it is easier to isolate and to bypass; (5) Thus we specify the electrical connections be a minimum of five inches outside the epoxy. And they must be brazed, to minimize added resistance.

In either case, every conductor end is brought out so that the 18 individual conductors in a coil can form 18 parallel cooling channels, allowing maximum water flow and minimum temperature rise. We estimate the water flow to be 46 GPM per coil at 50 PSIG. At a design power of 90.6 kW per coil, the resultant temperature rise is less than 8 degrees C. With 25-degree supply water, the coil temperature is below 35 degrees C. In general, for long service lifetime the maximum conductor temperature should stay below 60 degrees C with the epoxies usually used for this service.

Where each pair of conductors are brazed together externally, a cap is brazed over them as a pair and a single water fitting installed. Thus, for the 18 conductors and 36 conductor ends in each coil, there are 17 water fittings each serving a pair of conductors and two serving single conductor ends. This arrangement nearly halves the number of water fittings per coil, effecting a substantial savings of material and labor, as well as improving appearance.

Design: Field

The whole reason for the project is to achieve the specified field. The following plots show the field at five planes: (a) The centerline of the gas cell; (b) Midway from the centerline to the pressure foil (z = +85 mm); (c) At the pressure foil (z = +170 mm); (d) At the anode (z = +220 mm); and, (e) At the cathode (z = +270 mm).

Plots are given for the total field, the tilt of the field in the x direction, and the tilt in the y direction. Tilts are in degrees from normal. The plotted surface corresponds to the projection of the entire cathode emitting area, 300 mm high (y direction) by 1000 mm wide (x direction).

The uniformity over the cathode is +/-3 percent. The worst case tilt is 1.9 degrees in x, 1.0 degrees in y, and 2.0 degrees total. These plots are attached to the end of the report following the text.

Design: Inductance

Calculating the inductance of racetrack ovals is less straightforward than for circular coils. In this case, it is a challenge not worth solving, since we need only approximate inductances. We approximate the racetrack by a circle where the radius of the circle is chosen so that the mean turn of the circle and the mean turn of the racetrack enclose equal areas. We maintain the same 7 by 18 rectangular cross section for the circular equivalent coil and calculate its inductance using two different approximate methods in Grover's *"Inductance Calculations, Working Formulas, and Tables," Chapter 13, "Self-Inductance of Circular Coils of Rectangular Cross Section."* The two approximations in Grover are 1) treating each coil as a solenoid (long, thin winding) with a correction for the finite radial thickness and 2) treating each coil as a pancake (spiral wound clock spring) with a correction for the finite axial thickness. Both approximations yield a self-inductance of each coil of 43 millihenries and agree within 1 percent.

To estimate the total inductance of the coil pair, we resolve each of our circular approximation coils into two circular filaments according to the method of Lyle. The resultant estimate of the mutual inductance is 10 millihenries, for a total inductance of the pair of 106 millihenries.

The self-inductance is used to check the winding and connections of each coil. The total inductance is used in the power supply design.

These inductances are DC. Because the coils are mounted in conducting cans, which form massive shorted turns around them, the AC inductances are substantially lower. It is usually useful to estimate the AC inductance of each coil as a few millihenries (perhaps 1 to 5) and the AC mutual inductance as zero. Thus the total AC inductance is perhaps in the range of 3 to 10 millihenries. These are only crude guesses.

A disadvantage of the low AC inductance is that power supply ripple currents are increased. Conversely, the ripple currents only heat the containing cans and do not significantly modulate the inter-coil field in the gun and gas regions.

Design: Magnetic Forces

The two coils of the guide magnet attract each other and must be supported apart by spacers. There are many ways to estimate this force: (a) Assume each coil is a single circular filament; (b) Assume each coil is two circular filaments of equal radii (ala method of Lyle); (c) Assume each coil is nine circular filaments, one per double pancake; or, (d) Differentiate the mutual inductance with respect to the axial dimension, z. In all cases we assume the simplification of equivalent circular coils as discussed earlier for inductance calculations.

The *first approach* should give a slightly low answer because it under-weights the contributions of the turns closest to each other. By approximation (a) above one gets 3,970 pounds force, by (b) 4,325 pounds, and by (c) we get 10 percent more than the first, 4,400 pounds. We take the latter as a good approximation of the correct value. Since the method of

97

Lyle was used to estimate the mutual inductance, also assuming two circular current filaments per coil, differentiating with respect to z as in method (d) should be no better than method (b).

Note that in applying approximation (b) here, we did not include Lyle's adjustment to the mean turn radius. Lyle's corrected radius was used, however, in the previous calculation of the mutual inductance. We specify the power supply be capable of 110 percent of the design current. Thus, at maximum power supply current the attraction will be 121 percent of the above value, or 5325 pounds force. We take this as our design basis point.

Figures

Field plots for coil configuration 036S3

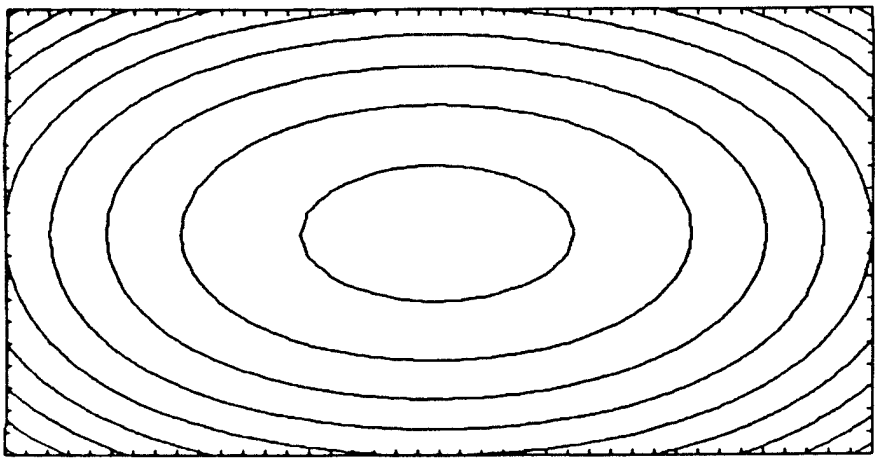

Figure 1 Field at the Cathode Surface 30x100 cm
Center Value = Minimum Value = 1456 Oe
Corner Values = Maximum Values = 1544 Oe
Value at Point of Peak Self Field = 1500 Oe
Contours are 10 Oe
Current = 1010 Amperes

98

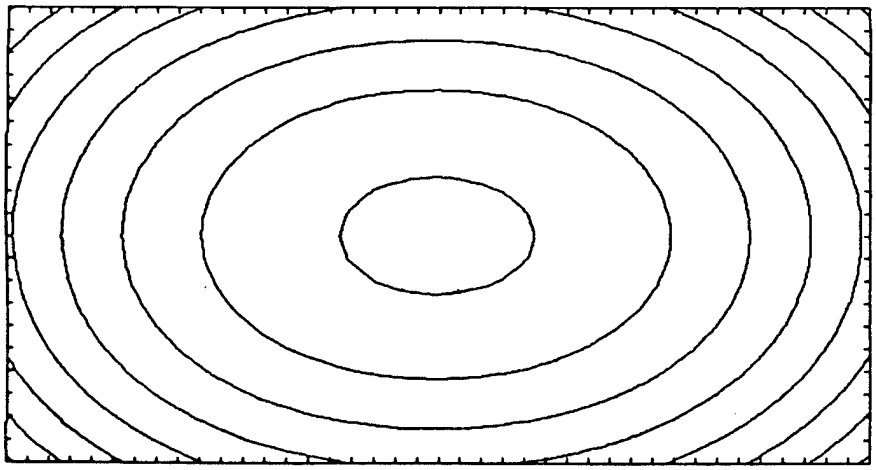

Figure 2 Field at Anode Plane 30x100 cm
Center Value = Minimum Value = 1468 Oe
Corner Values = Maximum Values = 1542 Oe
Contours are 10 Oe

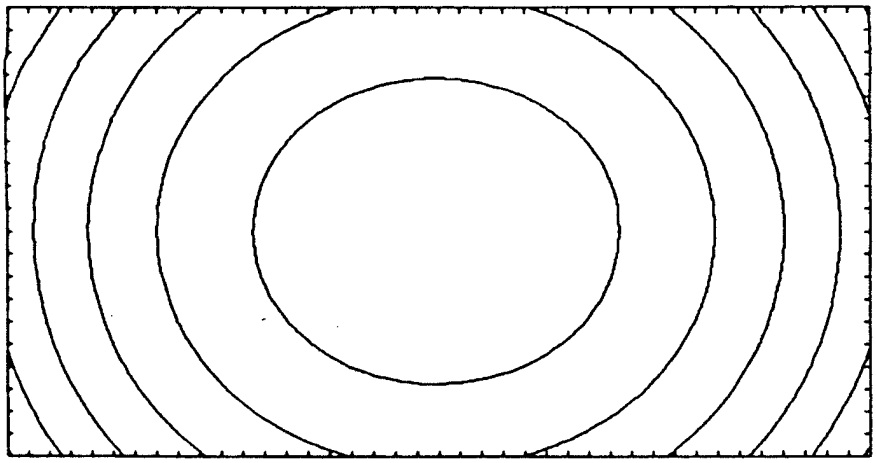

Figure 3 Field at Pressure Foil 30x100 cm
Center Value = Minimum Value = 1773 Oe
Corner Values = Maximum Values = 1530 Oe
Contours are 10 Oe

99

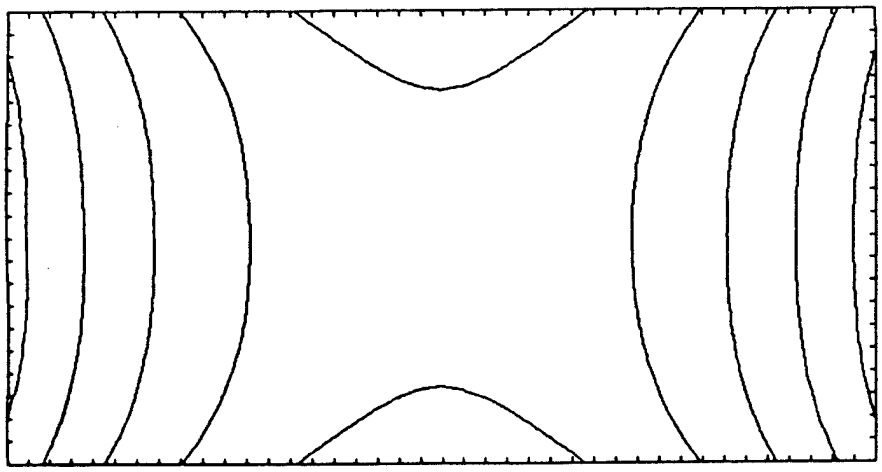

Figure 4 Field 8.5 cm from Cell Center Line 30x100 cm
Minimum Value = Top & Bottom Centers = 1465 Oe
Center Value = 1472 Oe
Maximum Value = Value at Peak Self Field = 1514 Oe
Contours are 10 Oe

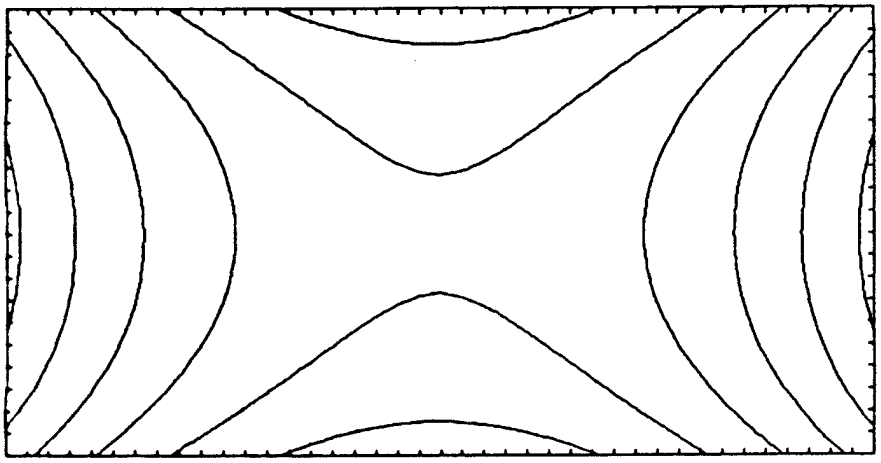

Figure 5 Field at Cell Center Line 30x100 cm
Minimum Value = Top & Bottom Centers = 1454 Oe
Center Value = 1471 Oe
Maximum Value = Value at Points of Peak Self Field = 1513 Oe
Contours = 10 Oe

Field tilt at the Cathode plane for Case 036S3

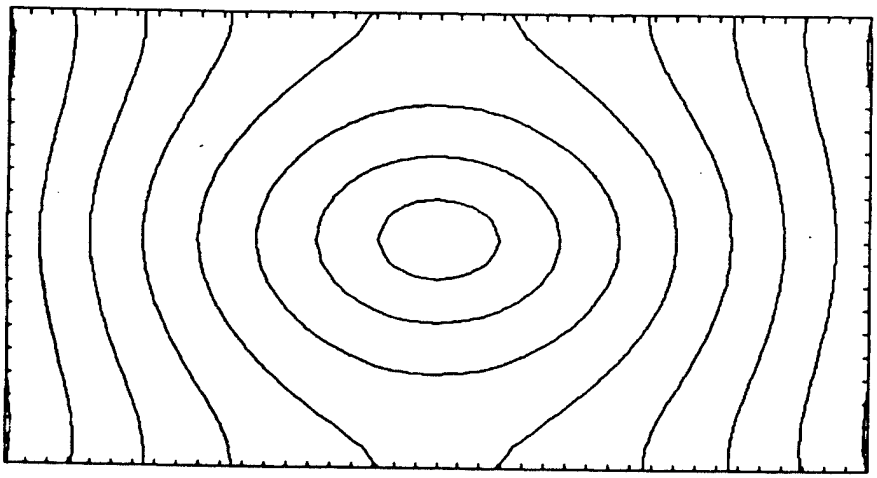

Figure 6 Total Tilt from Normal 30x100 cm
Center value = 0
Corner Values = Maximum Values = 2.0 degrees
Contours are 0.25 degrees

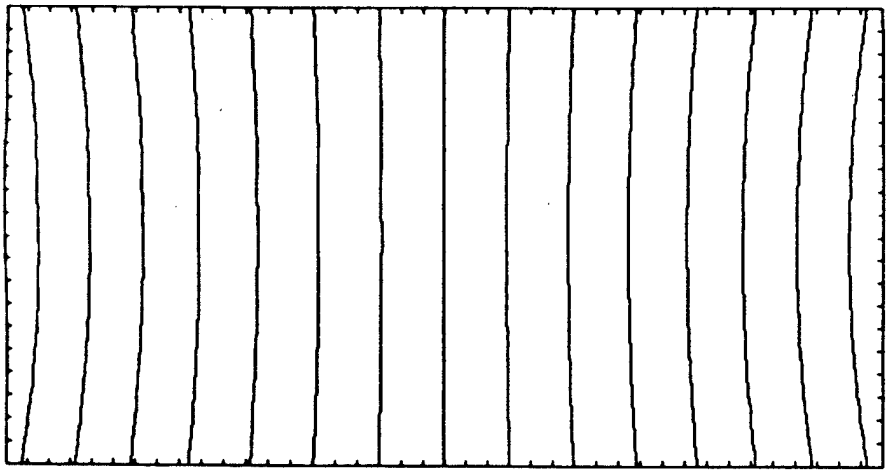

Figure 7 Horizontal Component of Field Tilt 30x100cm
Centerline Value = 0
Edge Values = Maximum Values = +/-1.9 degrees
Contours are 0.25 degree

101

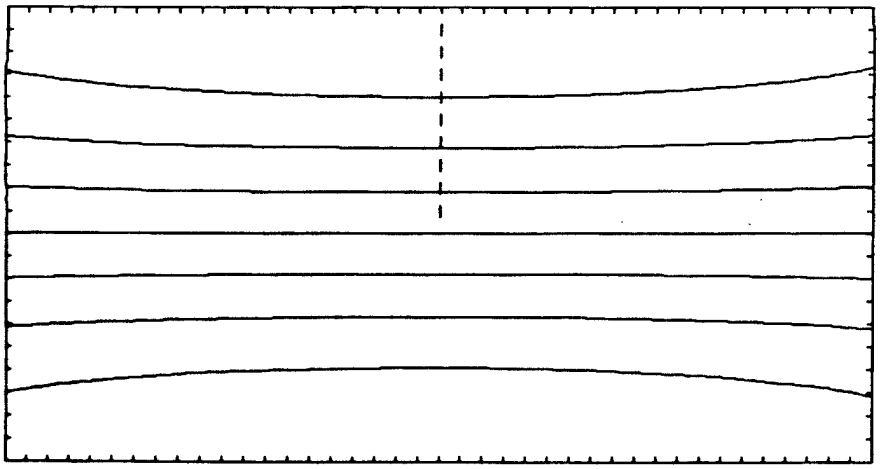

Figure 8 Vertical Component of Field Tilt 30x100 cm
Centerline Value = 0
Top & Bottom Values = Maximum Values = +/-1.0 degree
Contours are 0.25 degrees

102

Appendix 5

Conceptual Design of a KrF Laser Flow Loop

Final Report Presentation to Schafer Corporation

Prepared by
Kiran R. Magiawala, John E. Teodoro and H.W. Behrens
with Inputs from
Peter M. Livingston, Martin P. Wacks and Jon R. Augustson
11 February, 1999

Outline

- Objectives
- Program Deliverables
- Task Description
- Requirements
- Approach to a conceptual design
- KrF Laser Flow Loop Schematics
- First Iteration on the flow loop configuration
- Key Design Features
- Characteristics of Subsystems
  - laser cavity; upstream/downstream acoustic attenuators; thermalizer; heat exchanger; flow loop ducts and bends; blower; gas handling system
- Beam quality performance projection
- Conclusions
- Recommendations
- Back-up viewgraphs

Objectives

- To develop a conceptual design of the flow loop for KrF laser for Inertial Fusion Laser (IFL) facility including a system comprising of components including

  - blower, heat exchanger including cooling fluid subsystem, thermalizer, acoustic attenuators, flow loop ducting including test section and transition duct, flow loop thermal conditioning system, flow loop facility vacuum system, gas fill and thermal conditioning system, flow loop back-fill system, gas leak detection and room air recirculation safety subsystem

Program Deliverables

- Deliver a final report to customer describing the conceptual design of the KrF flow loop for Inertial Fusion Energy facility
- Submit the final report in form of a viewgraph format

Task Description

- Task 1: Based on system specifications and past experience, develop a conceptual design of the KrF laser flow loop system
- Task 2: Identify safety issues and mitigating technologies for operating the flow loop
- Task 3: Prepare a final report

Requirements

- Optical cavity gain height (flow direction; Lf): 30 cm
- Optical cavity gain width (e-beam axis direction; Lp): 30 cm
- Optical cavity gain length (optical direction; Lo): 100 cm
- Laser gas composition: χAr/χKr/χF2 0.6594/0.3375/0.0031
- Laser gas temperature: 323.15 °K
- Laser gas pressure: 1.1033x10^(05) N/M^2 (16 psia)
- Pulse repetition frequency: 5 Hz
- Beam quality budget (x diffraction limit): goal of <1.20
- Energy deposited into optical cavity by a two-sided e-beam per pulse: 9780 Joules

Approach to a Conceptual Design

- Over the past 18 years, TRW has designed, built and characterized five pulsed laser flow loops for fusion and communication devices
- Design tools developed under these programs and under TRW internal funded research include
  - Fluid mechanical, acoustical and thermal analysis based computational codes (PLACATE and its companion codes) validated by experimental results
  - Experimentally validated empirical design formulas for extending results for a new design
- Develop a conceptual design of the pulsed laser flow loop by compiling and exercising a TK Solver-based design tool
- Choose and integrate proven flow loop elements in the design as and where possible
- No mechanical, structural, thermal and vibrational analyses are were conducted for this conceptual design here

KrF Laser Flow Loop

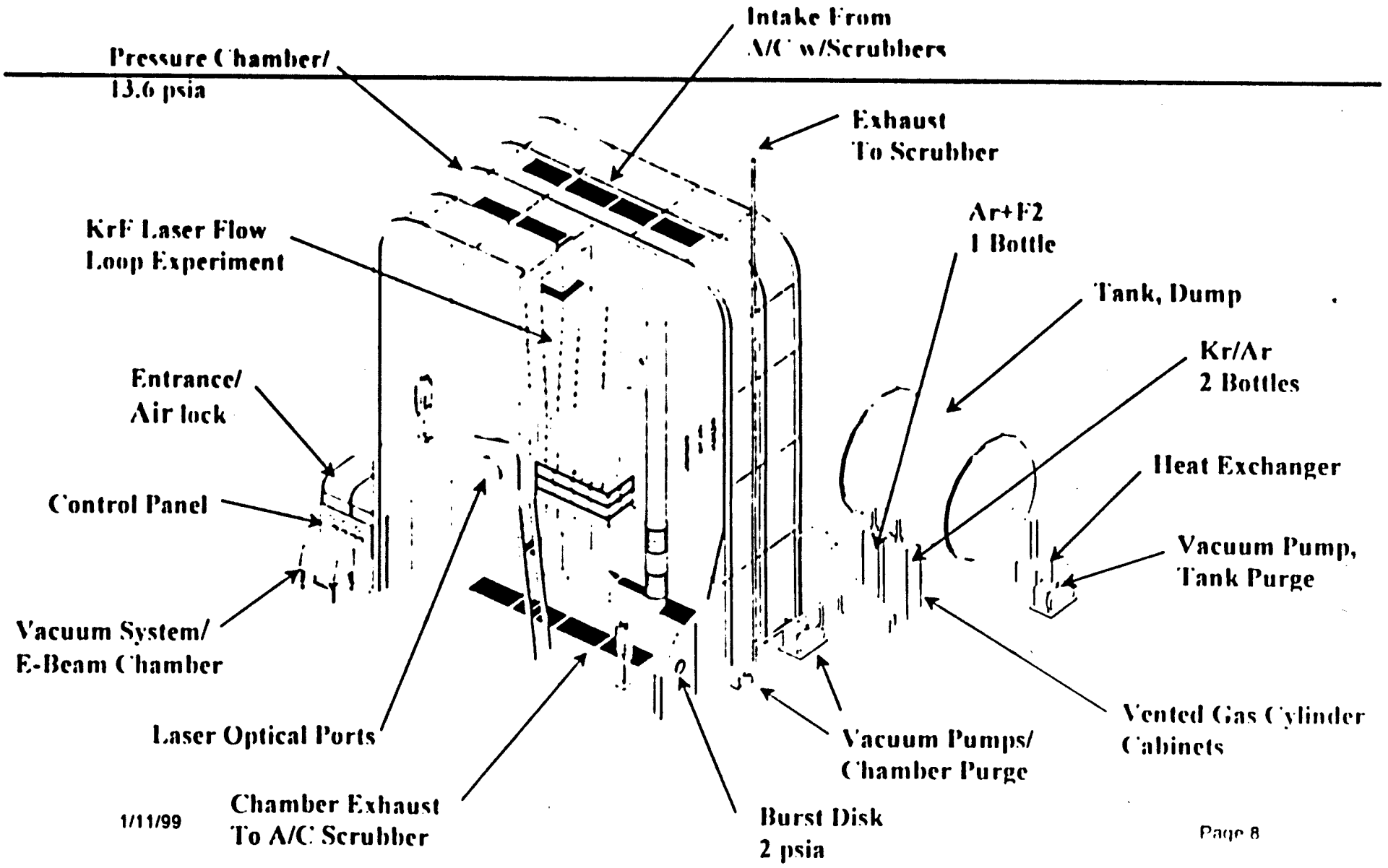

KrF Laser Flow Loop

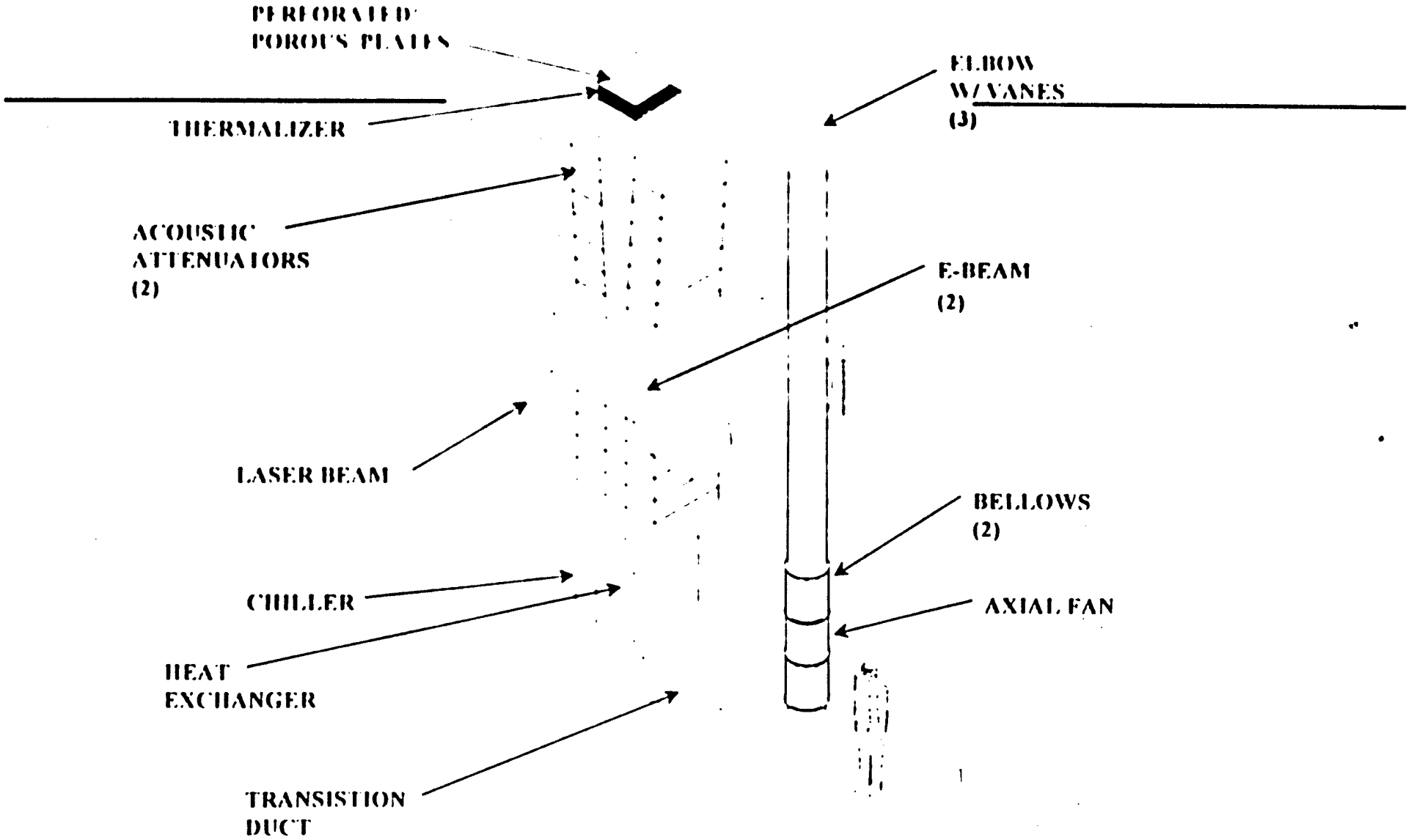

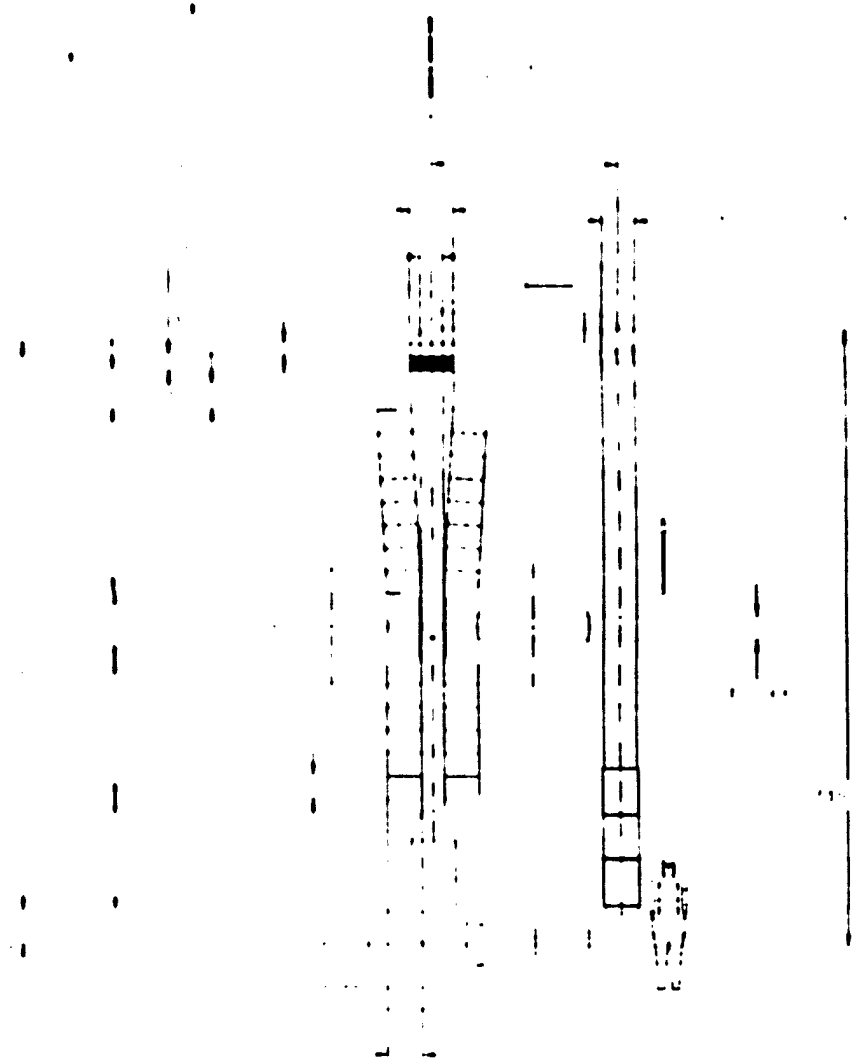

First Iteration on the Flow Loop Configuration

- TRW flow loop configuration concept was submitted to the customer for the review
- In order to install the flow loop in an existing laboratory, the customer recommended a few configuration based changes
  - Incorporate in the flow loop a detailed conceptual design of the e-beam including its magnets
  - Provide provision for a human factor-based height dimension to operate the e-beam hardware
  - Change from TRW proposed in-line heat exchanger configuration to a heat exchanger in the side leg of the flow loop to accommodate the overall laboratory height-based constructional constraint for flow loop integration
- These changes call for digging a ditch in the laboratory
- None of these changes affect the performance of the device
- See the enclosed revised schematics provided by the customer

First Iteration on the Flow Loop Configuration

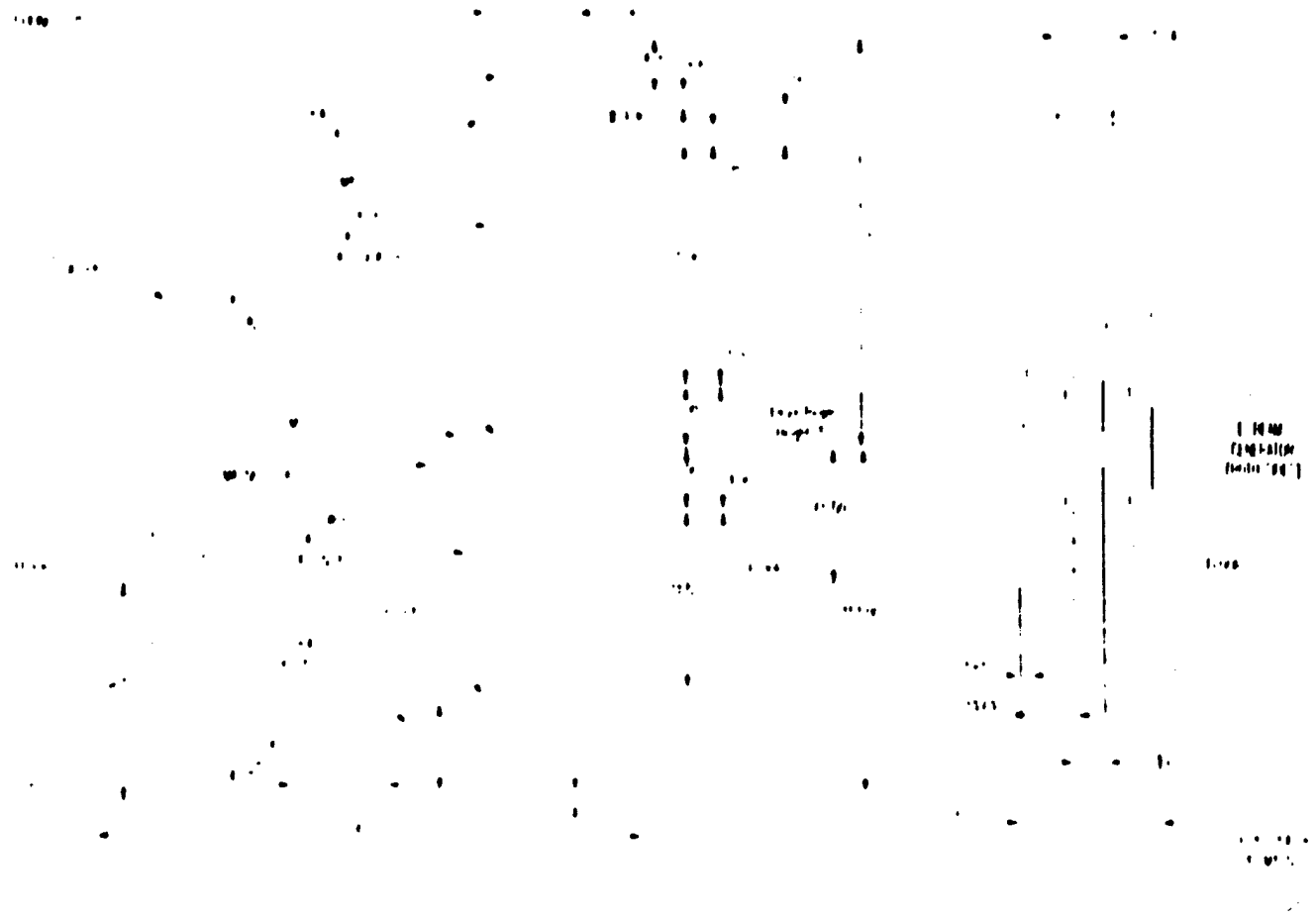

First Iteration on the Flow Loop Configuration

Key Design Features

- "End-Fed" loop configuration - permits easy integration with blower and other facility-based requirements
- Simple upper flow loop bend - conventional design that uses porous plate flow elements to achieve flow uniformity at minimum pressure drop
- Blower - vane and tube-axial type fan with inline direct-driven compact arrangement of vanes with laser gas compatible driver motor/casing that prevents any leakage of pressurized laser gases and can hold very low loop fill-up vacuum
- Canted thermalizer - provides damping of temperature non-uniformity in flow by canting entropy waves so entropy wave contribution to beam quality be reduced by phase averaging
- Boundary layer suction - distributed and concentrated suction in upstream acoustic attenuator to minimize boundary layers entering the cavity

Key Design Features (continue)

- Upstream acoustic attenuator - area contraction accelerates flow to reduce boundary layer growth
- Downstream acoustic attenuator - a straight duct type simple configuration
- Heat exchanger placement - proven finned-tube configuration that minimizes pressure drop-based blower load and hear transfer-based heat load to the flow loop
- Gas handling related safety issues and mitigating technologies for operating the flow loop - addressed by recommending use of an enclosed vacuum cell around the flow loop and laser gas supply cabinets, an airlock provision at the entrance to flow loop enclosure, room and breathing air circulation within the loop enclosure as per in clean rooms, a dump tank for sudden evacuation of the loop gases and a building exhaust scrubber

Characteristics of Subsystems
Laser Cavity

- Optical cavity gain height (flow direction; Lf): 30 cm
- Optical cavity gain width (e-beam axis direction; Lp): 30 cm
- Optical cavity gain length (optical direction; Lo): 100 cm
- Laser gain volume 90 liters
- For constant volume given energy input per pulse, Δp is 10.45 psia
- Leftover (after suction) boundary layer multiplication factors to each dimension 1.1
- Laser head volume 119.79 liters
- Flush factor 2.5
- Laser pulse rate of 5 Hz
- Laser gas velocity is 4.125 m/sec
- Laser gas flow rate of 3172.76 cfm
- Number of inter-pulse acoustic transients are 2.75
- E-beam placement with magnet coils was estimated and will be verified in the follow-on phase of the program

Characteristics of Subsystems
Upstream & Downstream Acoustics Attenuators

- Woven stainless steel cloth screens sandwiched between 50% open perforated plates with 0.060 inch diameter holes
- 316 Stainless steel 8 μ open corded fiber-based acoustic packing material with void fraction φ of 0.99 (or packing density of 1%) and permeability k of 4 x 10^(-05) m^2
- Select upstream attenuator contraction of 3° half angle and downstream attenuator with no divergence
- For conservative design select the following dimensions
  - Upstream attenuator (X/H) of 8
  - Downstream attenuator (X/H) of 6
  - Depth of the attenuators was 50 cms
  - Length of each partitioned cell in the attenuator 33 cms
- During the follow-on phase of the program, validate the attenuator design using PLACATE and its companion codes

Characteristics of Subsystems
Boundary Layer Suction

- 15% of the flow will be extracted through upstream attenuators for boundary layer control
- Both distributed (in all compartments) and concentrated suction (in the first compartment) will be employed
- Details on blowers (size and capacity) to be used will be addressed in the follow-on phase of the program after exercising appropriate computational codes

Characteristics of Subsystems
Thermalizer

- Thermalizer width 0.64 m
- Flow velocity upstream of the thermalizer 2.13 m/sec
- Hydraulic diameter of the honeycomb 0.001608 m
- Honeycomb solidity 0.12
- Flow direction length of a single slab of the honeycomb 0.01778 m
- For $\Delta Ti/\Delta To$ of 1000 (assume/verify) and ΔTi of +/- 2° K (assume/verify), total of 7 honeycomb slabs will be required
- Pressure head loss based on laser cavity gas velocity are 5.74 but 21.59 based on velocity upstream of the thermalizer
- Overall heat transfer coefficient will be 47.82 watts/m^2
- Overall length of the thermalizer including six of 0.01778 m gaps is 0.231 m
- 3° cant to flow (assume/verify)
- Choose and verify use of Aluminum or Nickel honeycomb material

Characteristics of Subsystems
Heat Exchanger

- The preliminary inputs were obtained from the original supplier of the heat exchanger Russell Coil Company
- Total heat load to be removed including gas heat and pump power (calculated through iterations) was estimated at 51019 Watts
- For a water carrying finned circular tube with Aluminum WK 20-12-09-36 core fitted in a 0.33 x1.1 m^2 cross section, a twelve pass version was selected to fit the flow direction dimension of 1.32 m
- For 40gpm room temperature water flow, outlet water temperature was estimated at 150 F
- ΔP gas side was estimated at less than 13 heads (based on laser cavity flow conditions
- Δp water side was estimated at less than 2 psid
- Detailed verification of these numbers will be conducted in the follow-on phase of the program

Characteristics of Subsystems
Flow Loop Ducts and Bends

- At the top end of the loop, downstream of the simple ducted header bend, use a Pall corporation Grade T 0.014 inch sintered-wire porous plate sandwiched between 50% open perforated metal with 0.064 inch diameter holes to provide uniform flow across the thermalizer
- Pressure drop across this assembly (including header insertion losses) are estimated at 15 heads based on laser cavity flow conditions
- One bellow on each side of the blower will be used to isolate blower vibration getting transmitted to the other portions of the loop
- Total of 6 miscellaneous pressure head losses in the loop include wall viscous losses, 2 downstream 90° turn losses and losses in bellows

Characteristics of Subsystems
Blower

- Total number of head loss in the loop (based on laser cavity flow velocity) was estimated at 37
- The safety factor of 2 was used on this number giving blower pressure requirement of 5.53 inch of water (10.61 Torr or 0.21 psid) at the loop flow rate of 3172.76 cfm
- Select a compact arrangement that prevents leakage of pressurized laser gas and can hold a very low fill-up vacuum
- Vane and tube-axial type B-LB fan with inline direct-drive (@3600 RPM) was selected from Howden Buffalo Corporation catalog
- Blower HP was estimated at 2.84 HP and with electric conversion efficiency of 55%, plug power of 5.17 HP will be needed

Characteristics of Subsystems
Gas Handling System

- F2 gas will be supplied in a premixed condition with Ar in a separate bottle at 1 psia with χAr=0.95 and χF2=0.05.
- Ar/F2 bottle and a separate Kr bottle will be kept in an individual gas supply cabinet (~ 750 Torr) and they will be connected to a scrubber.
- Flow loop will be housed in a vacuum enclosure (~750 Torr) and will be connected to a scrubber.
- Air lock provision will be provided at the entrance to the flow loop vacuum enclosure.
- Flow loop vacuum pump will be connected to a scrubber.
- Room/breathing air circulation (ceiling entrance/floor exit type clean room approach) equivalent to at least 10 times the breathing capacity of four personnel. Connected the room exhaust to a scrubber.

Characteristics of Subsystems
Gas Handling System (continue)

- Scrubber with activated Alumina or KCO3 + activated Charcoal with filter operational indicators.
- For emergency dump of the flow loop gases, provide a dump tank with ~ 12.3 times the volume of the flow loop itself. Flow loop volume was estimated at ~ 7230 liters. A dump tank with 10 ft in diameter and 40 ft in length will be sufficient.
- Keep this dump tank evacuated to hard vacuum during the test.
- This dump tank can also be used to fill the flow loop. For this operation, incorporate gas heaters for heating premixed laser gases.

Beam Quality Performance Projection

- Calculate beam quality estimates using Marechal's approximation
  - BQ = exp [1/2 ($\Delta\phi$rms)^2]
  - $\Delta\phi$rms = 2 x π x (L/λ) x β x (ρ/ρs) x ($\Delta\rho/\rho$)rms
  - L optical length, 2.2 m for a double pass resonator
  - λ wavelength, 248 nm
  - β Gladstone-Dale coefficient, 0.00028 (assume/verify)
  - ρ gas density, 2.2481 kg/m^3
  - ρs gas density at standard conditions, 2.2753 kg/m^3

Beam Quality Performance Projection (continue)

- Based on TRW's past design and experimentally validated database
  - $(\Delta\rho/\rho)$rms of 0.2077x10^(-05), for acoustic variations due to baseline flow disturbance at cavity flow Mach number of 0.0144
  - The scale Λ of these disturbances is estimated at 0.165 m
  - $(\Delta\rho/\rho)$rms of 1.2378x10^(-05), for thermal variations doe to baseline flow disturbances
  - $(\Delta\rho/\rho)$rms of 31x10^(-05), for window thermal boundary layer effect at ΔT (wall to window) of 10° K (assume/verify) with optical path length of 0.02905 m (2 x No of passes x thermal boundary layer thickness of 0.0073 m)
  - $(\Delta\rho/\rho)$rms of 1.5x10^(-05), for leftover acoustic disturbances because of the limitations of the attenuator design
  - $(\Delta\rho/\rho)$rms of 1.5x10^(-05), for entropy disturbances coming from the interaction of the leftover acoustic waves with the upstream thermalizer

Beam Quality Performance Projection (continue)

- Calculate individual $\Delta\phi$rms for each elements as 0.0320, 0.1909, 0.0631, 0.2313 and 0.2313 respectively
- For final numbers, estimate a square root of the sum of the squares for these $\Delta\phi$rms numbers to account for their incoherence and use this number, 0.3853, to calculate the final beam quality
- Final beam quality was estimated at 1.1
- For this case, $\Delta\phi$rms/ϕ or $\Delta\lambda$rms/λ was estimated at 0.0613 or 1/16
- These numbers will be verified in the follow-on phase of this program

Conclusions

- Based on the past experience of TRW, using requirements provided to us, a pulsed KrF laser flow loop was designed and medium homogeneity performance of this pulsed flow loop was verified by analysis
- For this conservative design of the pulsed laser flow loop, proven flow components were selected
- The safety issues and mitigating technologies for operating the flow loop were addressed by recommending the use of
  - an enclosed vacuum cell around the flow loop and laser gas supply cabinets
  - an airlock provision at the entrance to flow loop enclosure
  - room and breathing air circulation within the loop enclosure as per in clean rooms
  - A dump tank for sudden evacuation of the loop gases and
  - a building exhaust scrubber

Recommendations

- Resurrect the TRW computational code PLACATE (including its companion codes) that addresses in detail the acoustics, fluid mechanics and thermal issues associated with operation of a pulsed laser flow loop

- Incorporate any additional constructional and packaging related constraints that addresses the final placement of the flow loop at the venue of customer's choice and modify configurations of various flow loop elements accordingly

- Conduct final mechanical, structural, thermal and vibrational analysis and design of the flow loop that addresses various materials and operational issues involved

- Circumstances permitting, accomplish these tasks before the end of the month of September 1999

Back-Up Viewgraphs

- Physical and operational parameters of TRW designed excimer laser flow loops
- NRL excimer laser gas flow subsystem design by TRW
- Medium Homogeneity Measurements in a Repetitively Pulsed Excimer Laser, TRW AIAA Paper No. 90-1796
- Outputs files for TK solver parametric routines
  - Flow loop pressure drop calculations
  - Flow loop performance calculations
- Estimate of the optical quality of the image

TRW Space & Technology Group

PHYSICAL AND OPERATIONAL PARAMETERS OF TRW DESIGNED EXCIMER LASER FLOW LOOPS

TRW

PARAMETER	TRW EXCIMER LASER FACILITY	REP-RATE LASER FLOW LOOP	NRL XeCl FLOW LOOP
OPTICAL CAVITY LENGTH, CM	60	70	188
OPTICAL CAVITY WIDTH, CM	12.5	20	6.5
OPTICAL CAVITY HEIGHT, CM	12	20	12
CAVITY VOLUME, LITER	9	28	14.7
GAIN LENGTH, CM	50	50	120
GAIN WIDTH, CM	7.5	10	6.5
GAIN HEIGHT, CM	10	15	11
GAIN VOLUME, LITERS	3.75	7.5	8.6
FLOW LOOP VOLUME, LITERS	3285	4020	2830
EXPANSION RATIO	5.2	4.5	2.0
VOLUME FLOW RATE, LITER/SEC	4720	2830	2256
LASER GAS DILUENT	Ar	Ne	Ne
LASER GAS PRESSURE, ATM	3	4	4 nom. 5 max.

TRW Space & Technology Group

PHYSICAL AND OPERATIONAL PARAMETERS OF TRW DESIGNED EXCIMER LASER FLOW LOOPS (CONCLUDED)

TRW

PARAMETER	TRW EXCIMER LASER FACILITY	REP-RATE LASER FLOW LOOP	NRL XeCl FLOW LOOP
LASER GAS TEMPERATURE, °K	300	300	300
PULSE TIME, μSEC	-	-	0.20
PULSE REPETITION FREQUENCY, Hz	320	70	50
BEAM QUALITY BUDGET, X DL	<1.5	<1.5	<10
UPSTREAM SUPPRESSOR LENGTH / CAVITY HEIGHT	3.3	2.69	10.0
DOWNSTREAM SUPPRESSOR LENGTH / CAVITY HEIGHT	3.3	6.65	3.8
MAIN FLOW BLOWER POWER, HP	89.2	55.7	25
BOUNDARY LAYER SUCTION BLOWER POWER, HP	20	-	-
CAVITY FLOW MACH NUMBER	0.20	0.044	0.022
CAVITY FLOW VELOCITY (M/S)	65.5	20	10

Report Number TRW 49553-6001-UT-00

EXCIMER LASER GAS FLOW SUBSYSTEM DESIGN

H. W. Behrens
TRW Space and Technology Group
One Space Park
Redondo Beach, CA 90278

30 August 1988

FINAL REPORT

Contract Number N00014-86-C-2344

Prepared for

NAVAL RESEARCH LABORATORY
4555 Overlook Avenue, S.W.
Washington, DC 20375-5000

Unclassified

SECURITY CLASSIFICATION OF THIS PAGE

REPORT DOCUMENTATION PAGE

1a REPORT SECURITY CLASSIFICATION: Unclassified	1b RESTRICTIVE MARKINGS
2a SECURITY CLASSIFICATION AUTHORITY	3 DISTRIBUTION/AVAILABILITY OF REPORT
2b DECLASSIFICATION/DOWNGRADING SCHEDULE	
4 PERFORMING ORGANIZATION REPORT NUMBER(S): 49553-6001-UT-00	5 MONITORING ORGANIZATION REPORT NUMBER(S): N00014-86-C-2344
6a NAME OF PERFORMING ORGANIZATION: TRW Space & Defense; 6b OFFICE SYMBOL (If applicable):	7a NAME OF MONITORING ORGANIZATION: Naval Research Laboratory (6540)
6c ADDRESS (City, State and ZIP Code): One Space Park, Redondo Beach, CA 90278	7b ADDRESS (City, State and ZIP Code): 4555 Overlook Ave., S.W., Washington, DC 20375-5000
8a NAME OF FUNDING/SPONSORING ORGANIZATION; 8b OFFICE SYMBOL (If applicable): 1232:DL	9 PROCUREMENT INSTRUMENT IDENTIFICATION NUMBER
8c ADDRESS (City, State and ZIP Code): 4555 Overlook Ave., S.W., Washington, DC 20375-5000	10 SOURCE OF FUNDING NOS: PROGRAM ELEMENT NO; PROJECT NO; TASK NO; WORK UNIT NO
11 TITLE (Include Security Classification): Excimer Laser Flow Subsystem Design (U)	
12 PERSONAL AUTHOR(S): [illegible]	
13a TYPE OF REPORT: [illegible]	13b TIME COVERED: FROM 9/19/86 TO 6/30/88
14 DATE OF REPORT (Yr, Mo, Day): 1988 Aug 30	15 PAGE COUNT
16 SUPPLEMENTARY NOTATION	
17 COSATI CODES: [illegible] SUB GR	18 SUBJECT TERMS (Continue on reverse if necessary and identify by block number): Excimer Laser; Flow Subsystem; Flowing Gas Laser; Flow Loop; Acoustic Attenuation; Medium Homogeneity

19 ABSTRACT (Continue on reverse if necessary and identify by block number):

[illegible] flow subsystem for an XeCl laser with an optical cavity of [illegible] centimeters has been designed operating at 60 psig. The flow [illegible] with a projected medium contribution to beam quality of less than [illegible] subsystems include controls, heat exchanger, thermalizer and a laser gas [illegible]. The fabrication drawings are ready for sign-off except for the [illegible] because the blower will have to be ordered at the beginning of the [illegible] blower spec is included in the final report. The stress analysis [illegible] the flow loop at 60 psig has been completed and signed off.

20 DISTRIBUTION/AVAILABILITY OF ABSTRACT: UNCLASSIFIED/UNLIMITED ☐ SAME AS RPT ☐ DTIC USERS ☐	21 ABSTRACT SECURITY CLASSIFICATION: Unclassified
22a NAME OF RESPONSIBLE INDIVIDUAL: [illegible]	22b TELEPHONE NUMBER (Include Area Code): (202) 767-2813; 22c OFFICE SYMBOL: 6540

DD FORM 1473, 83 APR EDITION OF 1 JAN 73 IS OBSOLETE

Unclassified

SECURITY CLASSIFICATION OF THIS PAGE

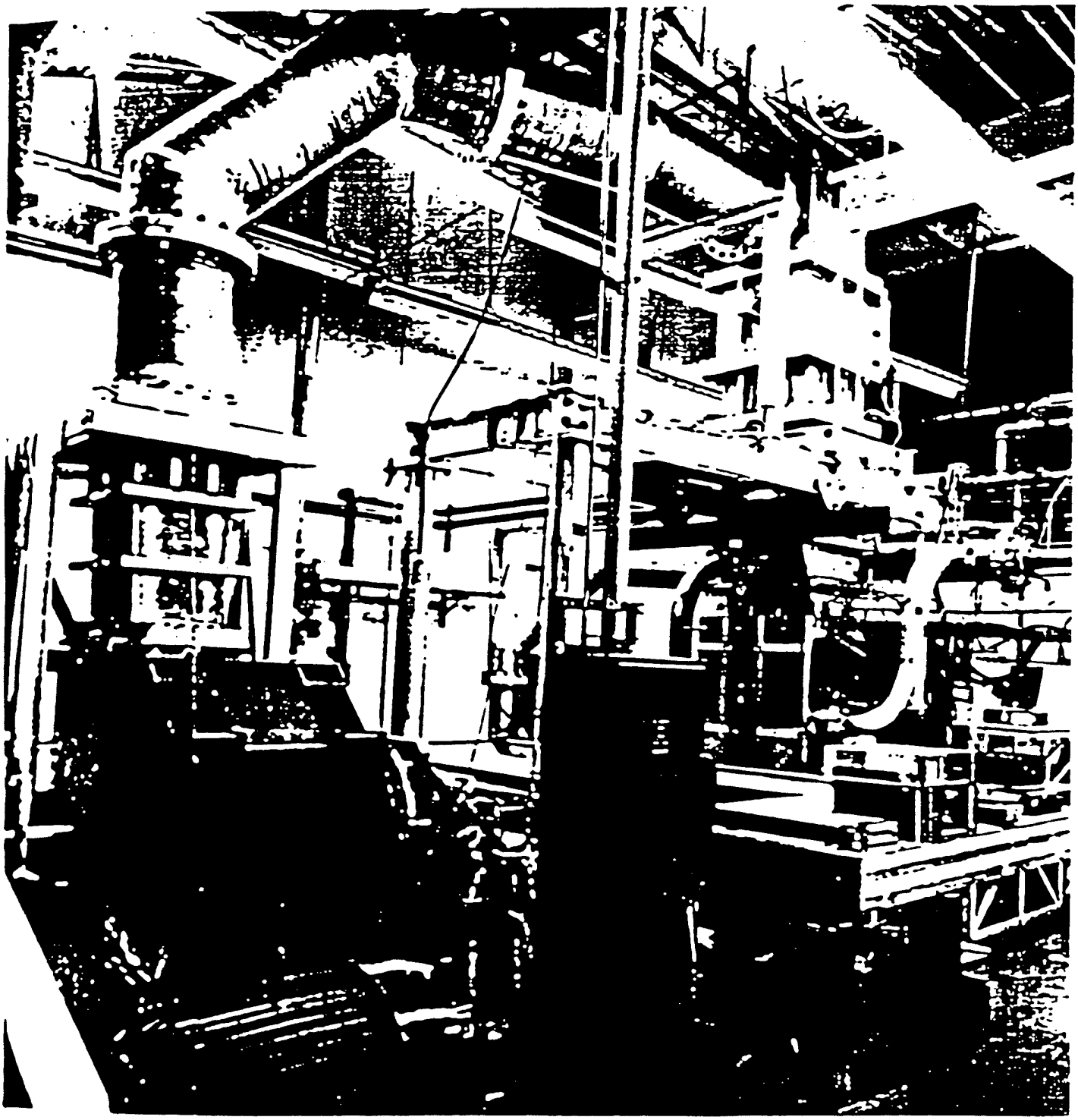

Figure 1.1. TRW EMRLD Excimer Laser Flow Loop.

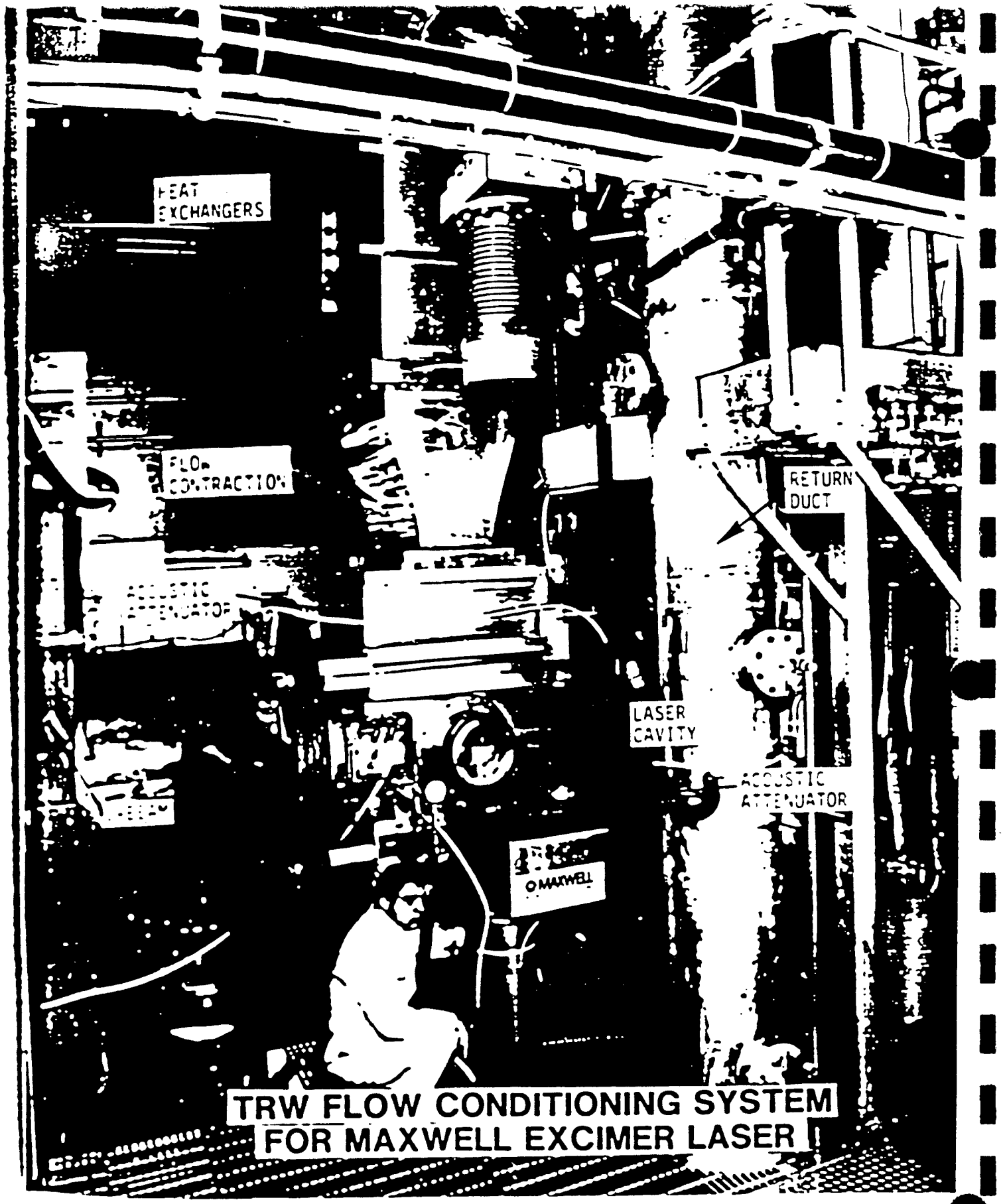

Figure 1.2. Maxwell Laboratories Excimer Laser Flow Loop.

Final Acoustic Analysis

The PLACATE simulation code has been used to investigate medium homogeneity for the modified flow loop design. The modifications, shown in Figure 3.14, include:

- an increase of the distance between upstream and downstream absorbers from 50 cm to 90 cm,
- the addition of one absorber to the upstream absorber section and the removal of two downstream absorbers,
- an increase of the cavity width from 10 cm to 12 cm,
- an increase of the depth of the absorbers from 10 cm to 18 cm,
- and, an increase of the mean flow speed from 8 m/sec to 10 m/sec.

Some results of the simulation are presented in Figures 3.15 and 3.16. The simulation was run for the first 20 milliseconds following energy deposition in the laser cavity. The position axis represents the distance from the center of the laser cavity, normalized by the 12 cm cavity width.

The evolution of the pressure distribution in the system is shown in Figure 3.15. The linear scale that is used has the result that at early times, the large amplitudes near the cavity are not legible. However, the efficiency of the absorbers is such that after about one half of a pulse period, no pressure disturbances are even discernable in the figure. The pressure fluctuations are plotted using a log scale in Figure 3.16. It is observed that the attenuation rate over one pulse period, is sufficient to reduce RMS density inhomogeneities to acceptable levels (RMS $\Delta\rho/\rho < 10^{-5}$).

Multiple Pulse Analysis

A simulation of two pulses was performed to determine the residual effects that may occur during steady state operation. Figures 3.17 - 19 contain the results of the two-pulse simulation. The pressure and temperature disturbances are presented in Figures 3.17 and 3.18. For the pressure distribution, no change is discernable between the two pulses.

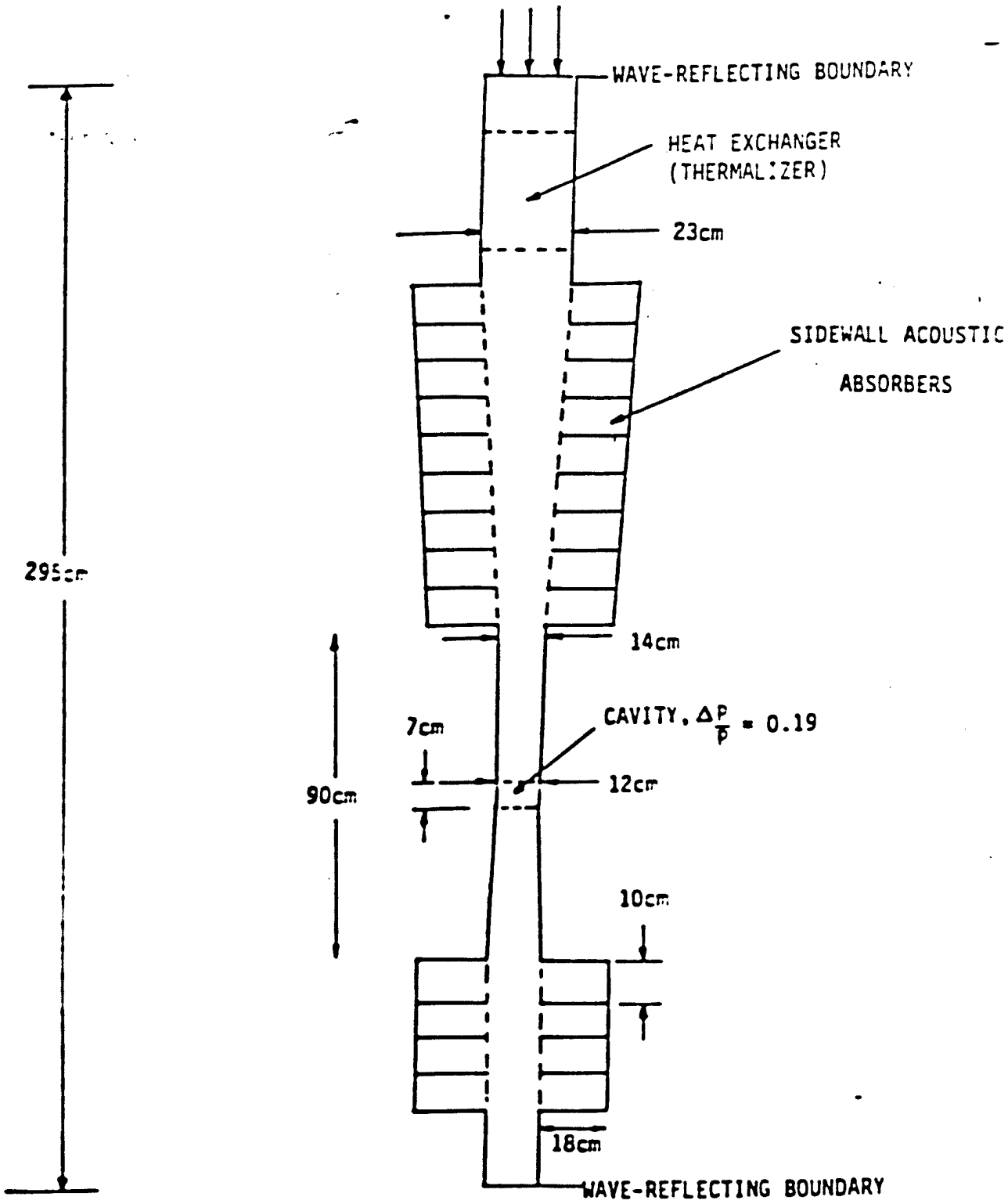

Figure 3.14. Revised PLACATE Simulation Configuration.

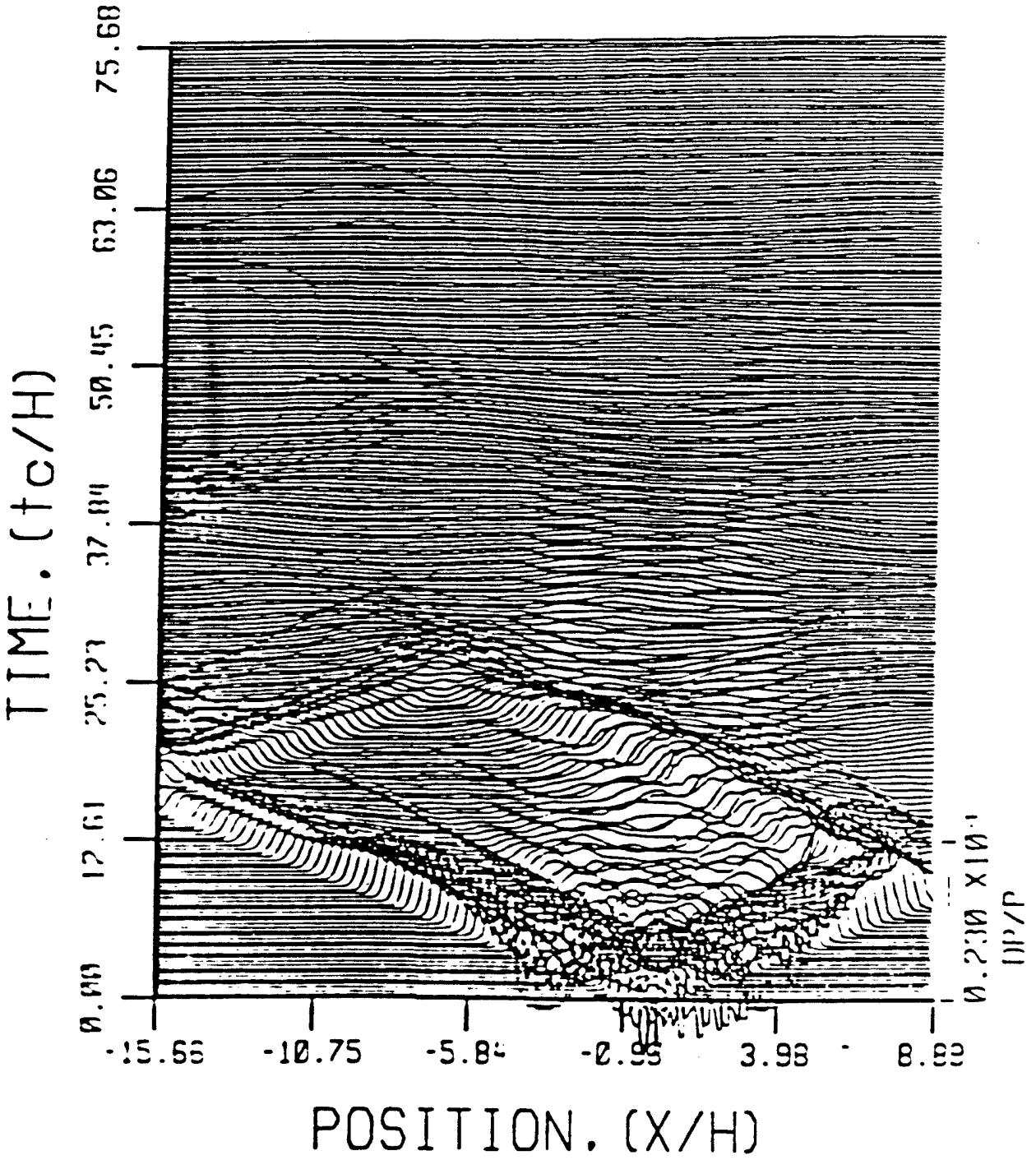

Figure 3.15. PLACATE Revised Simulation, Axial Pressure Waves in Channel.

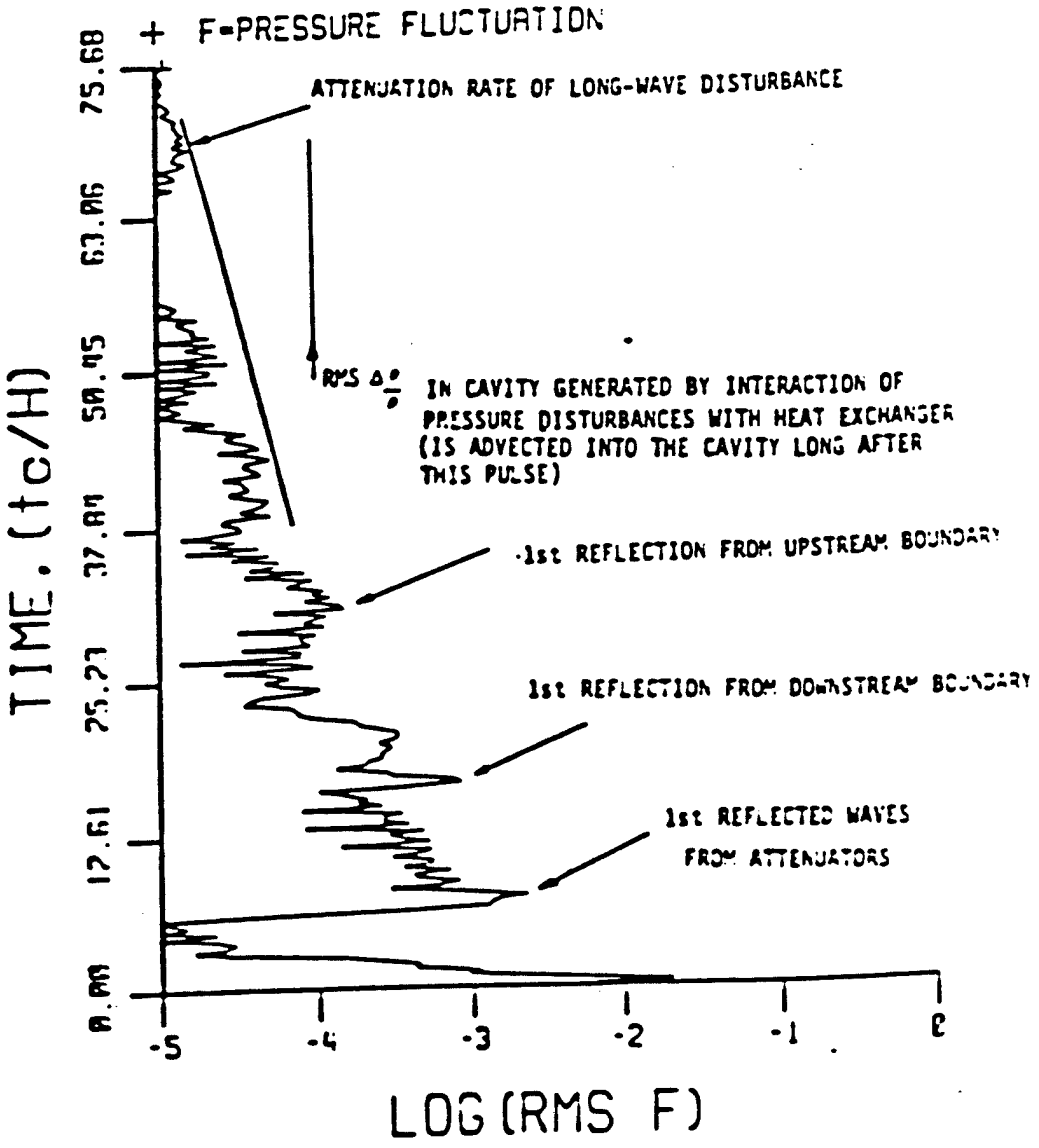

Figure 3.16. PLACATE Revised Simulation: RMS Medium Innomogeneity in Cavity.

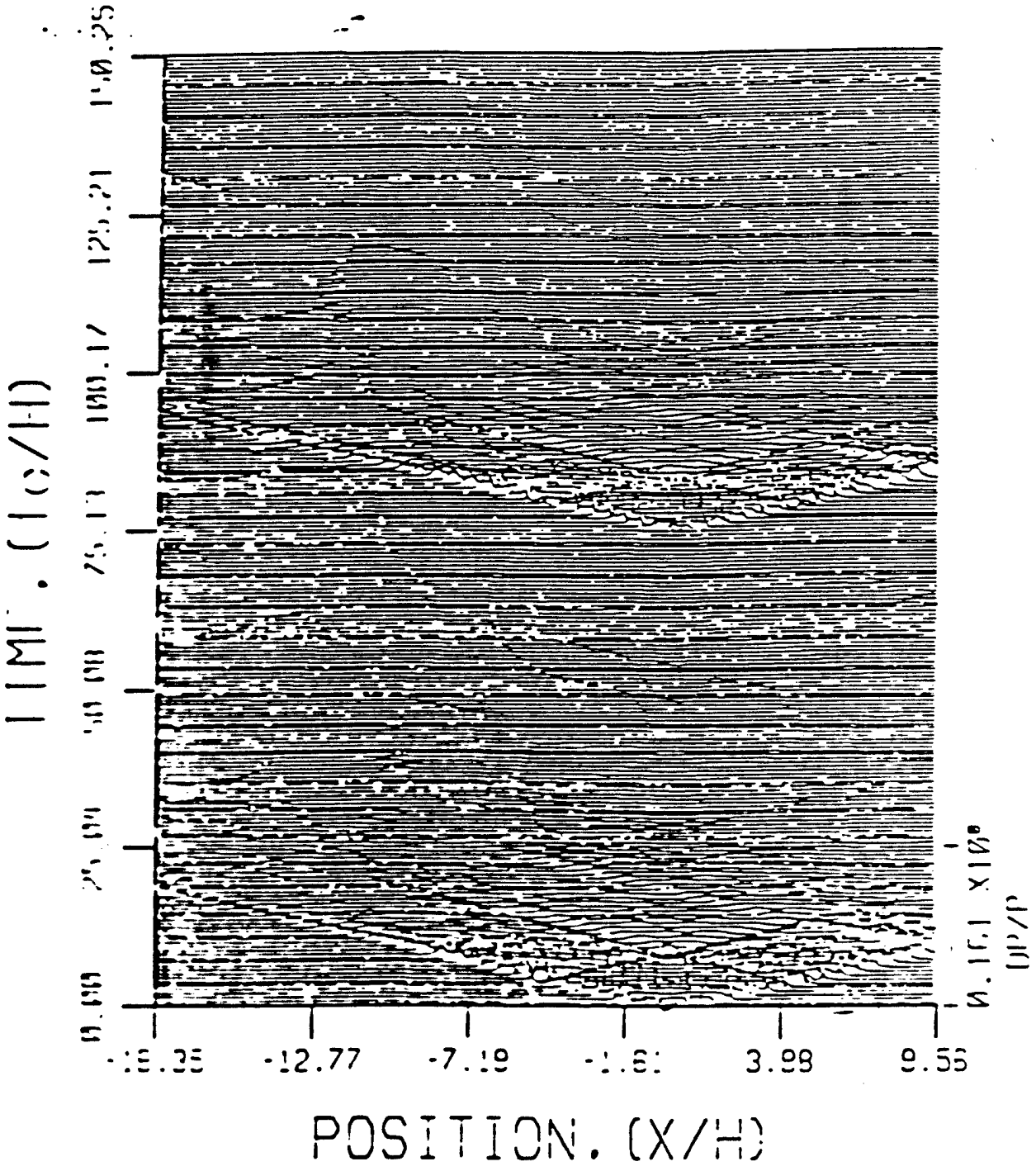

Figure 3.17. Pressure History - Two Pulse Case.

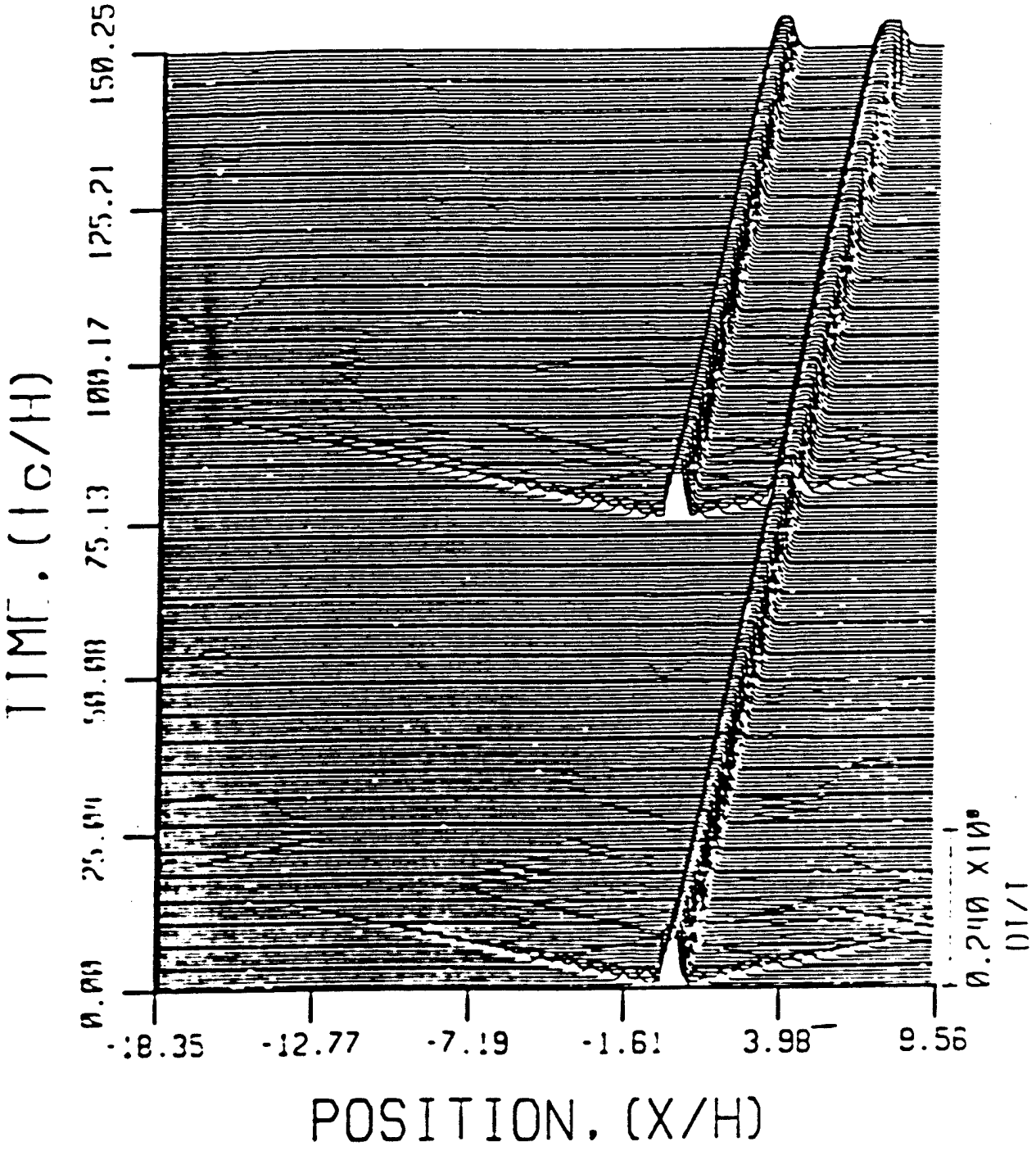

Figure 3.18. Temperature History - Two Pulse Case.

Also, for the temperature distribution, the only noticeable change is the hot region from the first pulse that is convected downstream of the cavity.

The RMS pressure in the cavity is shown in Figure 3.19. While some increase in the RMS pressure can be seen for the second pulse, the attenuation rate is nearly the same. The corresponding density disturbance is smaller by a factor of γ and is of the order of 1×10^{-5}.

The PLACATE simulations employ upstream and downstream boundary conditions that provide ideal reflections of the acoustic energy. This makes the simulation conservative because some portion of the pulse energy will propagate around the bends on both ends.

Entropy Wake

Upstream-traveling pressure waves will be generated by each pulse of the NRL excimer laser. The waves may be presented as a square pulse traveling upstream at the acoustic velocity. As the pulse passes the thermalizer, heat is transferred to the plate leaving a "cold spot" in the flow. This inhomogeneity may adversely affect laser beam quality. Analysis of the magnitude of the thermal disturbance generated by the interaction of the pulse with the upstream thermalizer has been performed.

Description of Problem

At the thermalizer location, the attenuated pressure waves may be represented by the acoustic approximation for the associated temperature and velocity disturbances to the mean flow. As the leading edge of the pulse passes the thermalizer, the temperature of the fluid increases by dT. Thus, heat diffuses into the colder plate and leaves a temperature profile in the fluid between T and T+dT. Then, as the trailing edge of the pulse passes, the temperature of all of the fluid decreases uniformly by dT. This results in a temperature profile between T-dT and T such that the fluid adjacent to the plate is at T-dT. Thus, heat diffuses into this cold layer from the plate. However, some cold fluid may be shed from the downstream end of the thermalizer before reheating significantly. The concern is that this "cold spot" may be convected into the laser cavity and result in poor beam quality.

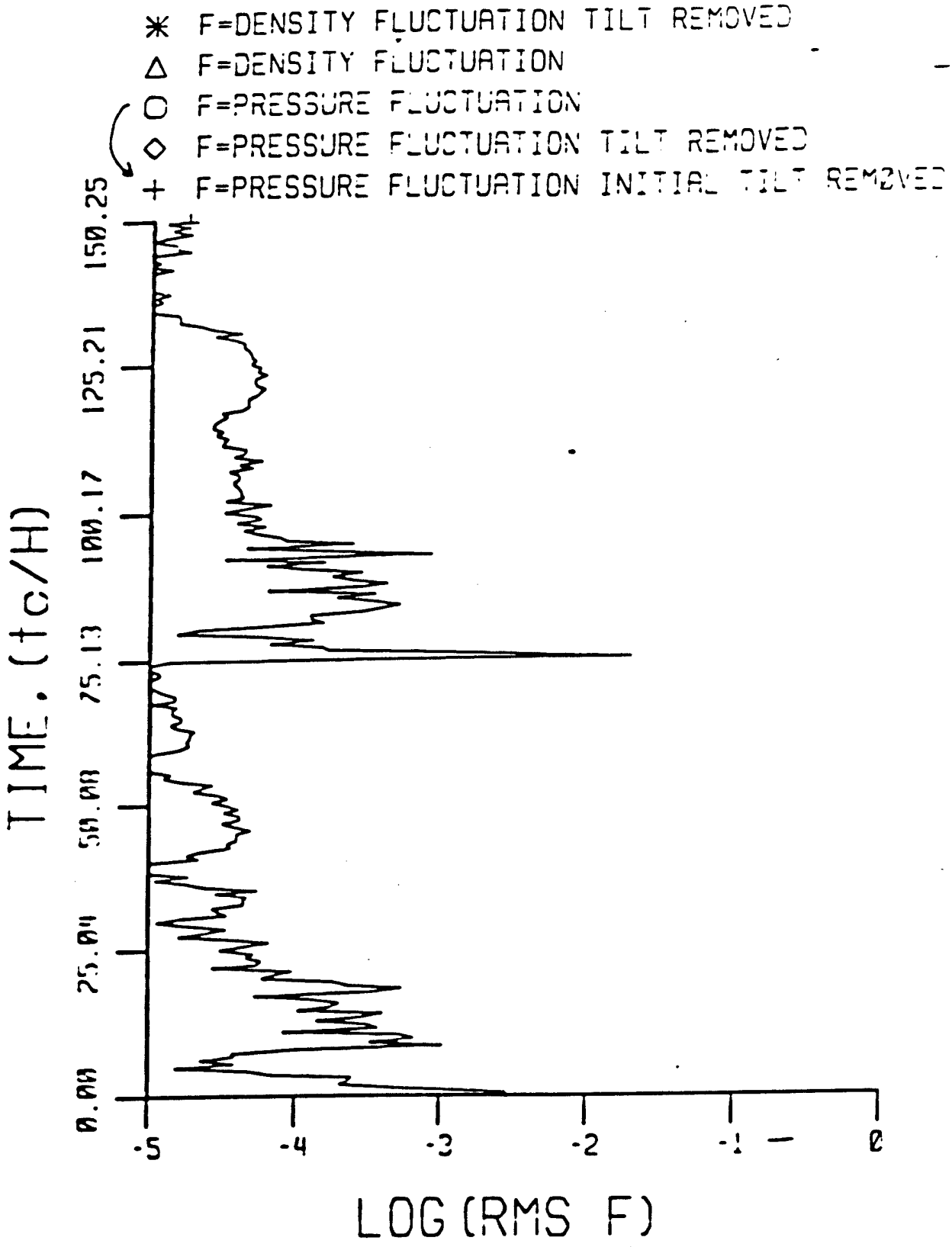

Figure 3.19. Cavity RMS Pressure History - Two Pulse Case.

Model of the Disturbance

The assumptions made in modeling the interaction between the pressure wave and the thermalizer are as follows. Fully-developed laminar flow is assumed to exist between flat plates of half-spacing δ. Also, the plates are assumed to be isothermal at the temperature of the mean flow. The pressure disturbance is approximated by an acoustic square-wave pulse. The time that the pulse is over the thermalizer is short compared to the convection time of fluid through the thermalizer. Therefore, streamwise gradients are neglected and the momentum and energy equations reduce to the diffusion type that have similarity solutions. The model is described in detail in Appendix 2.

Results

The solution of the governing equations yields the downstream temperature distribution as a function of time. After turbulent mixing removes gradients perpendicular to the flow direction, a mean temperature may be used to define the density profile in the flow direction. If no subsequent smearing or mixing of this profile occurs as the flow is convected into the laser cavity, the RMS density disturbance in the cavity can be approximated as a function of time. For values representative of the NRL excimer laser design, the maximum value was found to be:

$$\text{RMS } (\Delta\rho/\rho)_{max} = 4.3 \times 10^{-5}.$$

This corresponds to a beam quality below two and inhomogeneities due to other effects may be dominant.

Thermal diffusivity results in a decay of the residual temperature variations during the transit from the thermalizer to the laser cavity. This effect results in a factor of three reduction in the value listed above if only laminar diffusion occurs. An order of magnitude reduction can be expected for turbulent flow. Furthermore, since the size of the "cold spot" is of the same order as the plate spacing, and because the velocity profile in the thermalizer is not uniform, some convective smearing of the disturbance may occur before transition to turbulence

AIAA 90-1796
Medium Homogeneity Measurements in a Repetitively Pulsed Excimer Laser

J. M. Lin and T. J. Zukowski
TRW Space & Technology Group
Redondo Beach, CA

AIAA 21st Fluid Dynamics, Plasma Dynamics and Lasers Conference
June 18-20, 1990 / Seattle, WA

Medium Homogeneity Measurements In a Repetitively Pulsed Excimer Laser

Jane M. Lin* and Dmitri Zukowski+

TRW Space and Technology Group
Redondo Beach, CA

Abstract

Medium homogeneity measurements in the cavity of a repetitively pulsed excimer laser were conducted in an effort to characterize the performance of the laser flow loop. Optical index variations due to inherent baseline flow inhomogeneities and to pulsed energy deposition were evaluated interferometrically. For the baseline flow, measurements were made at three Mach numbers (0.05, 0.068 and 0.086) and with two flowing media (argon and neon). The flow loop achieved a 1.3×10^{-6} rms level of density uniformity at the highest Mach number. The rms density variations were found to increase as the square of the flow Mach number.

Under pulsed lasing conditions at 40 Hz rep-pulse rate, the magnitude of density variations following the first and twentieth pulses were found to decay to the level of the baseline flow in $Ut/V < 0.7$, i.e., in 70% of the time required to flush the e-beam excited gas from the cavity. At 70 Hz, rapid decay of pulse-associated disturbances was also observed. The results suggest that it may be possible to operate the laser at even higher pulse frequencies without degrading the medium uniformity in the cavity or the beam quality of the output pulses.

1. Introduction

In this paper, we describe the interferometric measurement of gas density variations in the cavity of a repetitively pulsed excimer laser. This work was motivated by the fact that density inhomogeneities in the lasing gas are the major source of refractive index variations in the cavity, and these variations, in turn, are a major source of beam quality (BQ) degradation. Thus, the attainment of good BQ demands that the gas density in the cavity be as spatially uniform as possible prior to energy deposition from an e-beam pulse.

In previous work, characterization of the sources of medium nonuniformity and development of means to control them were given by Baum, et.al. [1]. In their work, measurements were made of the density uniformity in the recirculating gas and in the flow following pulsed energy deposition in a closed-loop flow facility. A two dimensional unsteady code was developed to model the acoustic suppressor and to aid in the design of future flow loops [2]. Analytical models have also been developed to describe the response of heat exchangers to fluctuating gas temperature [3]. Many of these findings were incorporated in the design of the excimer laser flow loop whose performance is evaluated here.

---

* Member of Technical Staff, AIAA member
\+ AIAA member, current address: ST Systems Corp., Washington D.C.

We sought to establish the "noise" levels in the so-called baseline flow, i.e., in the quiescent closed loop gas flow, without pulsed e-beam pumping. In addition, we evaluated the magnitude of density variations following energy deposition. For actual pulsed lasing operation, we have found that the density variation decay to the baseline level in a time which is only 70% of that required to flush the e-beam excited gas from the cavity. These results suggest the feasibility of operating the laser at higher pulse frequencies without degrading the BQ.

2. Experimental Setup

2.1 Experimental Setup

A schematic of the closed loop laser flow system is shown in Figure 1. The major elements include a blower to recirculate the gas, a heat exchanger to remove the heat generated by the blower and the excess energy deposited by the e-beam, flow conditioning devices for velocity and temperature control, and acoustic suppressors to rapidly attenuate the pressure fluctuations in the recirculating gas and the overpressure generated following energy deposition.

2.2 Diagnostics

The primary diagnostic was interferometry. A double-pass Fizeau interferometer with an 800 mWatt argon-ion laser and a CCD camera was used to measure the spatial variation of optical path length in the lasing cavity. The interference patterns were photographically recorded with single-shot Polaroid and 16mm high-speed movie cameras. The exposure times were kept to a minimum to provide an instantaneous snapshot of the density nonuniformities. The movie camera was operated at 6000-8000 frames per sec for exposure times of 12.5-17 μsec. The exposure time of the Polaroid photos was approximately 35 μsec.

Measurements were made of the gas temperature at several locations in the flow loop. Thermocouples were located immediately downstream of the laser cavity and at the entrance and exit to the heat exchanger. Laser cavity sidewall temperature was monitored using a resistance sensor located close to the wall surface (~ 6 mm). Resistive sensors were also used to monitor the coolant temperature at the entrance and exit to the heat exchanger. Time histories of all sensors were recorded simultaneously on strip charts.

The loop was designed to operate with both argon and neon. Argon was selected as the primary test gas because of its relatively low cost and high index of refraction. The high index allowed us to maximize the optical sensitivity of the interferometer and thus enhance the signal levels relative to the noise of the system. The Reynolds and Mach numbers (Re and M) for flow with argon were selected to match the design operating values for neon as well. Measurements with argon were made at three Mach numbers (0.048, 0.068, and 0.086) and at a unit Reynolds number of about 2.3×10^6/meter. Measurements with neon were made at M=0.048, $Re = 2.3 \times 10^6$/m, and at M=0.035 and $Re = 1.1 \times 10^6$/m. The design M and unit Re for the flow loop were 0.044 and 2.1×10^{-6}/m, respectively.

2.3 Interferogram Evaluation

The magnitude of disturbances are evaluated in terms of a spatially rms averaged optical path differences (OPD) over a 10 cm diameter partial aperture of the laser cavity. This aperture is equivalent to more than 50% of the gain volume. Figure 2 gives the cavity dimensions, gain volume, and the evaluated field of view.

The interferograms were digitized either manually (using a digitizing tablet) or automatically (using a video source) and processed by VFAST!, a fringe analysis optical code developed by Phase Shift Technology. The code computes the phase difference integrated across the optical aperture. Aberrations due to tilt and focus are removed. Maps of the phase waveforms are generated and spatially averaged rms OPD values computed from the maps. Typical error from manual digitization is about 10%. The noise of the system due to nonuniformities in the operational laser beam, aberrations in the optical components of the interferometer, and distortions

on the windows of the laser cavity, was removed from the data by a point-by-point subtraction of the tare map from each phase map.

3. Experimental Results

3.1 Baseline Flow Characterization

The flow loop was designed to provide a gas mix, flow rate, and density uniformity to assure that the medium-produced beam aberrations would yield a beam quality less than 1.5. This requirement translates to a density uniformity in the laser cavity of $\Delta\rho/\rho = 1.3\times10^{-4}$ from all sources, from inhomogeneities inherent in the baseline flow as well as from those associated with pulsed flow.

Initially, the flow rate uniformity of the loop was checked to insure that there were no large scale variations which could cause density nonuniformities. A pitot probe was used to scan the flow channel. These tests were performed using neon at 4.00 atm and flow velocities of 15.7 and 22 m/sec (M = 0.035 and 0.048). We found the mean velocity variations to be less than 5% peak to peak (excluding the boundary layer region). It was concluded that these small variations had negligible effect on index variations in the cavity, and therefore, no further measurements were made. Temperature variations, which were expected to have a more pronounce effect, were characterized by interferometry.

Summarized in Table 1 are all test conditions and results for the baseline flow. Listed are the measured rms OPDs computed for a single pass of the excimer laser (0.350 μm wavelength). Also indicated are the equivalent rms density fluctuations, $(\Delta\rho/\rho)_{rms}$, which are related to OPD by OPD = $(\beta L/\lambda)(\rho/\rho_{ref})(\Delta\rho/\rho)$, where β is the Gladstone-Dale coefficient, L is the pathlength (0.70 m), and ρ/ρ_{ref} is the operating density ratio (ρ_{ref} is the density at STP). Each value represents the averaged result from a minimum of three tests at the same conditions. Except for the tare values (i.e., the system noise), all other data have the system noise subtracted out. Some sample interferograms and their corresponding phase waveforms are shown in Figures 3-5.

The interferogram given in Figure 3 represents the OPD distortion due solely to the optics and windows of the flow loop, without medium-induced aberrations. The rms OPD is about 0.04 waves. When the cavity is pressurized, an additional OPD contribution of 0.027 from pressure-induced stresses in the windows and from natural convection currents in the gas was measured. The rms OPD from all noise sources was about 0.067 waves. Interpreted in terms of flow-induced aberrations, this corresponds to an rms density disturbance level of $(\Delta\rho/\rho)_{rms} = 5.7\times10^{-5}$.

Figures 4 and 5 show typical interferograms for flow at M = 0.048 with argon and neon. These interferograms were taken when the temperature of the gas and cavity sidewall were matched. This insured that the measured aberrations were primarily due to acoustic disturbances and not caused by thermal disturbances generated at the heat exchanger and convected into the cavity. The gas temperature was controlled by varying the coolant flow rate; several flow rates were tried.

At M=0.048, the medium-induced rms density variation was measured to be about 5×10^{-5} to 7.5×10^{-5} for flow with argon. Slightly higher values of 8.3×10^{-5} to 1.1×10^{-4} were measured for neon. The higher values can be partially attributed to resolution of the interferometer. The OPDs measured for neon were generally less than 0.025 waves at 514 nm (or less than 0.04 waves at 350 nm) which is near the device resolution limit of 0.02 waves.

Figures 6 and 7 summarize the rms density variation for flow with argon as a function of Mach number. The data are plotted in terms of the parameters $(\Delta\rho/\rho)_{rms}$ and $(1/\gamma-1)(\Delta\rho/\rho)_{rms}$ where γ is the gas constant. They are shown in this manner for the reasons explained below.

Acoustic pressure fluctuations which arise in the baseline flow (from processes of gas recirculation) produce density

variations, or OPD variations, in two ways. Density aberrations can be generated by the isentropic compression or expansion of the gas as acoustic waves propagate through the cavity or, by the nonisentropic interaction of acoustic waves with different elements of the flow loop hardware (e.g., acoustic suppressor, flow conditioning devices, etc). If the disturbances affecting index of refraction changes were purely acoustic (isentropic disturbances), one would expect the density variations to be related to pressure variations by $(\Delta\rho/\rho)_{rms} = (1/\gamma)(\Delta P/P)_{rms}$ or, in terms of Mach number, as $(1/\gamma)(\Delta P/P)_{rms} = \alpha_p M^2$, where α_p is a correlation constant. If these disturbances were the result of entropy waves (i.e., nonisentropic sources), one would expect the density variation to scale with pressure and Mach number as $(\Delta\rho/\rho)_{rms} = (1-1/\gamma)(\Delta P/P)_{rms} = (\gamma-1)\alpha_p M^2$. Therefore, by showing the density variation in terms of either $(\Delta\rho/\rho)_{rms}$ or $(1/\gamma-1)(\Delta\rho/\rho)_{rms}$, some insight can be gained as to the dominant source of disturbance.

In addition to the current results, Figures 6 and 7 also include the interferometric measurements made in an excimer laser flow loop similar to the one evaluated here [1]. The proportionality factor $\alpha_p = 0.015$, was determined in these experiments by a correlation of the measured pressure fluctuations with Mach number.

Figures 6 and 7 show clearly that the rms density fluctuation increases with flow Mach number. In both cases, there is good correlation with M^2. For example, $(\Delta\rho/\rho)_{rms}$ increases by nearly a factor of two from 8×10^{-5} at M= 0.048 to 1.2×10^{-4} at M= 0.86. A least-square fit to the data gives a proportionality constant of 0.012 for $(\Delta\rho/\rho)_{rms}$ and 0.018 for $(1/\gamma-1)(\Delta\rho/\rho)_{rms}$. From these results, it is evident that both isentropic and nonisentropic disturbances are sources of density variations in the baseline flow. In the range of Mach numbers tested for this flow loop, there is no evidence that one source is predominant.

In addition to isentropic and nonisentropic acoustic disturbances, thermal disturbances produced at the heat exchanger and convected into the cavity are also a source of density aberrations. To determine the magnitude of these effects, a series of experiments were performed in which the temperature difference between the gas leaving the heat exchanger and the coolant was varied. The temperature difference was quantified as a temperature mismatch between the gas and flow loop sidewall. Figure 9 shows the interferogram corresponding to a four degree mismatch. In this case, the $(OPD)_{rms}$ was measured to be 0.163 or $(\Delta\rho/\rho)_{rms} = 1.4\times10^{-4}$, which is higher than the design requirements for the flow loop. Plotted in Figure 8 is the effect of the temperature mismatch on $(\Delta\rho/\rho)_{rms}$. The figure shows clearly that thermal disturbances from the heat exchanger can greatly affect the level of density uniformity in the cavity. A 50% increase in $(\Delta\rho/\rho)_{rms}$, from 10^{-4} to 1.5×10^{-4}, was measured for a four degree temperature difference. It is evident that thermal disturbances must be prevented.

3.2. Inhomogeneities Under Pulsed Lasing Conditions

Interferometric measurements of flow aberrations within the lasing cavity were made as a function of time following energy deposition by the e-beam at rep-rates of 40 and 70 Hz. At 40 Hz, more than 20 consecutive pulses were achieved. At 70 hz, only three pulses were fired.

A series of interferograms at selected time intervals showing the evolution of disturbances following e-beam deposition is given in Figures 10 and 11. The first sequence shows the history following the first pulse, the second shows that following the twentieth pulse in the same pulse train. The direction of the flow and of the e-beam are marked. For clarity, the location of the original e-beam excited slug of gas at several times is also shown pictorially. Indicated in the figures are three times, the absolute time, t, and two dimensionless times, F=Ut/W (the flush factor) and ct/W (the number of acoustic wave transits across the laser aperture).

Here, t is the time elapsed after the pulsed energy deposition and c is the speed of sound in the gas. A flush factor of unity is defined as the time required to flush the original slug of gas completely from the cavity. For the flow conditions shown (40 Hz rep-rate at M=0.048), each slug of gas is displaced from the cavity and replaced by undisturbed flow 1.96 times between pulses (or the flush factor is 1.96). In terms of acoustic passes, ct/W, there are roughly 20 passes before the gas directly heated by the e-beam clears the cavity, and another 20 passes before the next pulse.

Prior to energy deposition, the character of the flow is consistent with that found in earlier tests; Figure 10a is similar to Figures 5 and 6 except that there are many more fringes. The rms density fluctuation in the cavity is about 1.2 x 10^{-4}, which is near the high end of the range of values measured for the baseline flow. At t=0+, immediately after the e-beam is fired (Figure 10b), the disturbances due to heating are so large that the interferogram appears blurred. However, by Ut/W=0.16 or ct/W=3.33 (Figure 10c), an interference pattern with highly distorted fringes can be clearly seen. A notable feature in the photo is a narrow band near the top within which two distinct lines appear. The band apparently marks the interface between the gas that was originally in the gain volume and that which was behind it, in the rest of the cavity (see sketch for correspondence). Below the band the fringes are distorted; while above the band, the fringes are fairly straight. In subsequent photos (10c-f), the band and distorted fringes (i.e. the e-beam heated gas) move downward through the cavity at the flow velocity of 15.7 m/sec. By Ut/W = 0.31 or ct/W = 6.46 (Figure 10f), the trailing edge of the original slug is completely within the field of view. By Ut/W=0.55 or ct/W=11.5, only a few fringes are distorted which suggests that nearly all pulse-associated disturbances are flushed from the cavity. By Ut/W=0.63 (ct/W=13.1), the fringe pattern is similar to that prior to the e-beam pulse. At later times, Ut/W> 0.7 (ct/W >14.58), there is no evidence of any residual density inhomogeneity from the energy deposition; the fringes remain undistorted. In terms of slug location, beyond Ut/W=0.75 or ct/W=15.6, all of the original gas has cleared the viewing aperture.

The character of the flow following the twentieth pulse is similar to that following the first as seen in Figure 11. The major features, such as the band of disturbances which mark an apparent interface between the disturbed and undisturbed flow and the propagation of the heated slug through the cavity, are all evident. Like the first pulse, all pulse-associated inhomogeneities appear to be attenuated by Ut/W=0.7.

Figure 12 gives a comparison of the rms density variation as a function of Ut/W for the two pulses just described. Prior to the firing of the e-beam, a series of three interferograms was analyzed to determine the baseline noise level. The averaged OPD level for this series is $(\Delta\rho/\rho)_{rms}$=1.2 x10^{-4}. Between Ut/W = 0+ to 0.55, the cavity is flushed and the aberrations in the thermally-distorted gas were too large to be analyzed. By Ut/W = 0.55, the trailing edge of the slug which was originally within the gain volume just clears the aperture (see Figures 10i and 11i) and $(\Delta\rho/\rho)_{rms}$ = 10^{-3}. Between 0.55 to 0.7, the rms density disturbances diminish rapidly, by nearly an order of magnitude to 1.3x10^{-4}. Beyond Ut/W=0.7 or ct/W=14.6, the rms disturbances cannot be distinguished from the baseline flow noise level.

For the twentieth pulse, a similar behavior is observed. Specifically, the rms density variation decays to nearly the baseline level by Ut/W = 0.7.

These results indicate that the acoustic suppression system in the flow loop rapidly and effectively attenuates the pressure waves generated in the cavity by the energy deposition. By the time the thermally distorted gas is flushed out of the cavity, the residual cavity pressure fluctuations (from the initial overpressure) are too small to be detected. The density uniformity in the cavity returns to the pre-pulse or baseline noise level in Ut/W=

0.7 (ct/W = 14.58). Even after more than 20 pulses, there is no degradation in the baseline flow medium homogeneity. These results suggest that the flow loop can be operated at higher pulse repetition rates without exceeding the cavity density uniformity and beam quality allowed. The current results suggest that a rep-rate of 100 Hz, corresponding to a flush factor of 0.7, is possible.

We now move on to the results at the higher rep-rate. Figure 14 shows the interferometric time history for the first pulse in a series of three at 70 Hz. The rms density variation with time is given in Figure 13. The flow Mach number is again 0.048. At this higher rep-rate, the flush factor is 1.12 and the total number of acoustic passes prior to the subsequent pulse is 23. The energy deposition per pulse was estimated to be 50-100% higher than that at 40 Hz, although no direct measure of the energy was made.

The features seen in Figure 14 are similar to those in Figures 10 and 11. In particular, the band of irregular fringes is clearly visible and inhomogeneities are seen to propagate through the cavity. A direct comparison however, indicates one difference. At the higher rep-rate, longer times are required to attenuate the pulse-associated disturbances. For example, in Figure 10 only the last remnants of the distorted fringes are apparent by Ut/W = 0.31 or ct/W = 11.46, while in Figure 14, large distortions are still evident at that time. Beyond Ut/W = 0.78 (ct/W = 16.25), the fringe pattern is similar to that prior to the e-beam pulse.

The longer time required to attenuate pulse-associated disturbances is clearly shown in Figure 13 where the rms density variation as a function of time is given for the two pulses. The slower attenuation at 70 Hz is not surprising and can be attributed to the more than 50% greater energy deposited per pulse. By Ut/W = 1 (ct/W = 20.83), the density uniformity in the cavity is about the same for both cases. Note that Figure 13 does indicate that just prior to the second pulse at 70 Hz, $(\Delta\rho/\rho)_{rms}$ is slightly higher than the baseline. Although this can be partially attributed to the digitizing error inherent in the interferogram evaluation, this result suggests that for high frequency operation, further fine tuning of the acoustic suppression system may be necessary in order to achieve the 1.3×10^{-4} homogeneity level requirement imposed on the laser.

Overall, the medium homogeneity measurements in pulsed flow indicate that the required design density uniformity of $(\Delta\rho/\rho)_{rms}$=1.3×10^{-4} in the laser cavity is achieved.

To conclude, some results for neon are presented. The interferometric time histories shown in Figures 15 and 16 are those following the first and twentieth pulses (from a train of 23 in neon) at the 40 Hz rep-rate. These have been included for comparison with the analogous argon cases and for reference. No difference in behavior for the two gases was observed. As in the argon flow, the Mach number for flow with neon was 0.048. Since the sound speed in neon is larger than in argon, the flow velocity is higher (22 m/sec) than for argon and the flush factor therefore, is also higher (2.75). Note also that the frames shown in Figures 15-16 and in Figures 10-11 are at corresponding absolute times and not at corresponding normalized times, Ut/W and ct/W.

4. Summary

Medium homogeneity measurements of the baseline flow and of the flow under pulsed lasing conditions in a repetitively pulsed excimer laser were conducted in an effort to characterize the performance of the laser flow loop. The primary objectives were to determine the magnitude and sources of disturbances which contribute most significantly to index of refraction changes in the laser cavity. The major findings are summarized as follows.

1. The magnitude of density fluctuations in the baseline flow was measured to be within the design requirements for BQ

considerations. A value of $(\Delta\rho/\rho)_{rms}$ $=1.3\times10^{-4}$, corresponding to a BQ=1.5, was measured for flow with argon at M = 0.048 and unit Re=2.3×10^{6}/m. Similar homogeneity levels were measure for flow with neon at the same Mach and unit Reynolds numbers.

2. The cavity density variation observed in this experiment showed an M^2 correlation. The data indicate that both isentropic and nonisentropic acoustic fluctuations are sources of density inhomogeneities.

3. Thermal disturbances produced at the heat exchanger due to a temperature mismatch between the flowing gas and sidewall and convected into the cavity, were a source of large density fluctuations. A 50% increase in $(\Delta\rho/\rho)_{rms}$ was measured for a four degree temperature difference.

4. There was no evidence of a degradation in the homogeneity level in the laser cavity from one pulse to the next under rep-pulsed operation. At 40 Hz pulse rate (flow with argon and also with neon at M = 0.048), the magnitude of density variations following the first and twentieth pulse in the same pulse train, were found to decay to the pre-pulse level in less than the time required to flush the cavity of the e-beam excited gas. A post-pulse $(\Delta\rho/\rho)_{rms}$ of 1.3×10^{-4} was achieved within Ut/W = 0.7 (flush factor = 0.7).

5. The acoustic suppressor rapidly and effectively attenuates the pressure wave generated in the cavity by the energy deposition. By the time the thermally distorted gas is flushed out of the cavity (Ut/W = 1.0 and ct/W = 20.83), the cavity pressure fluctuations are too small to be detected.

6. The loop can be operated at a pulse repetition rate of 70 Hz without exceeding the cavity density aberrations allowed for a beam quality budget of 1.5.

Acknowledgments

The authors gratefully acknowledge Dr. H. W. Behrens and Dr. Craig Zahnow for their valuable guidance and advice. This work was performed under subcontract #MKL-RK85-1020 for Maxwell Laboratories, Inc., San Diego, CA.

References

1. Baum, E., G. Koop., V. Kulkarny, K. Magiawala, and J. Shwartz, "Density Homogeneity Control in Repetitively Pulsed Gas Lasers", Sixth International Symposium on Gas Flow and Chemical Lasers, Jerusalem, Israel, 1986.

2. Baum, E., K. Magiawala, V. Kulkarny, and J. Shwartz, " Modeling of Tapered Duct Acoustic Suppressors for Pulsed Chemical Lasers", Lasers 85, Proceedings, ed. by C. P. Wang, SOQE, 1986.

3. Kulkarny,V., K.Magiawala, and J.Shwartz, "Analysis of Thermal Homogenizers for Closed-Cycle Excimer Laser Flows", AIAA Paper No. 85-1602.

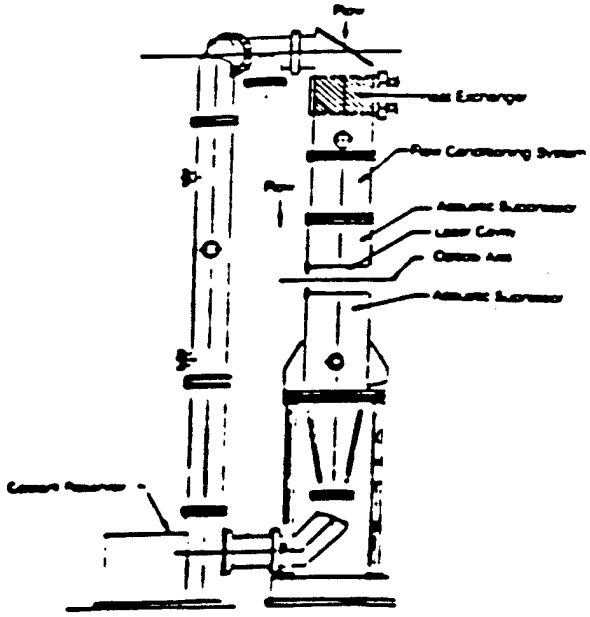

Figure 1 Schematic of Closed-Loop Pulsed Laser Flow System

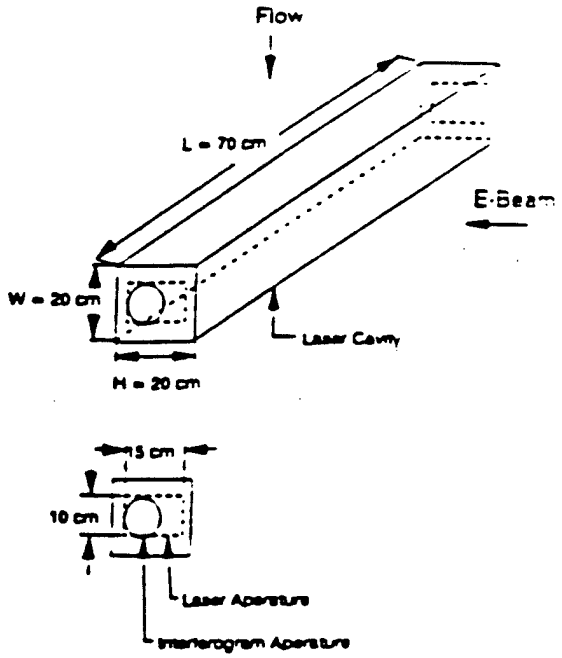

Figure 2. Rep-Laser Cavity Configuration

Table 1. Measured rms OPD for Baseline Flow (λ = 350nm)

GAS	MACH NUMBER	UNIT RE (m^{-1})	$\left(\frac{\rho}{\rho_{std}}\right)$	COOLANT FLOW RATE	$\lvert\Delta T\rvert$ (deg K)	RMS OPD $\frac{\Delta\lambda}{\lambda}$	EQUIV RMS $\left(\frac{\Delta\rho}{\rho}\right)$
None	0	0	NA	none	0	0.040	NA
Argon	0	0	2.08	none	0	0.067	5.7×10^{-5}
Argon	0.048	2.3×10^{6}	2.08	none	0	0.056	4.8×10^{-5}
	0.048	2.3×10^{6}	2.08	low	0.	0.075	6.4×10^{-5}
	0.048	2.3×10^{6}	2.08	high	0.12	0.088	7.5×10^{-5}
	0.048	2.3×10^{6}	2.08	high	3.0	0.176	1.5×10^{-4}
	0.048	2.3×10^{6}	2.08	low	4.0	0.163	1.4×10^{-4}
Argon	0.068	2.3×10^{6}	1.50	low	0.85	0.068	7.9×10^{-5}
	0.068	2.3×10^{6}	1.50	high	0	0.103	1.2×10^{-4}
	0.068	2.3×10^{6}	1.50	low	3.9	0.131	1.6×10^{-4}
Argon	0.086	2.1×10^{6}	1.06	low	0	0.069	1.2×10^{-4}
Neon	0.035	1.1×10^{6}	2.60	none	0	0.041	1.1×10^{-4}
Neon	0.048	2.3×10^{6}	4.00	none	0	0.046	8.3×10^{-5}
	0.048	2.3×10^{6}	4.00	low	0.3	0.049	8.7×10^{-5}
	0.048	2.3×10^{6}	4.00	high	0.2	0.063	1.1×10^{-4}
	0.048	2.3×10^{6}	4.00	low	0.59	0.044	1.2×10^{-4}
	0.048	2.3×10^{6}	4.00	high	0.9	0.048	1.3×10^{-4}
	0.048	2.3×10^{6}	4.00	none	3.7	0.023	2.5×10^{-4}

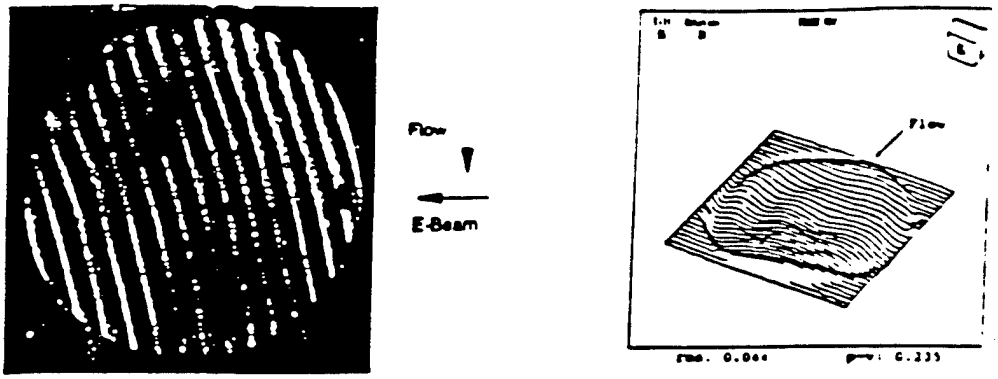

Figure 3. Interferogram and phase waveform of evacuated laser cavity. P < 30 torr.

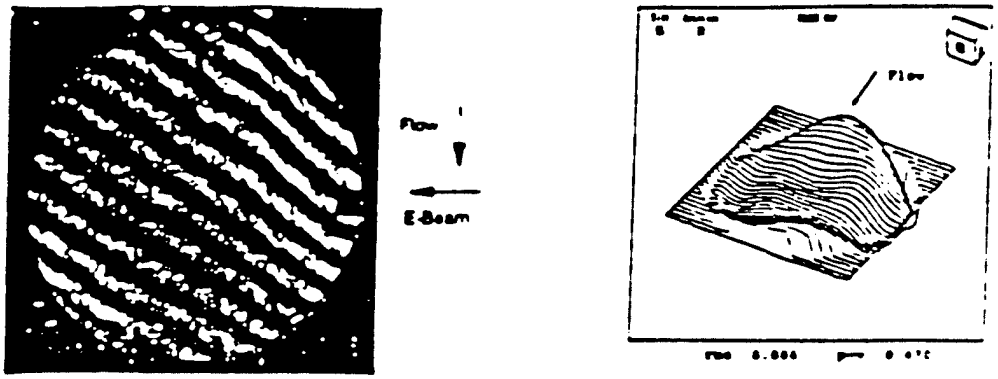

Figure 4 Interferogram and phase waveform of baseline flow with Argon. M = 0.048

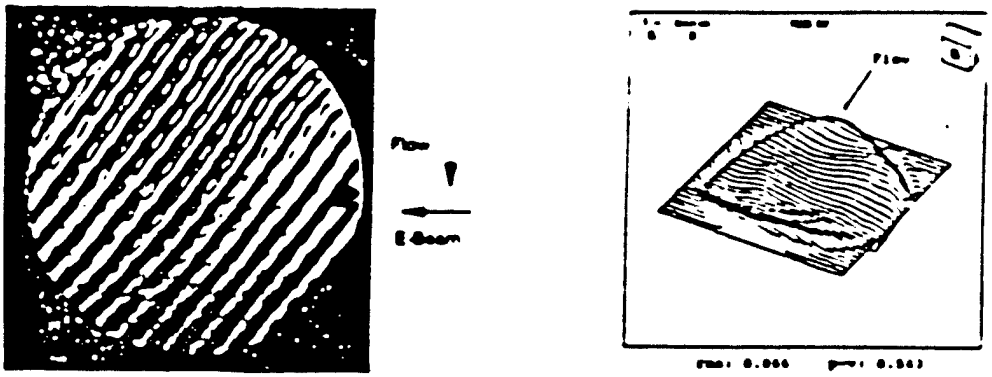

Figure 5. Interferogram and phase waveform of baseline flow with Neon, M = 0.048

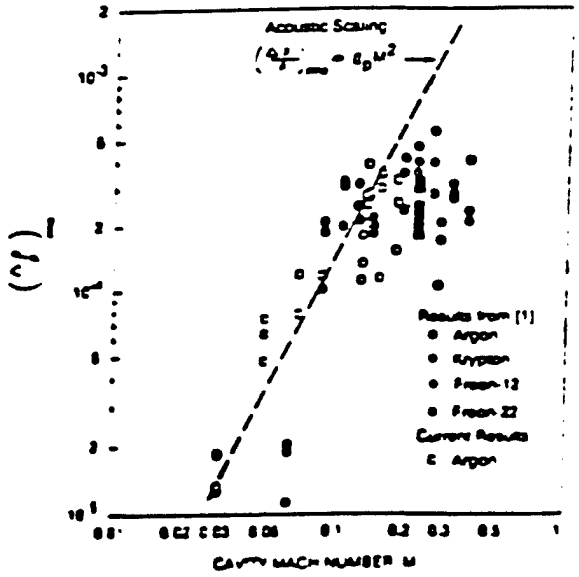

Figure 6 Baseline flow rms cavity density variations scaled as isentropic disturbance.

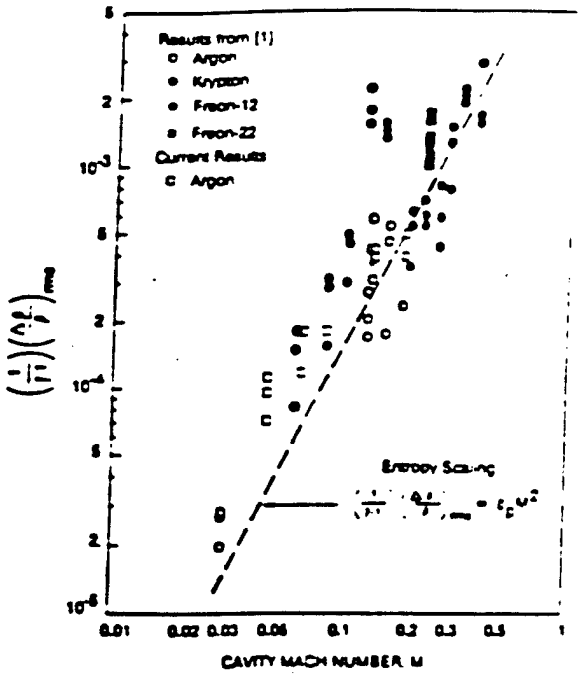

Figure 7. Cavity density variation scaled as nonisentropic disturbance.

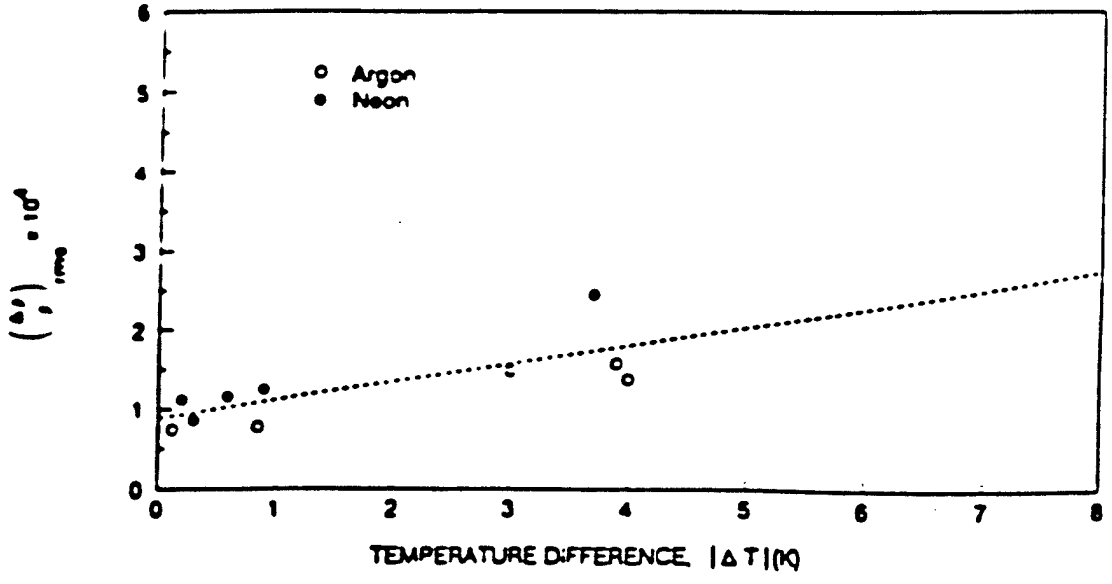

Figure 8. Effect of gas and cavity sidewall temperature difference on rms density variation, (|ΔT| = Tgas - Tsidewall)

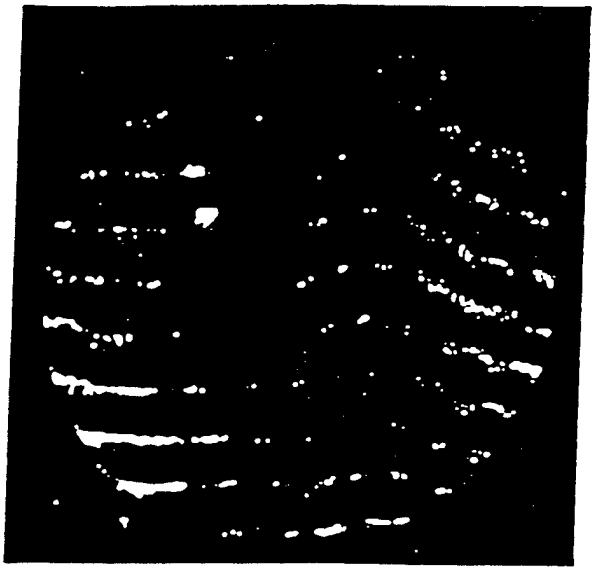

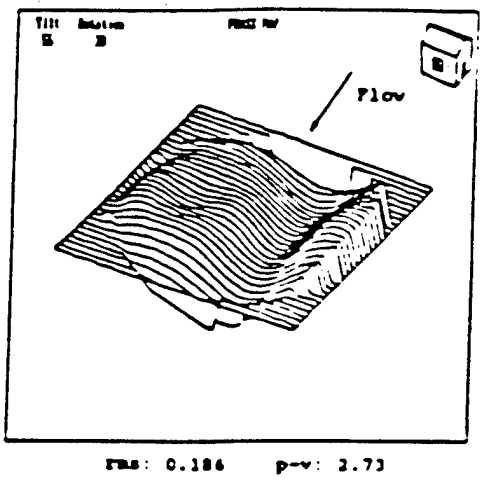

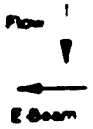

Figure 9. Interferogram and phase waveform of baseline flow with sidewall and gas temperature mismatch, argon flow, M = 0.048.

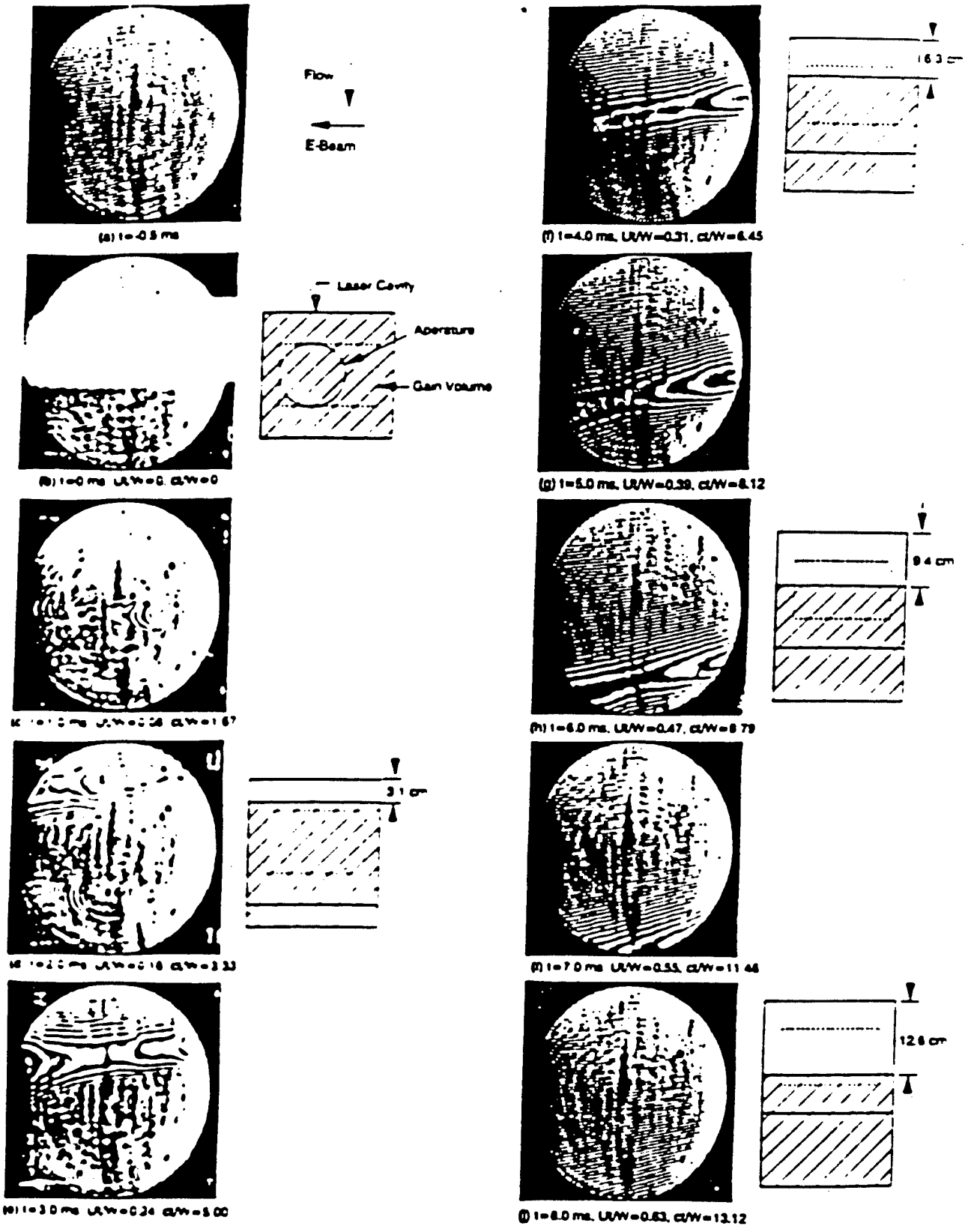

Figure 10 Interferogram time history following first pulse in flow with Argon at M = 0.048, 40 Hz rep-rate. ▭ Excited Gas

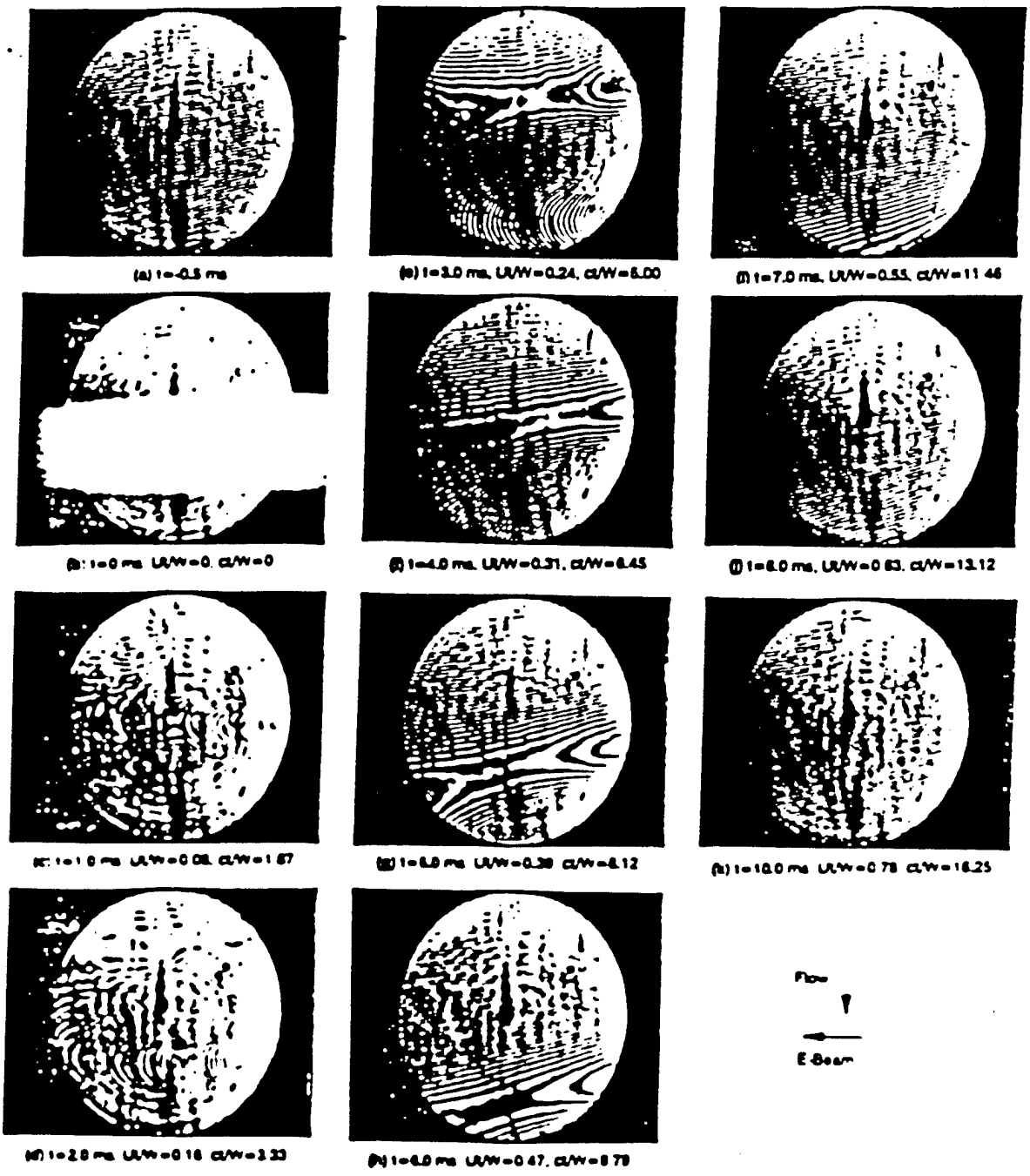

Figure 11. Interferogram time history following twentieth pulse in flow with Argon at M = 0.048, 40 Hz rep-rate.

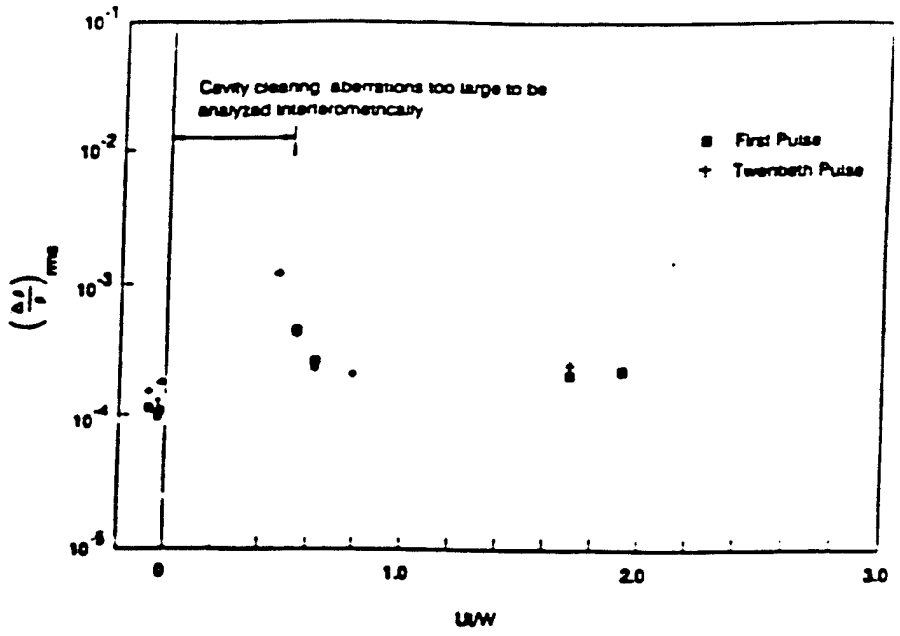

Figure 12. RMS density variation as function of flush factor (Ut/W) following first and twentieth pulses in argon flow, M = 0.048, 40 Hz rep-rate.

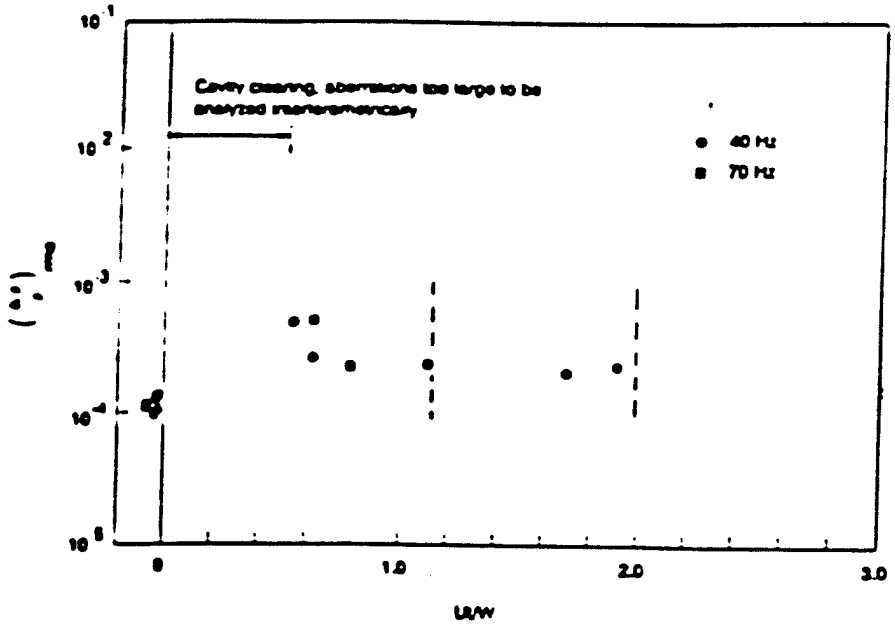

Figure 13. RMS density variation as function of flush factor (Ut/W) following first pulse in argon flow, M = 0.048.

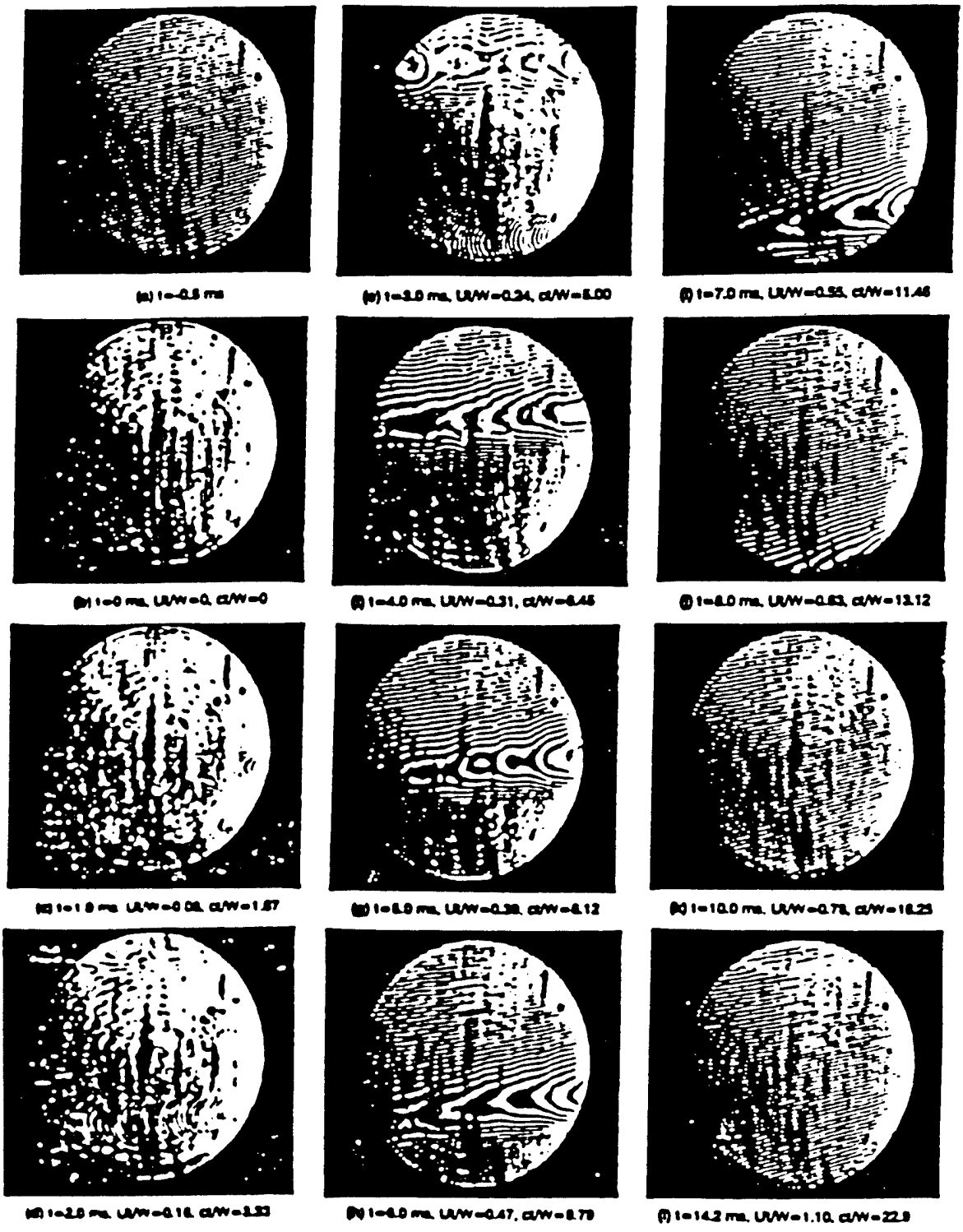

Figure 14. Interferogram time history following first pulse in flow with Argon at M = 0.048, 70 Hz rep-rate.

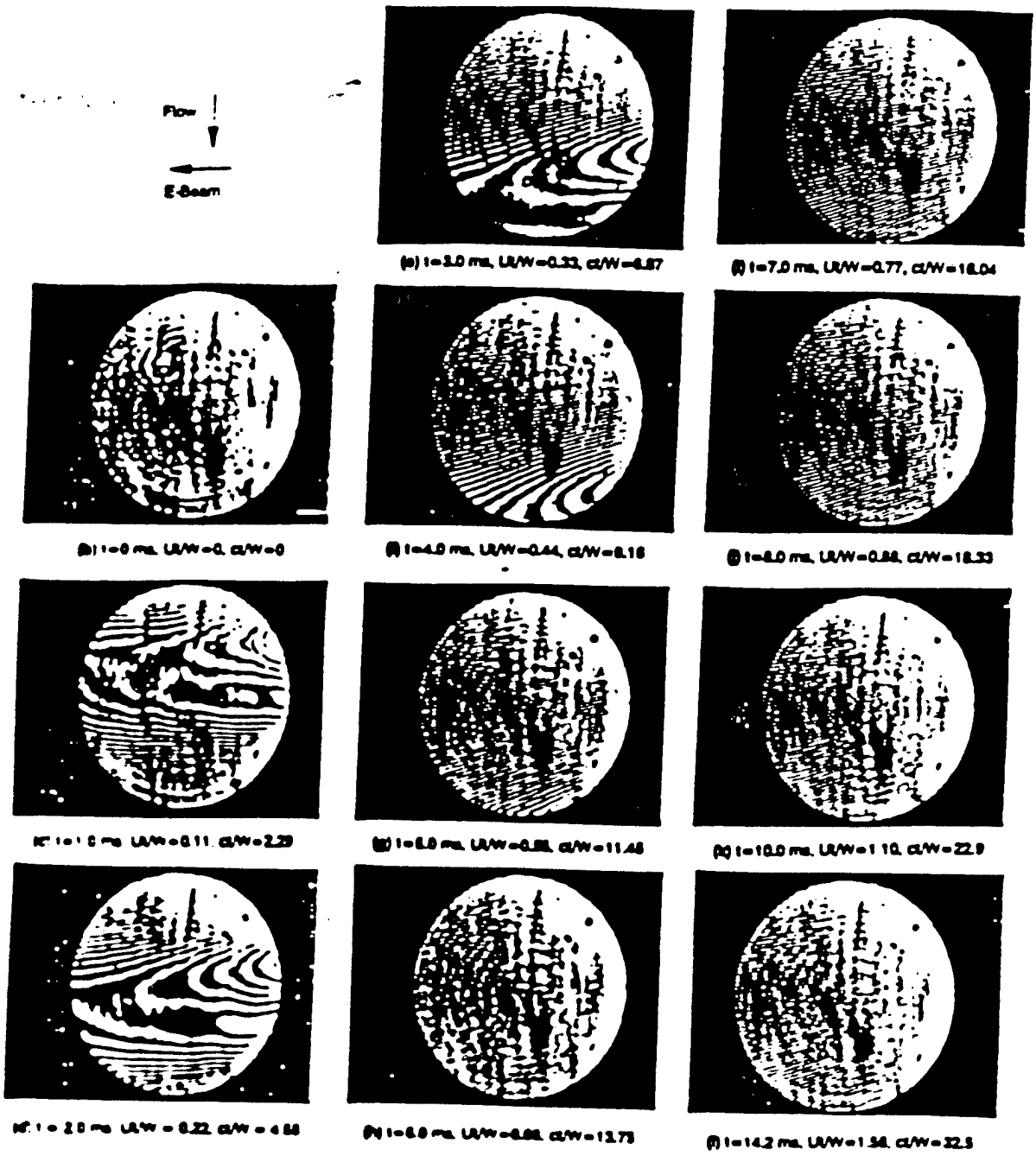

Figure 15. Interferogram time history following first pulse in flow with Neon at M = 0.048, 40 Hz rep-rate.

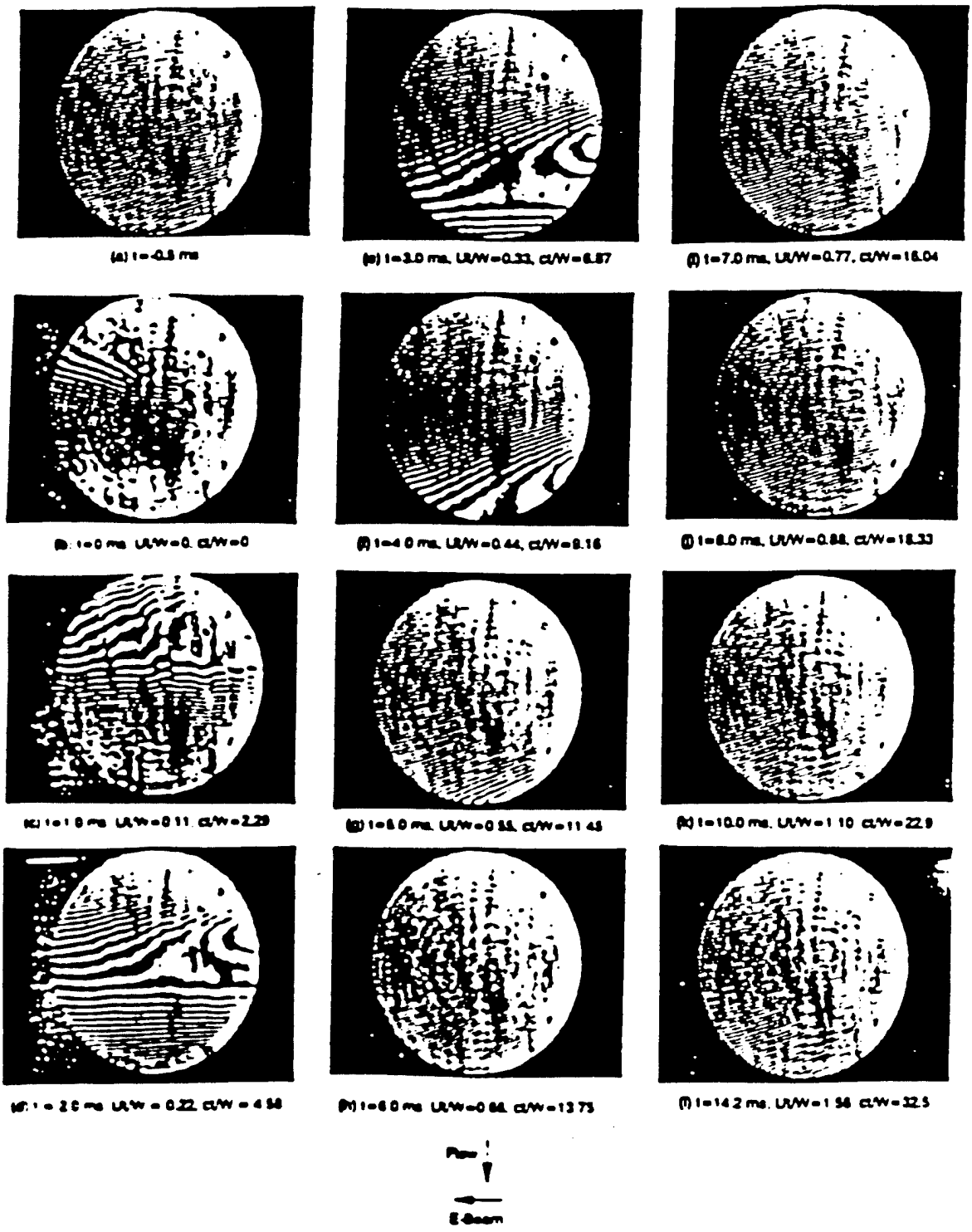

Figure 16. Interferogram time history following twentieth pulse in flow with Neon at M = 0.048, 40 Hz rep-rate.

				Selection of the porous plate 09/25/98 09/26/98 09/28/98 10/11
.0000191	μa		kg/(m*sec)	Viscosity of air at NTP; 1 atmosphere and 293 15 K
1.205	Rhoa		kg/m^3	Density of air at NTP; 1 atmosphere and 293 K
				Reference - Pall Corporation Data on air: PSS-700E
.000356	t		m	Figure 4, pp 9, Grade T 0.014 inch thick
86.2	dpa1		N/m^2	Data point1
1.524	Ua1		m/sec	Data point1; 300 cuft/(min*sqft) or 5 ft/sec
1379 17	dpa2		N/m^2	Data point2
15.24	Ua2		m/sec	Data point2; 3000 cuft/(min*sqft) or 50 ft/sec
	C	.06545534		Porous plate drag constant
	k	1.288E-10	m^2	
	permeabil	1.13491E-5	m	Porous plate permeability
				Calculations for pressure drop in laser gas
				Reference 9/21/98 model
2 2481	RhoKrF		kg/m^3	Laser gas density; T 323.15 K
00002625	μKrF		kg/(m*sec)	Laser gas viscosity; T 323.15 K
2 127	Uthrmlzr		m/sec	Velocity of laser gas upstream of the porous plate
	ΔpKrF	175 203337	N/m^2	Pressure drop in laser gas for the porous plate
4 125	Uflow		m/sec	Lase head flow velocity
	q	19 1264133	N/m^2	One head loss in laser @ cavity conditions with Uflow
	quth	5 0853472	N/m^2	
	hdlsquth	34 452581		ΔpKrF/quth across the porous plate based on Uthrmlzr
	hdlsqufl	9 16028186		ΔpKrF/q across the porous plate based on Uflow
				Sandwich this Rigimesh within in two perforated plates
	nprfpr			
	Δperfpr	11 1877638	N/m^2	Head loss across 2 sandwitchnig perforated plates
33	Lpp		m	
	Lop		m	
18 1875	Din		inch	Input from IMS/HB Compaby 09/28/98 Vaneaxial fan type B-LB,
	Uin	8 93361538	m/sec	Velocity in top circular section of the loop
	nupinsn			Assume number of head loss in header due to sudden expansion
	Δpinsnsert	89 7098502	N/m^2	Insertion loss at the porpos plate upsteam plenum
	Δptotalhdr	276 100951	N/m^2	Total pressure loss in top leg header (insertion+perforated plate+
	ntotalhdr	14 4355843		Total number of heads loss in header based on Uflow
				Carry this number in blower selection
	Resideleg	353443 738		Reynold's number of the laser gas flow in side legs
285 84	a0		m/sec	
	Min	031253902		Mach number of the flow in other circular legs
16	p		psia	Pressure of the laser gas
1 6648	γ			Gamma for the laser gas
015	fourl			Reference Shapiro Vol 1, pp 184/187, 4f with ε/D ~ 0.00012, ε ~
8 811	Llaserleg		m	
495	flength			

Lotherlegs	4.361445	m	All other legs (top/bottom/side) are assued to be smaller in length
L3legs	13.084335	m	Total length of the three other 3 legs
Δpin3legs	38.1140015	N/m^2	
nwallfr	1.99274171		Number of wall friction head losses based in 3 leags based on Uf
			Use the above number in nmisc for blower power calculations

KrF Laser Flow Loop Design: 09/18/98, 09/21/98, 09/22/98, 09/23/98
09/28/98; 10/01/98; 10/03/98; 10/05/98, 10/07/98

For physical/operational parametes see customer requirements

Gas composition: χAr=0.6594; χKr=0.3375, χF2=0.0031
Use TRW GASPROP code to calculate gas properties

16	p		psia	Operating pressure for the flow loop
54.742	Mwt		kg/kgmol	Calculated value from TRW GASPROP code outputs
323.15	T		K	
8314	R0		J/(kgmol*K)	Universal gas constant (pp 77, Thompson)
	Rho	2.24809298	kg/m^3	
380.9011	Cp		J/(kg*K)	Calculated value from TRW GASPROP code outputs
	Cv	229.025027	J/(kg*K)	Calculated value from TRW GASPROP code outputs
1.6648	γ			Specific heat ratio
.000026246	μ		kg/(m.sec)	Viscosity
3	L'		m	Dimensions of an acrtive cavity
3	Lc		m	
1	Lo		m	
	Vactive	09	m^3	Active volume of the laser cavity
	mvactive	202328368	kg	Mass of the laser gas in active volume
				See customer inputs; neglect energy going out into laser beam
				Assuming nlasing very small number (assume/verify)
9.00	dE		J	Energy Dumped into active volume of the laser gas per pulse by 2 e-b
	dT	211.056696	K	Instantaneous constant volume temperature rise
	dp	10.4499679	psia	Instantaneous constant volume pressure rise
	dp/p=dT/T	653122994		dp/p=ΔT/T
..	ε'			Multiplication factors for boundary layers etc (assume/verify)
..	εc			See pp A-17 AVCO paper
..	εo			
	Lfp	33	m	Dimensions of the floow loop cross section for a laser head
	Lpp	33	m	
	Lop	1.1	m	
	Vlasemd	11979	m^3	Volume of the laser head section
2.5	ff			Flush factor
	FF	2.5		See pp 5, NRL Report
5	PulseRate		Hz	Laser pulse rate
	Uflow	4.125	m/sec	Laser head flow velocity
	Flowrate	3172.76093	ft^3/min	Total flow rate, see HB Bulletin C3300, September, 1996
	q	19.1263535	N/m^2	One dynamic head (@ cavity flow conditions)
10	nhex			See pp 13, NRL Report (assume/TBD)

	nthrmlzr	6		Number of head loss in thermalizer, see calculations in later portion of
6	nmisc			Miscellaneous, wall viscous losses, turns and bellow see 09/28 98 TK
				nmisc=nwallfr+nturns+nbellow; 2+3+1=6 see 09/28/98 TK file 2 assu
15	nhrdppp			See 09/25/98 to 09/28/98 work on header and porpus plate selection
	ntotal	37		Total number of head loss based on Uflow
	dptotal	2.76630189	inch H2O	
2	sm			Operatinal safety margin (assume/vanfy)
				See pp 12; NRL Report
	smdptotal	5.53260378	inch H2O	Use this number for selecting a blower
	DesignFR	3172.76093	ft^3/min	Use this number for selecting a blower
	Pumppow	2119.30995	N*(m/sec)	Blower power with safety margin
	BlowerHP	2.84199464	HP	Blower Horse Power; safety margin is included herein
55	nse			Efficiency number input form IMS/HB Company 09/28/98
	HPplug	5.16726298	HP	Plug power
				Use vaneaxial fan type B-LB direct dnven @3600 RPM
1.204	Rhoairstp		kg/m^3	Density of air at stp (pp 640; Thompson)
	SCFMaire	5924.13752	scfm	
	smdpaireq	2.96306915	inch H2O	Pressure head for air equivalent design with safety margin
	BlHPaireq	2.84199464	HP	Blowe Horse Power (air equivalent), safety margin is included herein
3	lebeam			E-BEAM FLANGE ACOOMODATION DISTANCE
	Lebeam	99	m	
				ACOUSTIC ATTENUATORS/THERMALIZER/HEAT EXCHANGER
	aC	285.843153	m/sec	Velocity of sound in laser gas
	N	2.75		Number of interpulse acoustic transients
	lupupatt			
	Lupupatt	33	m	Length upsteam of the upstream attenuator
8	lupstatt			Upstream attenuator
	Lupstatt	2.64	m	
3	θ		Degree	Half angle of expansion for the upstearm channel in degrees
	Wuschate	.641302209	m	Width at the entrance to the upsteam attenuator
	lthrmlzr			
	Lthrmlzr	231	m	Length of a thermalizer section
5	lupthrmlzr			
	Lusthrmlzr	165	m	Chamber length upsteam of the thermalizer
5	ldsupthrm			
	Ldsupthrm	165	m	Chamber length downstream of the thermalizer
6	ldownstatt			Downstream attenuator
	Ldownsatt	1.98	m	Length of the diownstream attenuator
5	ldsdsatt			
	Ldsdsatt	165	m	Length of a section downstream of the downstream attenuator
4	ldshex			
	Ldshex	1.32	m	Length of the downstream heat exchanger (assume/venfy)

.5	fdsdshex			
	Ldsdshex	.165	m	Length down sream of the downstream heat exchanger
2	fwdshex			Best guess (check with CATIA); accomodates for the width of the heat
0	fmisc			
	Lmisc	0	m	Length of the misc section (assume/verify with CATIA)
	Llegtotal	8 151	m	Total length of the laser leg of the flow loop
	Vupatchnl	1.58662216	m^3	Volume of the upstream attenuator flow channel See page 2-13 Mark
	Vlaserleg	4 19848475	m^3	Total volume of the laser leg of the flow loop
18 1875	dotherlegs		inch	Diameter of the duct/tube for other legs (See Fax by IMS H-Bdated 09
14 908	Lotherlegs		m	Length of other leags (assume/verify from CATIA)
	Vflowloop	6697 2315	liter	Total volume of the entire flow loop (verify from CATIA)
				Check for the missing volumes of the top and bottom bends in the las
3	fdepthatt			
	Depthatt	495	m	Depth of an acoustic attenuator
				Packing material. See pp 47 of NRL Report Φ ~ 0 99. k ~ 4 x 10^(-5)
				packing density ~ 1%. 8 micron fiber with from perforated plate
1	fattcmp			
	Wattcmp	33	m	Width of the compartment in acoustic attenuator
				Boundary layer suction
	Dhydraulic	507692308	m	Hydraulic diamater in the actual laser cavity
	ReDh	179380 686		Reynold's Number based on hydraulic diameter
		3 3	m	
	Re_	1165974 46		Reynold s number based on lenght to cavity entrance from thermalize
				Assueme the following
	δ	2 94133421	inch	Boundary layer thickness Turbulant flowwith zero pressure gradient. p
	δ1	367666777	inch	Displacement thickness
	δ2	285963048	inch	Momentum thickness
	δT	285963048	inch	Thermal boundary layer thickness = Momentum thickness (assume/ve
				HEAT EXCHANGER
	Lasem	48900	Watts	Total energy dumped into cavityby 2 e-beams per second. N*(m/sec)=
	Heatload	51019 3099	Watts	Total heat load (e-baem enrgy+pup power) to be removed by the heat
	mdotlotal	3 36623822	kg/sec	
				THERMALIZER
				For Pr=0 70. use V. Kulkarney's memo dated 11 September. 1981
64	Wthrmlzr		m	Width of thermalizer
	Uthrmlzr	2 12695313	m/sec	Flow velocity upstream of thermalizer
12	HCo			Honeycomb solidity
001608	HChd		m	Honeycomb hydraulic diameter
	RethHChd	332 898958		Reynold's number based on honeycomb hydraulic diameter

.01778	LHC		m	length of a single slab of a honeycomb
	σ	.1328597		Honeycomb size parameter, Reference V Kulkamy
1000	DTR			Requirement ΔTi/ΔTo (assume/verify): ΔTi ~+/- 2 K (assume verify)
1.06	PLOT			Figure 5, Reference V. Kulkamy
	NHC	6.51675026		Calculated number of honecomb slabs
	Nhc	7		Selected number of honecomb slabs
.32	PLOTA			Figure 6, Reference V. Kulkamy
	nΔpHC	21.5867352		Number of pressure head loss across honeycomb based on Uthrmlzr
	nΔpTH	5.73924675		Number of pressure head loss across honeycomb based on Uflow
	Ltotalthrm	.23114	m	total length of the thermalizer unit with unit spacing in between the sla
7.6923	PLOTB			Figure 6, Reference V. Kulkamy
	hthrmlzr	47 8239584	Watts/(m^2*K	Overall heat transfer coefficient for thermalizer note Joule/sec=Watt
				MEDIUM HOMOGENEITY
				Beam quality: Goal 1.5: 09/23/98 M Wacks input
				Baseline flow aberrations
				Use Marechal's approximation, See pp 26-46 NRL Report
				Acoustic disturbances caused by gas recirculation
	Mcavity	014430991		Cavity flow Mach number
015	αp			
	dRhoRho1	2 0767E-6		RMS acoustic variations due to baseline flow disturbances
	Λ1	165	m	Scale of these disturbances
				Measured temperature fluctuations in baseline flow
004	dTm		K	
	dRhoRho2	1 23782E-5		RMS thermal variations due to baseline flow disturbances
				Thermal disturbances from heat exchanger thermalizer
	ΔTwallgas		K	Twall-Tgas See AIAA 90-1796, pp 10
	dRhoRho3	00031		Window boundary layer effects
				Pulsed flow aberrations
				verify with detailed PLACATE Code analysis
000015	AN1			Acoustic effects (assume verify with detailed PLACATE Code analysi
	dRhoRho4	000015		See pp 46 NRL Report
000015	AN2			Entropy disturbances (assume, verify with detailed PLACATE Code an
	dRhoRho5	000015		See pp 46 NRL Report
14 69	pref		psia	Reference pressure
293 15	Tref		K	Reference temperature
	Rhostp	2 27525639	kg/m^3	
2	NoofPass			Number of passes in laser amplifier (assume/verify)
	OPL	2 2	m	Optical path length
000000248	λ		m	Wavelength of laser
00028	β			Gladstone-Dale Coefficient @ λ of interest (assuem/verify)
	ΔΦ1	032023398		RMS
	ΔΦ2	190874827		RMS
	ΔΦ4	231304501		RMS

	ΔΦ5	.231304501		RMS
	OPLδT	.02905383	m	Optical path length for ΔTwallgas related disturbances
	ΔΦ3	.063129919		RMS
	BQ1	1.00051288		Beam quality
	BQ2	1.01838353		Beam quality
	BQ3	1.00199468		Beam quality
	BQ4	1.0271119		Beam quality
	BQ5	1.0271119		Beam quality
	ΔΦrms	.385289019		Root sum squared of all ΔΦs
	BQ	1.07704784		Beam quality

See the header design and porous plate selection 09/25/98 amd 09/26

FLOW LOOP

FLOW LOOP ENGINEERING DESIGN

Flow loop lay-out

Flow loop structural analysis

Engineenng design

GAS SUPPLIES

FLOW LOOP OPERATIONAL SAFETY/MITIGATING TECHNOLOGI

Objective and Approach

- Objective: Assess the effect of optical inhomogeneities in the amplifier gain media on the optical quality of the intensified target image relayed to the pellet location.
- Approach:
  - Create optical phase screen in front of last optic in the train.
  - Divide the screen into subscreens with random phases according to inhomogeneity scale lengths. Screen phase variance will be a free parameter.
  - Convolve the (incoherent) target image with the imhomogeity-degraded point-spread function.
  - Maximum tolerable image degradation (irradiance non-uniformity) sets the limit on the maximum allowable path inhomogeneity. The latter becomes a top level technical requirement for the design.

Basic numerical design considerations

- Short KrF wavelength insures all parts of the beam line are in the near field The use of a thin random phase screen is thus justified
- Distance R_1 in the drawing is effectively infinity
- I assumed a 20 cm optic and a 30 cm final amplifier.
- I used an inhomogeneity scale length of 16 5 scaled to 11 cm taken from Kirin's work
- Here the image is 0 36 cm in diameter
- The 400 x 400 near field scales to 1 unit = 0 05 cm
- The 400 x 400 focal plane field scales as 502 6r (r, cm).
- Assumed focal length, 50 m
- Note that the results will strongly depend on the ratio of the inhomogeneity scale length to the entrance aperture. Problem is similar to propagation of a laser beam through the atmosphere. The role of the coherence diameter there is our scale length here

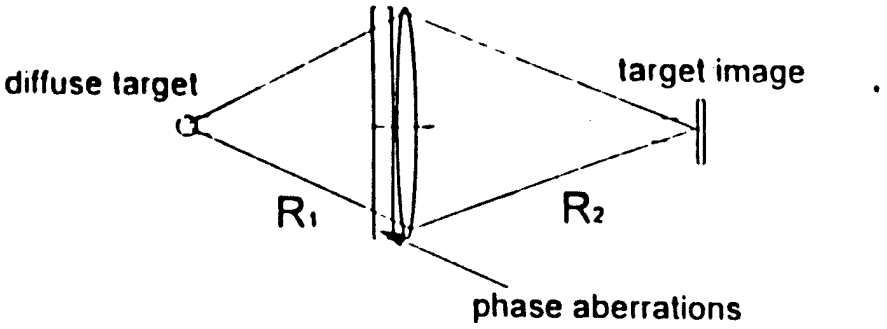

Point spread function and the diffraction-limited image in the pellet plane

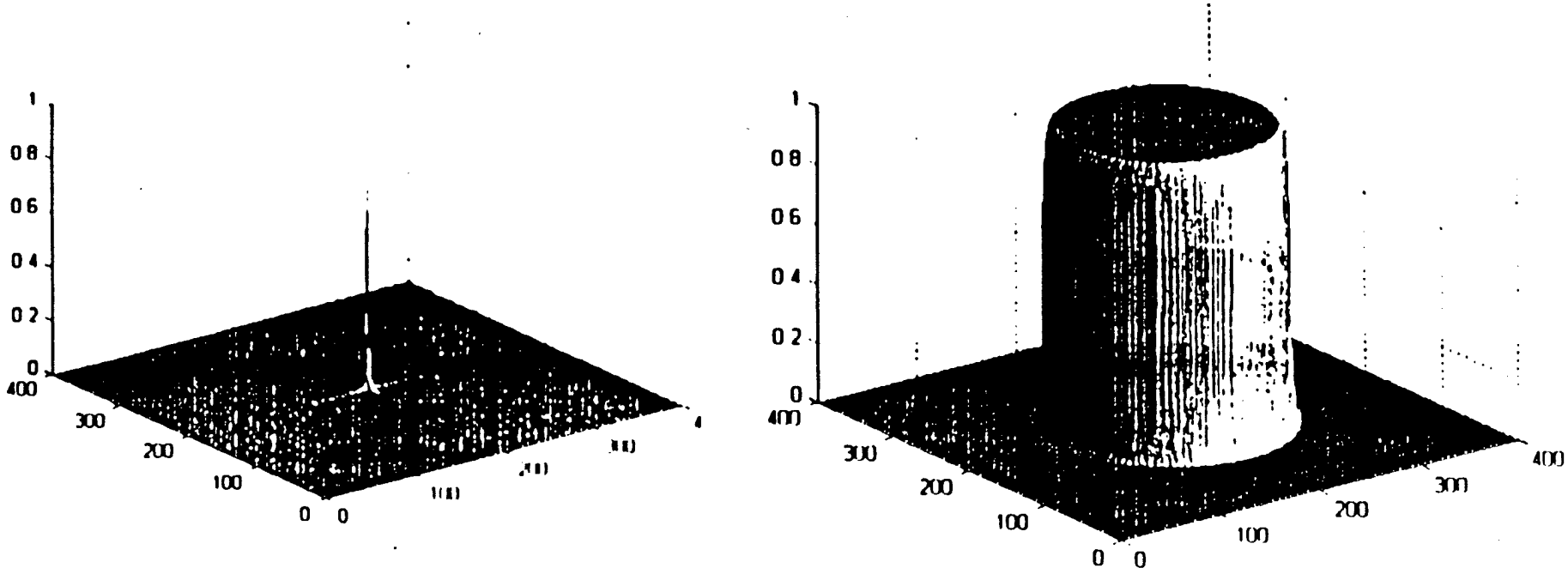

Nearly diffraction-limited imaging reveals sharp irradiance edges and a smooth top

Sigma = 0.0316 waves

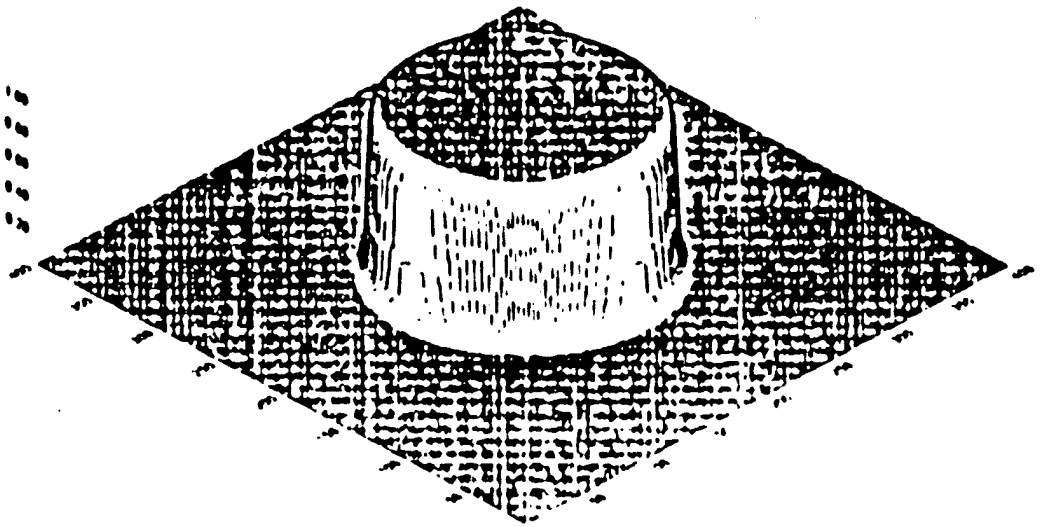

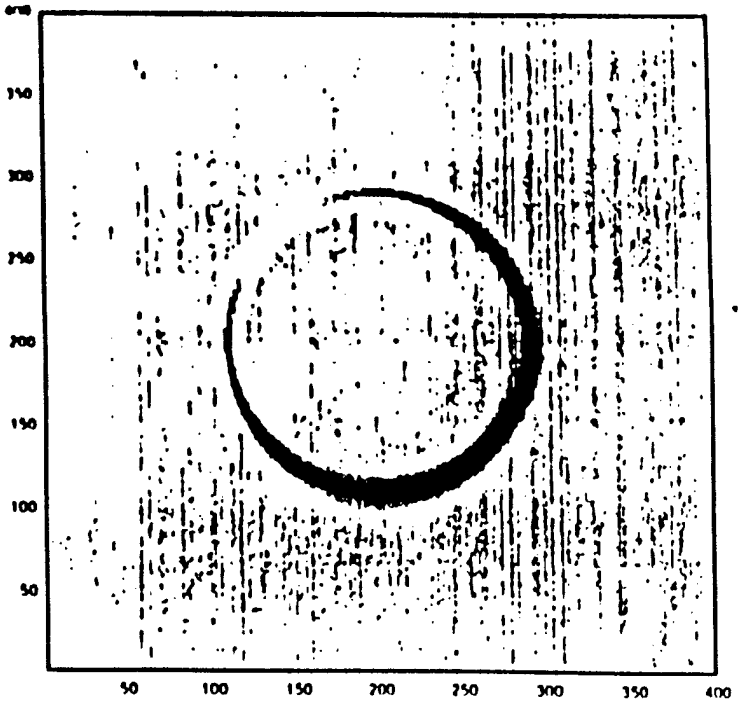

At sigma = 1.01 waves, some profile rounding occurs.

Some aliasing also is noticeable in the 'foot' around the figure. Note: ratio of aperture to scale area is 3.3: 1, therefore one should not expect enormous distortion.

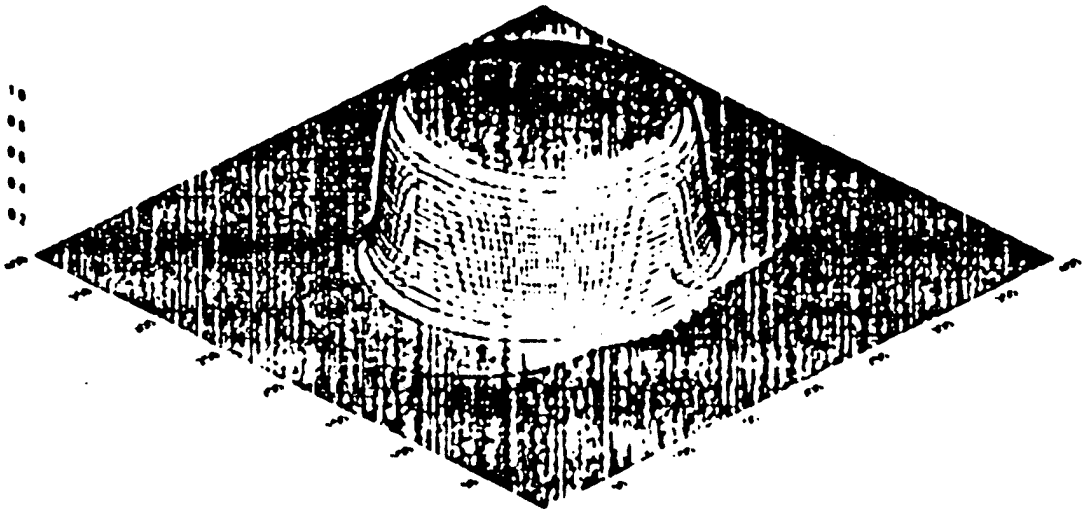

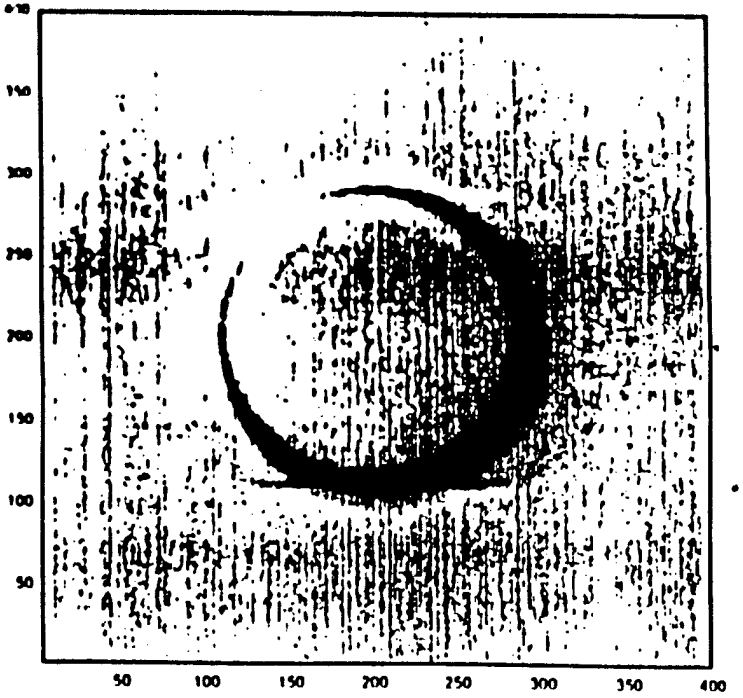

For the same phase standard deviation, reducing the scale relative to the aperture increases image rounding.

Sigma = 1.01 waves
scale reduced to give 25
statistically independent
patches across aperture instead
of four.

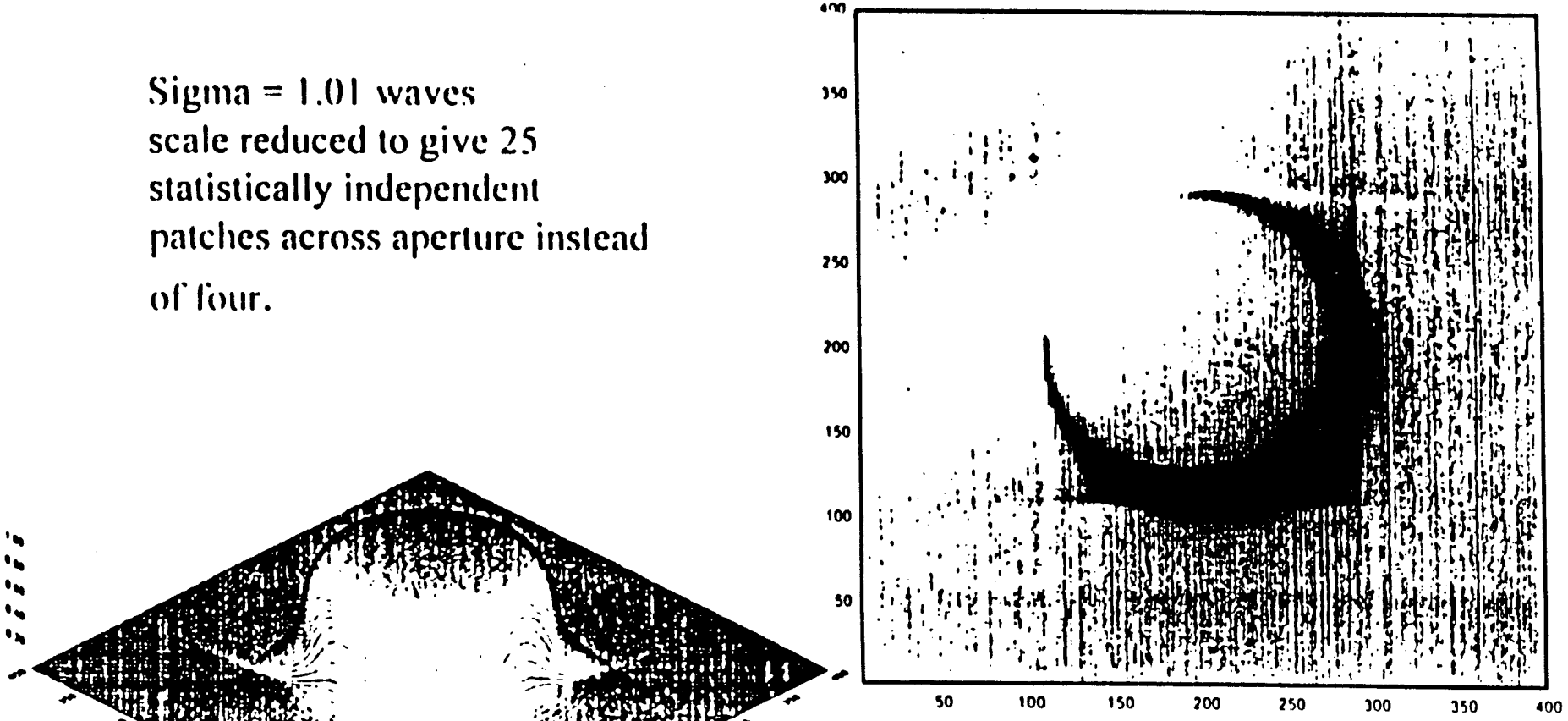

Observation

- Imaging of finite objects in the presence of turbulence (phase inhomogeneities) differs from far-field turbulence-induced 'speckle' in the same way that viewing the maiden through the shower glass differs from observing star twinkle: the maiden's outline doesn't twinkle, but the stars do. The large number of picture elements involved in a finite image interfere with a deterministic and random component. The effect of the random component in the composition of the image is to act as a spatial low pass filter causing the sharp (high spatial frequency) part of the image to be attenuated. For this reason, the proposed KrF system will be much more tolerant of phase inhomogeneities than a system that had a coherent point source. (A true stroke of genius!). However, the appropriate measure is the allowable 'droop' in intensity across the image allowable as each beam line tiles the target. If the droop becomes too large, additional beam lines must be added to maintain a prescribed level of uniformity. Thus optical path inhomogeneities limits become a part of the top level technical requirement levied on the system design.